

UNCLASSIFIED

---

AD 275 949

*Reproduced  
by the*

ARMED SERVICES TECHNICAL INFORMATION AGENCY  
ARLINGTON HALL STATION  
ARLINGTON 12, VIRGINIA



---

UNCLASSIFIED

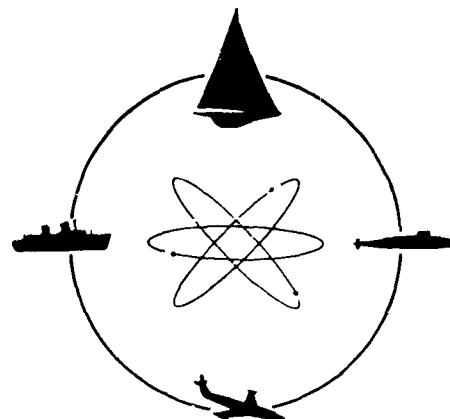
NOTICE: When government or other drawings, specifications or other data are used for any purpose other than in connection with a definitely related government procurement operation, the U. S. Government thereby incurs no responsibility, nor any obligation whatsoever; and the fact that the Government may have formulated, furnished, or in any way supplied the said drawings, specifications, or other data is not to be regarded by implication or otherwise as in any manner licensing the holder or any other person or corporation, or conveying any rights or permission to manufacture, use or sell any patented invention that may in any way be related thereto.

275 949



STEVENS INSTITUTE  
OF TECHNOLOGY

CASTLE POINT STATION  
HOBOKEN, NEW JERSEY



## DAVIDSON LABORATORY

MAY 16 1962

### WAVE FORCES ON SUBMERGED BODIES

by *Charles J. Henry, Milton Martin, and  
Paul Kaplan*

Navr 263(15)

RESEARCH WAS CARRIED OUT UNDER  
THE BUREAU OF SHIPS  
FUNDAMENTAL HYDROMECHANICS RESEARCH PROGRAM  
S-R001 01 01

ADMINISTERED BY  
DAVID TAYLOR MODEL BASIN

R-808

June 1961

WAVE FORCES ON SUBMERGED BODIES

*by Charles J. Henry, Milton Martin, and Paul Kaplan*

Report 808  
Project HY 1862  
June 1961

CONTRACT No. 263(15)  
RESEARCH WAS CARRIED OUT UNDER THE  
BUREAU OF SHIPS  
FUNDAMENTAL HYDROMECHANICS RESEARCH PROGRAM  
SR001-01-01

ADMINISTERED BY  
DAVID TAYLOR MODEL BASIN

DAVIDSON LABORATORY  
Stevens Institute of Technology  
Castle Point Station  
Hoboken, New Jersey

## TABLE OF CONTENTS

	<u>page</u>
Nomenclature	ix
Abstract	xiii
I.    Introduction	1
II.   Experimental Setup	3
A.    Apparatus	3
B.    Calibration	4
C.    Test Procedure	6
D.    Data Reduction	7
III.  Discussion of Results	9
A.    Vertical Plane	9
B.    Horizontal Plane	9
IV.   Comparison with Theory	13
V.    Conclusions	17
VI.   References	19
Appendix A	A-1
Appendix B	B-1

## LIST OF TABLES

<u>Table</u>	<u>Page</u>
I. Model Characteristics	21
II. Test Conditions and Frequency of Encounter (cycles per second)	23
III. Wave Speeds	25

## LIST OF ILLUSTRATIONS

### Figure

1. Seakeeping Installation Tank No. 2
2. Experimental Apparatus
3. Block Diagram of Instrumentation
4. Oscillating Beam
5. Phase Diagram
6. Heave Force per Unit Wave Amplitude versus Wave Length/  
Body Length at  $0^\circ$  Heading Angle
7. Heave Force per Unit Wave Amplitude versus Wave Length/  
Body Length at  $30^\circ$  Heading Angle
8. Heave Force per Unit Wave Amplitude versus Wave Length/  
Body Length at  $60^\circ$  Heading Angle
9. Heave Force per Unit Wave Amplitude versus Wave Length/  
Body Length at  $90^\circ$  Heading Angle
10. Pitching Moment per Unit Wave Amplitude versus Wave  
Length/Body Length at  $0^\circ$  Heading Angle
11. Pitching Moment per Unit Wave Amplitude versus Wave  
Length/Body Length at  $30^\circ$  Heading Angle
12. Pitching Moment per Unit Wave Amplitude versus Wave  
Length/Body Length at  $60^\circ$  Heading Angle
13. Pitching Moment per Unit Wave Amplitude versus Wave  
Length/Body Length at  $90^\circ$  Heading Angle
14. Side Force per Unit Wave Amplitude versus Wave Length/  
Body Length at  $30^\circ$  Heading Angle (without Conning Tower)
15. Side Force per Unit Wave Amplitude versus Wave Length/  
Body Length at  $60^\circ$  Heading Angle (without Conning Tower)
16. Side Force per Unit Wave Amplitude versus Wave Length/  
Body Length at  $90^\circ$  Heading Angle (without Conning Tower)
17. Yawing Moment per Unit Wave Amplitude versus Wave Length/  
Body Length at  $30^\circ$  Heading Angle (without Conning Tower)
18. Yawing Moment per Unit Wave Amplitude versus Wave Length/  
Body Length at  $60^\circ$  Heading Angle (without Conning Tower)

Figure

19. Yawing Moment per Unit Wave Amplitude versus Wave Length/  
Body Length at  $90^\circ$  Heading Angle (without Conning Tower)
20. Side Force per Unit Wave Amplitude versus Wave Length/  
Body Length at  $30^\circ$  Heading Angle (with Conning Tower)
21. Side Force per Unit Wave Amplitude versus Wave Length/  
Body Length at  $60^\circ$  Heading Angle (with Conning Tower)
22. Side Force per Unit Wave Amplitude versus Wave Length/  
Body Length at  $90^\circ$  Heading Angle (with Conning Tower)
23. Yawing Moment per Unit Wave Amplitude versus Wave Length/  
Body Length at  $30^\circ$  Heading Angle (with Conning Tower)
24. Yawing Moment per Unit Wave Amplitude versus Wave Length/  
Body Length at  $60^\circ$  Heading Angle (with Conning Tower)
25. Yawing Moment per Unit Wave Amplitude versus Wave Length/  
Body Length at  $90^\circ$  Heading Angle (with Conning Tower)
26. Roll Moment per Unit Wave Amplitude versus Wave Length/  
Body Length at  $30^\circ$  Heading Angle (with Conning Tower)
27. Roll Moment per Unit Wave Amplitude versus Wave Length/  
Body Length at  $60^\circ$  Heading Angle (with Conning Tower)
28. Roll Moment per Unit Wave Amplitude versus Wave Length/  
Body Length at  $90^\circ$  Heading Angle (with Conning Tower)
29. Phase Lag of Heave Force versus Wave Length/Body Length  
at  $0^\circ$  Heading Angle
30. Phase Lag of Heave Force versus Wave Length/Body Length  
at  $30^\circ$  Heading Angle
31. Phase Lag of Heave Force versus Wave Length/Body Length  
at  $60^\circ$  Heading Angle
32. Phase Lag of Heave Force versus Wave Length/Body Length  
at  $90^\circ$  Heading Angle
33. Phase Lag of Pitching Moment versus Wave Length/Body  
Length at  $0^\circ$  Heading Angle
34. Phase Lag of Pitching Moment versus Wave Length/Body  
Length at  $30^\circ$  Heading Angle
35. Phase Lag of Pitching Moment versus Wave Length/Body  
Length at  $60^\circ$  Heading Angle



## Figure

36. Phase Lag of Pitching Moment versus Wave Length/Body Length at  $90^\circ$  Heading Angle
37. Phase Lag of Side Force versus Wave Length/Body Length at  $30^\circ$  Heading Angle (without Conning Tower)
38. Phase Lag of Side Force versus Wave Length/Body Length at  $60^\circ$  Heading Angle (without Conning Tower)
39. Phase Lag of Side Force versus Wave Length/Body Length at  $90^\circ$  Heading Angle (without Conning Tower)
40. Phase Lag of Yawing Moment versus Wave Length/Body Length at  $30^\circ$  Heading Angle (without Conning Tower)
41. Phase Lag of Yawing Moment versus Wave Length/Body Length at  $60^\circ$  Heading Angle (without Conning Tower)
42. Phase Lag of Yawing Moment versus Wave Length/Body Length at  $90^\circ$  Heading Angle (without Conning Tower)
43. Phase Lag of Side Force versus Wave Length/Body Length at  $30^\circ$  Heading Angle (with Conning Tower)
44. Phase Lag of Side Force versus Wave Length/Body Length at  $60^\circ$  Heading Angle (with Conning Tower)
45. Phase Lag of Side Force versus Wave Length/Body Length at  $90^\circ$  Heading Angle (with Conning Tower)
46. Phase Lag of Yawing Moment versus Wave Length/Body Length at  $30^\circ$  Heading Angle (with Conning Tower)
47. Phase Lag of Yawing Moment versus Wave Length/Body Length at  $60^\circ$  Heading Angle (with Conning Tower)
48. Phase Lag of Yawing Moment versus Wave Length/Body Length at  $90^\circ$  Heading Angle (with Conning Tower)
49. Phase Lag of Roll Moment versus Wave Length/Body Length at  $30^\circ$  Heading Angle (with Conning Tower)
50. Phase Lag of Roll Moment versus Wave Length/Body Length at  $60^\circ$  Heading Angle (with Conning Tower)
51. Phase Lag of Roll Moment versus Wave Length/Body Length at  $90^\circ$  Heading Angle (with Conning Tower)
52. Variation of Velocity Corrections with Depth
53. System of Coordinates

# NOMENCLATURE

$A_{22}, A_{33}, A_{42}$	Virtual inertias
$a$	Wave amplitude
$a_1, a_2$	Amplitude of motion of model and strut, respectively
$b$	Distance from centerline to tip of fin (Appendix A) and strut semi chord (Appendix B)
$C(\kappa)$	Theodorsen function
$c$	Wave speed
$D$	Maximum diameter of model
$d$	Distance from wave wire to CB of model
$d_c$	Correction factor for depth of submergence
$d_o$	Correction factor for roll moment due to conning tower
$g$	Gravitational constant
$h$	Depth of submergence to coordinate axis
$h_m$	Depth to midspan of conning tower in model diameters
$h_o$	Depth to model centerline in model diameters
$h_1$	Depth of submergence to model centerline for each test in model diameters
$h_2$	Common depth of submergence = 2.5D
$I_{zz}$	Mass polar moment of inertia of model about the z axis
$i$	$\sqrt{-1}$
$J_n(\kappa)$	$n^{\text{th}}$ order Bessel function of the first kind
$K$	Roll moment

$k$	Wave number, $k = 2\pi/\lambda = g/c^2$
$k_\beta$	Stiffness of balance in yaw
$k_\delta$	Stiffness of balance in side sway
$k_1, k_2$	Stiffness of balance and bridge in side sway
$L$	Model length and lift force on strut (Appendix B)
$L_o$	Amplitude of lift on strut
$L_o'$	Amplitude of lift on strut per unit span
$L_{2D}$	Total two dimensional lift on strut
$L_h(\kappa, AR)$	Unsteady lift coefficient corrected for aspect ratio
$l$	Distance from center of balance to CB, positive if CB is forward
$M$	Pitch moment about CB
$m$	Stripwise mass of the displaced fluid $\pi\rho R^2$ (Appendix A) and mass of model (Appendix B)
$m_1, m_2$	Mass of model and strut, respectively
$N$	Yaw moment about CB
$N_o$	Amplitude of yaw moment
$N_{\dot{y}}, N_{\ddot{y}}, N_{\dot{\beta}}, N_{\ddot{\beta}}, N_{\beta}$	Hydrodynamic yaw moment derivatives relative to CB of model
$R$	Radius of circular cross section of model
$t$	Time
$T_w$	Wave period
$V$	Model or ship speed
$v, w$	Lateral and vertical orbital velocities, respectively
$v_o, w_o$	Values of $v, w$ taken at center of cross section
$x, y, z$	Orthogonal cartesian coordinates fixed in the model

$x_b$	Distance from origin to bow
$x_s$	Distance from origin to stern
$x_1, x_2$	Displacement of masses $m_1$ and $m_2$
$Y$	Side force
$Y_o$	Amplitude of side force
$Y_y, Y_y, Y_\beta, Y_\beta$	Hydrodynamic side force derivatives relative to CB of model
$y_o$	Amplitude of model oscillation in y direction
$Z$	Heave force
$\alpha$	Phase lag correction for offset between CB and wave wire
$\beta$	Phase lag obtained from records and distortion of balance in yaw (Appendix B)
$\beta_o$	Amplitude of distortion of balance in yaw
$\gamma$	Phase lag correction due to electrical filters
$\delta$	Distortion of balance in y direction
$\delta_o$	Amplitude of $\delta$
$\epsilon$	Phase lag relative to wave height at CB of model
$\epsilon_1, \epsilon_2$	Phase lag of $x_1$ and $x_2$ , respectively
$\eta$	Wave height at CB
$\eta_c$	Frequency of wave encounter
$\theta$	Heading angle
$\kappa$	Argument of Theodorsen function, $= 2\pi b/\lambda$
$\phi$	Velocity potential and phase lag of lift force on strut
$\mu$	Argument of Bessel functions, $= 2\pi b \cos \theta/\lambda$
$\xi$	Distance from center of gravity to center of bouyancy, positive if CB is forward

$\rho$	Mass density of water
$\omega$	Circular frequency of wave encounter
$\omega_1^2, \omega_2^2$	Uncoupled natural frequencies, $\omega_1^2 = k_1/m_1, \omega_2^2 = k_2/m_2$

## ABSTRACT

A series of experiments, in which the forces and moments acting on a slender, submerged body-of-revolution moving under regular waves were measured, provided data to verify theoretical predictions of these forces and moments. The measured and predicted results over a range of speeds, heading angles, and wave lengths agreed. The measured and predicted roll moments, acting on the same model but with a conning tower, did not agree; however, the measured and predicted heave and side forces and the pitch and yaw moments did agree.

## I. INTRODUCTION

In the development of optimum underwater vehicles, increasing importance has been given to the prediction of motions due to wave forces. In the past, these predictions were attempted theoretically, and expressions for the forces and moments acting on a spheroid moving obliquely under regular waves were developed (reference 1). As a result of choosing this simple model, the expressions for the forces and moments were in closed form. However, the range of shapes to which the results applied was limited. An extension to more general shapes, using strip theory, provided more practical results for the case of slender bodies in head seas. An empirical correction factor applied to the theoretical results provided agreement between theory and experiment. This correction accounted for wave-body interactions. An extension of Lagally's Theorem to unsteady flows provided means for predicting the forces and moments acting on a slender body-of-revolution moving obliquely under waves (reference 2). Again using strip theory but including the wave-body interactions, a method was found by which the forces due to added masses of fins could be included with the prediction of forces and moments on a slender body (reference 3). The results of reference 3 agree with those of reference 2.

Previous experimental investigations were for head seas only. These results did not provide information for the oblique seas case. Therefore, a series of experiments was conducted with a slender body-of-revolution at various heading angles and several forward speeds and wave lengths. Measurements of the magnitude and phase of the heave and side force and the yaw and pitch moment which acted on the model showed good agreement with the values predicted by the theory

in reference 3. In another series of tests, a conning tower was attached to the model. The measured roll moment showed poor agreement with the theory; however, the other measured forces and moments showed good agreement with theory.



## II. EXPERIMENTAL SETUP

### A. APPARATUS

The experiments were performed in the Seakeeping Facility (Figure 1) described in reference 4.

#### 1. Model

A series-58 Hull was used in all tests. This family of bodies-of-revolution is described in reference 5. The model dimensions are given in Table I. The afterportion of the model was altered by cutting off the last three inches to accomodate the sting. The effect of this change was neglected; the model length used in all calculations was 4.5 feet. For the calculation of the inertial properties of the model, the water contained in the free-flooding cavities within the model was assumed to move rigidly with the model. The conning tower was an airfoil-shaped fin with a chord length of 0.45 foot and a span of 0.293 foot with the leading edge 1.27 feet aft of the bow.

#### 2. Sting, Carriage, and Bridge

A sting, connected to a faired vertical strut, supported the model. The strut was supported from a carriage running on a rail beneath the truss-type bridge that spanned the tank. The angle of the bridge relative to the wave crests was adjustable. An internal balance between the sting and model measured the desired forces and moments (Figure 2).

#### 3. Preliminary Tests

Preliminary tests of this apparatus indicated two difficulties. The vibrations caused by the rolling carriage wheels and other extraneous sources completely obscured the desired outputs from the balance. In addition, the flexibility

of the supporting structure permitted appreciable vertical and horizontal motions of the model. The resulting dynamic and hydrodynamic effects could not be neglected.

Supports extending to the walls and ceiling trusses of the building decreased the vertical oscillations of the bridge considerably, but the horizontal motion remained. Much of this motion was due to flexibility in the bridge-rail-carriage system and could not be reduced easily.

#### 4. Instrumentation

The transducers used as sensing elements in the balance were Schaevitz linear differential transformers.

To provide the necessary information to correct for dynamic effects, accelerometers installed at the center-of-gravity of the model measured the horizontal and vertical accelerations. Low-pass filters reduced the noise in the outputs of the Schaevitz gages and the accelerometers.

A resistance wave-wire supported from the carriage at a known distance ahead of the model measured the wave height.

The five filtered outputs from the balance, the two filtered outputs from the accelerometers, and the unfiltered wave-wire output were recorded (Figure 3).

### B. CALIBRATION

#### 1. Filters

A sinusoidal signal was fed into the primary terminals of eight transformers. The outputs from the secondaries of seven of these transformers were fed into the recorder, each through its own filter. The output of the eighth transformer was put directly into channel eight of the recorder. In this way, eight signals from a single source

were recorded simultaneously, with and without the effect of the filters, under the same electrical conditions as used in the experiments (Figure 4). The attenuation and phase shift of each channel, relative to the unfiltered one (channel eight), obtained at several input frequencies covering the range anticipated gave the information necessary to correct for the electrical attenuation and phase shift due to the filters. The filters effectively suppressed high-frequency noise and passed the desired signal, which was in the range 0.6 to 2.5 cycles per second. Spot checks with differing amplitudes of the common input signal gave no difference in the results.

## 2. Accelerometers

The accelerometers were mounted on beam as shown in Figure 4. The beam was oscillated at a known amplitude and at several frequencies and the accelerometer outputs were passed through filters and into the recorder. The amplitude and frequency of the recorded signal were plotted against the amplitude of the acceleration at the accelerometer. Correcting for the filter attenuation at each frequency gave a linear calibration curve.

## 3. Wave-Wire

The unfiltered output from the resistance wave-wire was recorded on channel eight of the recorder. After recording a zero position, the wave-wire was moved known distances to either side of the zero position to obtain the calibration curve.

## 4. Balance

An initial check of the balance characteristics while they were mounted in the model but in air showed that the cross coupling among the force and moment components was negligible and that each component was linear. An extensive calibration was then done in air.

### C. TEST PROCEDURE

Tests were made over a range of speeds, wave lengths, and heading angles (Table II). In addition, Table II shows the frequencies of encounter ( $\eta_c$ ) for each condition as given by the relation

$$\eta_c = \frac{V \cos \theta + c}{\lambda} \quad (1)$$

where  $V$  = speed of advance of the model

$\theta$  = heading angle relative to wave direction

$c$  = wave speed

$\lambda$  = wave length.

Each day's testing began and ended with a calibration of the balance and wave wire. The bridge was moved to give the desired heading angle and then was braced as described previously. To get the desired wave length, the period of the wave-maker was set at the desired value ( $T_w$ ) given by

$$T_w = \sqrt{\frac{2\pi\lambda}{g}} \quad (2)$$

where  $g$  is the gravitational constant. The corresponding wave speeds were found from

$$c = \sqrt{\frac{g\lambda}{2\pi}} \quad (3)$$

For wave-length/body-length ratios of 1.0 and 1.5, the wave amplitude was set at 1/20 of the wave length. At the longer wave lengths, smaller amplitudes were used so as not to stress the wavemaking equipment.

A constant-speed electric motor drove the carriage through a gear and pulley system. The gear ratio and pulley radius were adjustable to give a range of speeds in discrete steps of varying size.

Starting the model as soon as the regular wave train was established over the course of the test minimized the

interference of the wave system reflected from the beach. The zero speed tests were made with the model near the middle of the tank; the beam sea tests were made across the middle of the tank. Thus, the tests were usually completed before the reflected wave reached the model.

After each run, the model was returned to the starting position and the next speed was set. This procedure was repeated with the conning tower attached.

#### D. DATA REDUCTION

Analysis of the experimental data gave the magnitude and phase angle of the forces and moments acting on the model.

Five or six cycles from each run were chosen and the data reported were the values averaged over this segment. The frequency of encounter determined from the recorded wave height agreed with the values given in Table II. The wave height was obtained from this record using the calibration curve described previously. Similarly, the magnitudes of the forces and moments were computed from the corresponding records and calibration rates. In addition, the force and moment magnitudes were corrected for the filter attenuation at the frequency of encounter according to the following relation:

$$\text{tape magnitude} \times \frac{\text{calibration rate}}{\text{filter attenuation}} = \text{force magnitude} \quad (4)$$

These results divided by the wave amplitude gave force per unit wave amplitude. The factor  $d_c$  corrected for minor variations in depth of submergence and was given by

$$d_c = \frac{\exp \left( - \frac{2\pi D}{\lambda} h_2 \right)}{\exp \left( - \frac{2\pi D}{\lambda} h_1 \right)} \quad (5)$$

where  $D$  = maximum model diameter,

$h_1$  = depth of submergence for each test, and

$h_2$  = common depth of submergence =  $2.5D$ .

The predicted values of force and moment per unit wave amplitude were computed for a depth of 2.5 model diameters by taking the product of the results of equations 4 and 5 divided by the corresponding wave amplitudes.

The phase angle ( $\beta$ ) between the maximum recorded force and the recorded wave-crest was taken from the record for each component. This value was corrected for the phase shift due to the filter ( $\gamma$ ) at the frequency of encounter and for the phase difference between the wave-height at the wave-wire and the wave-height above the center-of-buoyancy (CB) of the model ( $\alpha$ ). The latter correction may be found from the relation:

$$\alpha = \frac{d}{\lambda} (360^\circ) \cos \theta \quad (6)$$

where  $d$  is the distance from the wave-wire to the CB. The desired phase angle ( $\epsilon$ ) between the force maximum at CB and the time at which a wave-crest is over the CB was then found from

$$\epsilon = \beta - (\alpha + \gamma) \quad (7)$$

A vector diagram in Figure 5 shows the phase relations which, in general, were found throughout the investigation. Also shown in Figure 5 is a phase correction ( $\delta$ ) due to dynamic effects.

### III. DISCUSSION OF RESULTS

#### A. VERTICAL PLANE

The measured heave force and pitching moment magnitudes were corrected to 2.5 diameters submergence (Figures 6 through 13). The corresponding phase angles are shown in Figures 29 through 36. The scatter and inconsistencies in these results are indicative of the inadequacies of the experimental setup. Most of the scatter in the vertical plane results is due to poor measurement of the wave-height. Otherwise, these measurements are considered dependable.

No differences were found in the measurements with and without the conning tower.

#### B. HORIZONTAL PLANE

##### 1. Dynamic Effects

In the theoretical analysis, the model was constrained to move in a straight line at constant speed. The flexibility of the supporting structure in the experiments caused the model to oscillate slightly in response to periodic wave forces. An investigation was made of the effect of this motion on the measured forces and moments.

The natural frequencies of the apparatus for all rotations of the model and for vertical translation of the model were sufficiently high; therefore, corrections for dynamic effects were neglected. The natural frequency in vertical translation was about 10 cps, and the natural frequency in roll was about 20 cps. The largest frequency of

encounter was 2.38 cps which was less than  $1/4$  of the lowest of these natural frequencies and resulted in a magnification factor in the measured force of less than 2 percent.

However, the horizontal motion of the model-strut-carriage mass with the elastic support of the rail and bridge acting as a spring had a natural frequency of about 2.4 cps. At short wave lengths and high speeds, the magnification of lateral effects due to resonance was, therefore, not negligible. The derivation of the corrections for this dynamic response is discussed in Appendix B. Several corrected values are plotted in Figure 16 (the flagged points) for the side force and Figure 19 for the yaw moment, as examples of these results. This correction was less than 10 percent of the measured values for the side force magnitude and 5 degrees for the phase lag for 90 percent of the data. The moment corrections are less than those for the side force. These corrections are based on crude guesses of the worst possible conditions.

## 2. Without Conning Tower

A sinusoidal curve was visually faired through the data at the wave encounter frequency from which the measurements of the magnitude and phase angle of the side force and yaw moment were obtained. The resulting loss in accuracy caused the increased scatter, particularly in the phase angles when compared with the data for the vertical plane.

## 3. With Conning Tower

The contribution of the force on the conning tower to the force on the body in the horizontal plane was not large; therefore, significant changes in the side force and yaw moment were not observed.

The roll moment, however, was entirely due to the force on the conning tower. The roll moment magnitudes are shown in Figures 26 through 28 and the phase lags in Figures 49 through 51.



The analysis of the roll moment data was hampered by the same dynamic effects as the side force and yaw moment. However, for the roll, the dynamic magnification due to resonance was negligible since the natural frequency of oscillation in roll of the model was about 20 cps. There still remains the effect of the transverse oscillatory motion of the model at the frequency of wave encounter and at the natural frequency of transverse oscillations. Due to the smaller magnitude of the roll moments, the relative error introduced by the transverse oscillations caused greater scatter and more inaccuracy in this component. Again, a sinusoidal curve was faired through the record at the frequency of wave encounter resulting in the same loss in accuracy mentioned previously.

#### IV. COMPARISON WITH THEORY

Considering the loss in accuracy due to the poor wave-height measurement and due to dynamic effects, the agreement between theoretical and experimental results is good. The discrepancies may be due to poor experimental conditions as well as to inaccuracies in the theory.

The measured heave force and pitch moment magnitudes and phase lag show good agreement with theory at the large wave-lengths. At short wave-lengths a discrepancy in the phase angle is evident. This discrepancy may be due to the assumptions involved in slender-body theory, which would not be appropriate at small wave lengths. The theoretical and experimental magnitudes are in good agreement at short wave-lengths.

The side force and yaw moment magnitudes and phases indicate that the same conclusions apply. Agreement between theory and experiment is good for magnitudes and phase lag at the long wave-lengths but at short wave-lengths, slender-body-theory apparently does not give an accurate prediction of the phase angle. The experimental and theoretical magnitudes are in good agreement at short wave-lengths.

The discrepancy between the measured roll moment magnitudes and the corresponding predicted values, is largely due to the transverse oscillations of the model. However, a cursory investigation showed that better agreement was obtained using the following corrections to the theory. First, the wave orbital velocity at the midspan of the conning tower was used to calculate the roll moment. The theory presented in reference 3 uses the velocity at the centerline of the model. The variation of the wave orbital velocity with depth

is shown in Figure 52. The corrected roll moment magnitudes are shown as dashed lines in Figures 26 through 28. At each heading better agreement between the corrected theory and experiment is achieved at higher speeds, whereas, at zero speed, the original good agreement is now poor. Secondly, the theoretical roll moment at zero speed is calculated on the basis of two-dimensional theory. At zero speed, the roll moment is given by:

$$L = z_o m \frac{\partial v}{\partial t}$$

where,  $z_o$  = distance from x-axis to midspan of conning tower,

$m$  = added mass of conning tower,

$\frac{\partial v}{\partial t}$  = normal component of orbital acceleration near the conning tower.

A better approximation for  $m$  than that used in the theory of reference 3 might be

$$m = \frac{6.3 \rho a^2 b}{\sqrt{a^2 + b^2}} \cdot 2b \quad (8)$$

from reference 6. In this equation

$\rho$  = density of fluid

$a$  = semi-chord length

$b$  = semi span

The factor of 2 in equation 8 was included to account for the presence of the body. The zero speed roll moment magnitude calculated with this value of added mass is shown in Figures 26 through 28 as a dash-dot line. The original good agreement between theory and experiment is again realized with this correction. The magnitude of this correction decreases as speed increases since the contribution to the total force on the conning tower of added mass effects decreases.

These corrections are discussed here to indicate possible approaches to a more exact theory. It is not intended that these corrections should be included with future theoretical computations based on the theory in reference 3. If more exact theoretical results are desired a more exact theory is needed.

## V. CONCLUSIONS

The flexibility of the model supports caused considerable hash and some dynamic effects, which accounts for much of the scatter in the plotted data, especially in the horizontal plane. Nevertheless, the theory developed in reference 3 predicts with reasonable accuracy the forces and moments acting on a slender body moving obliquely under regular waves.

Two consistent discrepancies were found. The measured phase lags for all forces and moments at the 90-degree heading angle exceeded the computed values at all speeds. This discrepancy diminished as the wave length increased and at the highest wave length the phase lags agreed with theory in all cases tested. Secondly, the measured roll moment magnitudes do not agree with the theory at the higher speeds. Both of these discrepancies are indicative of the inadequacies of slender-body-theory.

## VI. REFERENCES

1. Havelock, T. H., "The Forces on a Submerged Body Moving Under Waves," Trans. Institute of Naval Architects, Vol. 96, 1954.
2. Cummins, W. E., "Hydrodynamic Forces and Moments Acting on a Slender Body of Revolution Moving Under a Regular Train of Waves," DTMB Report No. 910, December 1954.
3. Kaplan, P. and Hu, P., "Virtual Mass and Slender-Body Theory for Bodies in Waves," DL Note 543, June 1959.
4. Numata, E., Spens, P., and Muley, A., "New Facilities at Stevens for Research in Seakeeping Qualities of Ships," DL Report No. 677, October 1957.
5. Landweber, L. and Gertler, M., "Mathematical Formulation of Bodies of Revolution," DTMB Report 719, September 1950.
6. Yu Yeetak, "Virtual Mass of Rectangular Plates and Parallelepipeds in Water," Journal of Applied Physics, November 1945.

TABLE I: MODEL CHARACTERISTICS

Length-diameter ratio	7.34
Length	4.5 feet
Maximum diameter	0.613 feet
Maximum cross sectional area	0.295 feet <sup>2</sup>
Wetted surface	6.366 feet <sup>2</sup>
Projected area	1.999 feet <sup>2</sup>
Volume	0.797 feet <sup>3</sup>
Prismatic coefficient	0.600
Weight in air	21.0 pounds
Buoyant force minus weight in water	28.7 pounds
LCB aft of bow	2.005 feet
LCG aft of bow	2.047 feet
Center-of-balance aft of bow	2.671 feet

TABLE II: TEST CONDITIONS AND FREQUENCY  
OF ENCOUNTER (CYCLES PER SECOND)

		HEADING ANGLE $\theta$ (degrees)			
$\lambda/L$	$V$ (ft/sec)	0	30	60	90
1.0	0	1.055	1.055	1.055	1.055
	2.02	1.504	1.444	1.280	1.055
	3.96	1.936	1.818	1.496	1.055
	5.95	2.378	2.201	1.717	1.055
1.5	0	.895	.895	.895	.895
	2.02	1.219	1.176	1.058	.895
	3.96	1.530	1.445	1.213	.895
	5.95	1.848	1.720	1.372	.895
2.0	0	.746	.746	.746	.746
	2.02	0.970	0.940	0.858	.746
	3.96	1.186	1.127	0.966	.746
	5.95	1.407	1.318	1.076	.746
2.5	0	.668	.668	.668	.668
	2.02	0.848	0.824	0.758	.668
	3.96	1.020	0.973	0.844	.668
	5.95	1.197	1.126	0.933	.668



TABLE III: WAVE SPEEDS

$\lambda/L$	$\lambda$ (feet)	$c$ (ft/sec)
1.0	4.5	4.75
1.5	6.75	5.60
2.0	9.0	6.71
2.5	11.25	7.52

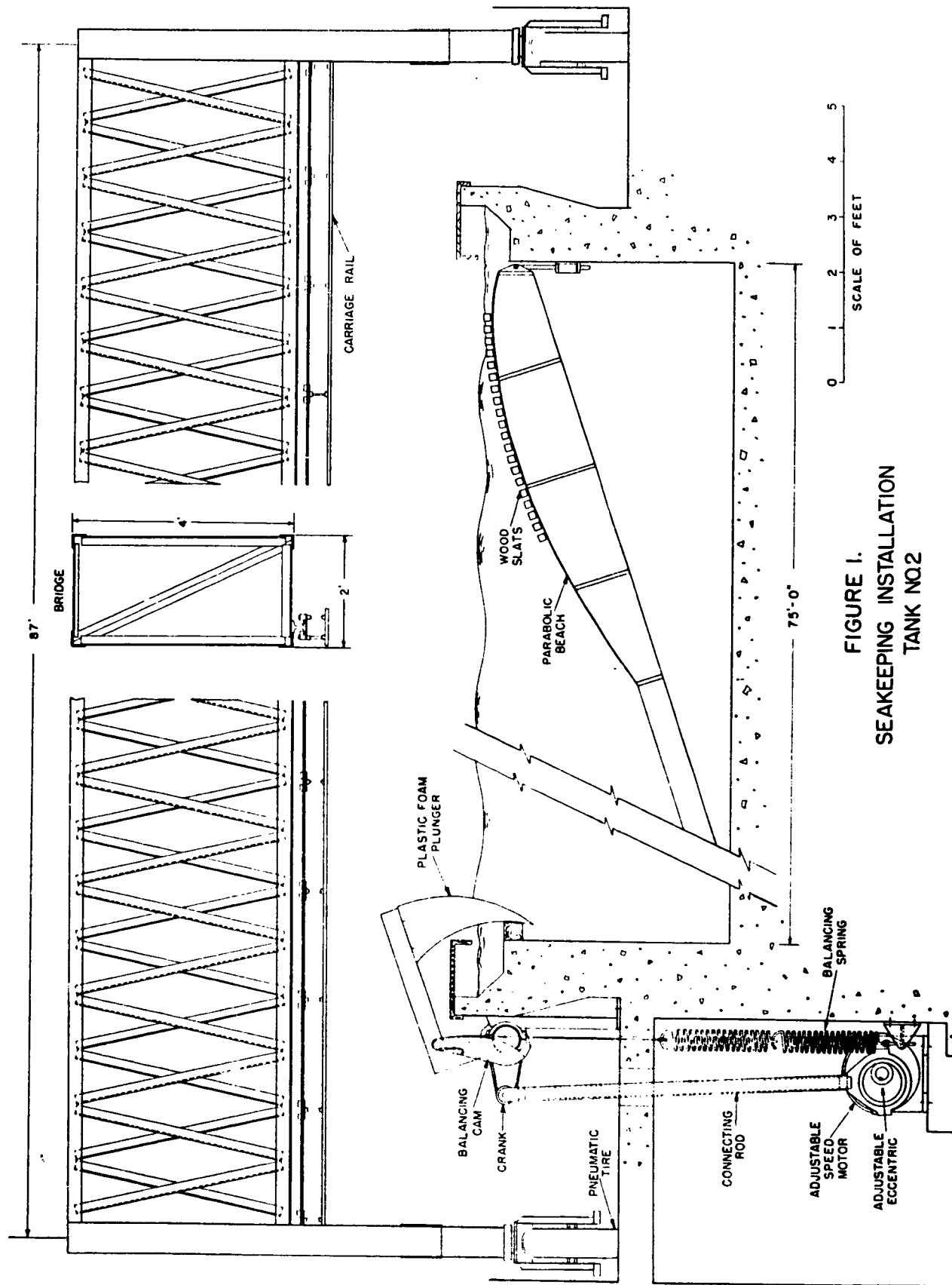


FIGURE 1.  
SEAKEEPING INSTALLATION  
TANK NO. 2

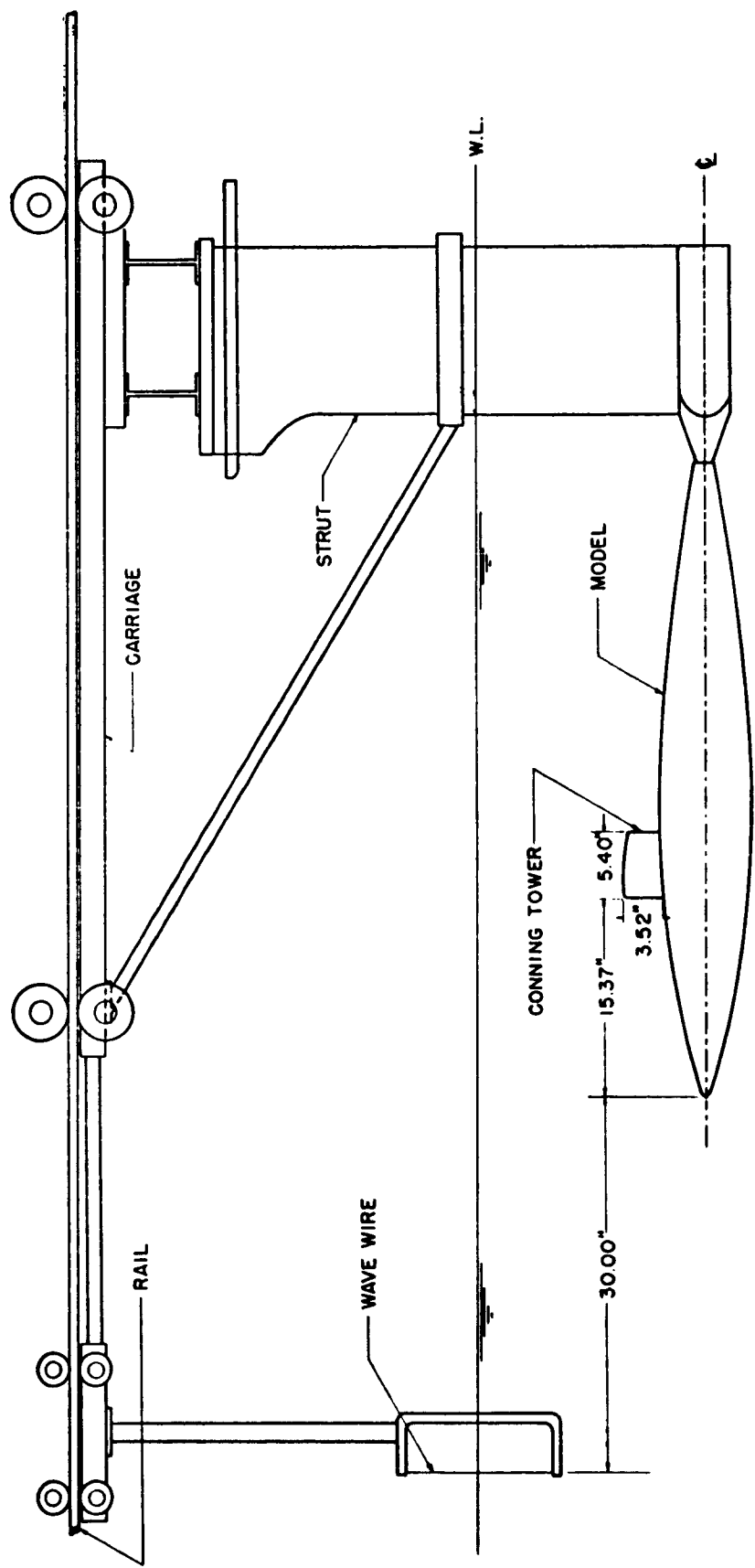
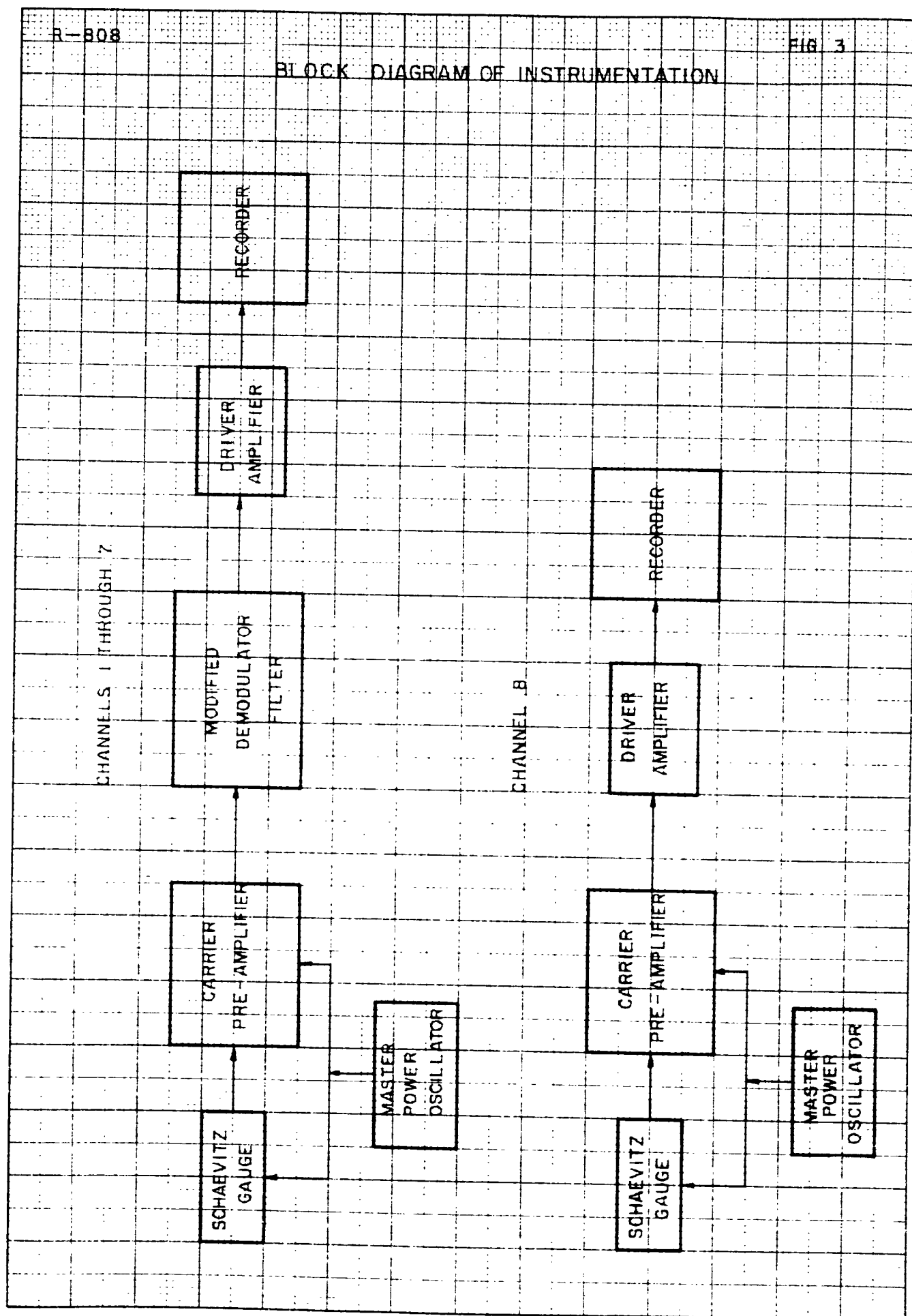


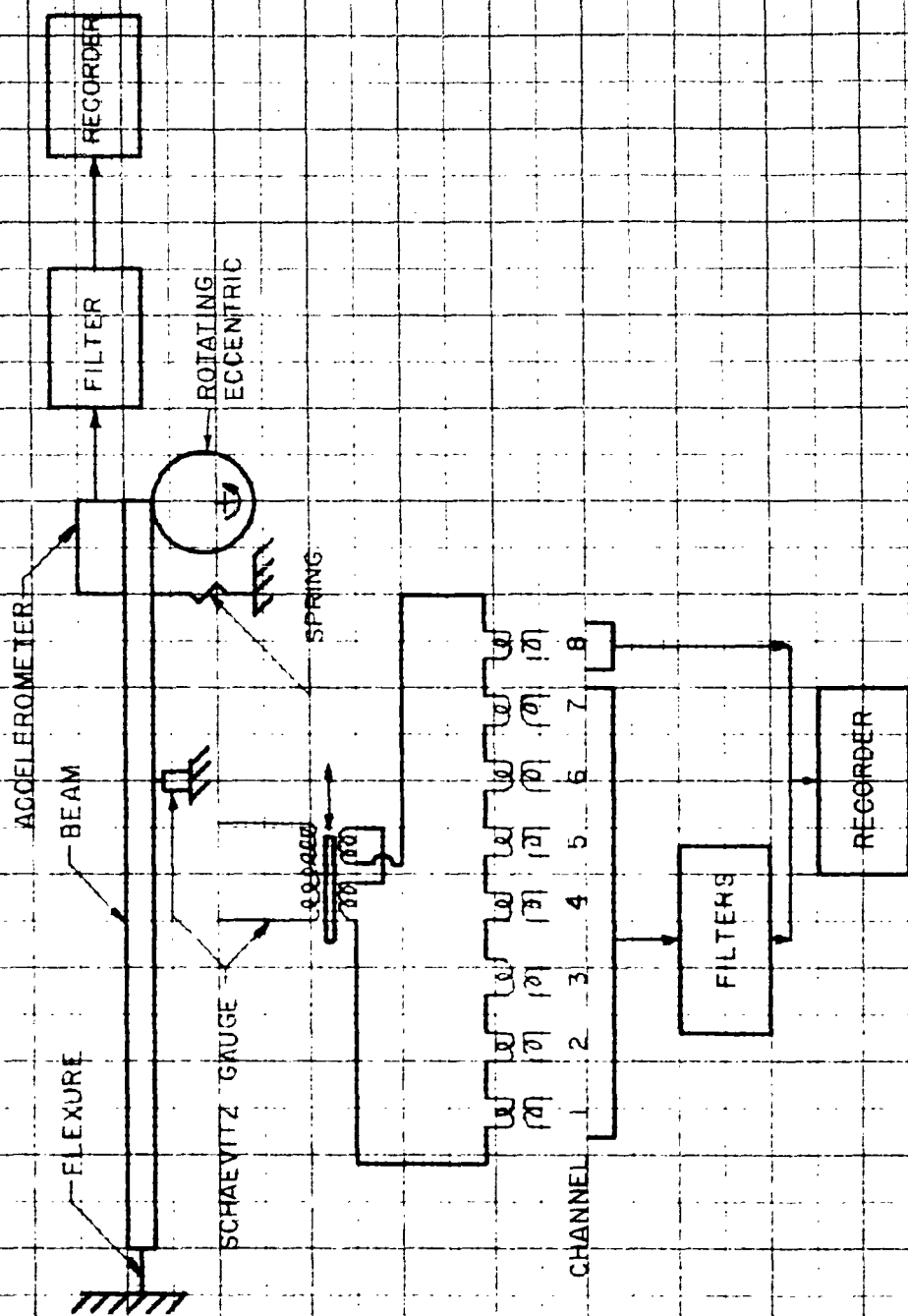
FIGURE 2. EXPERIMENTAL APPARATUS

## BLOCK DIAGRAM OF INSTRUMENTATION

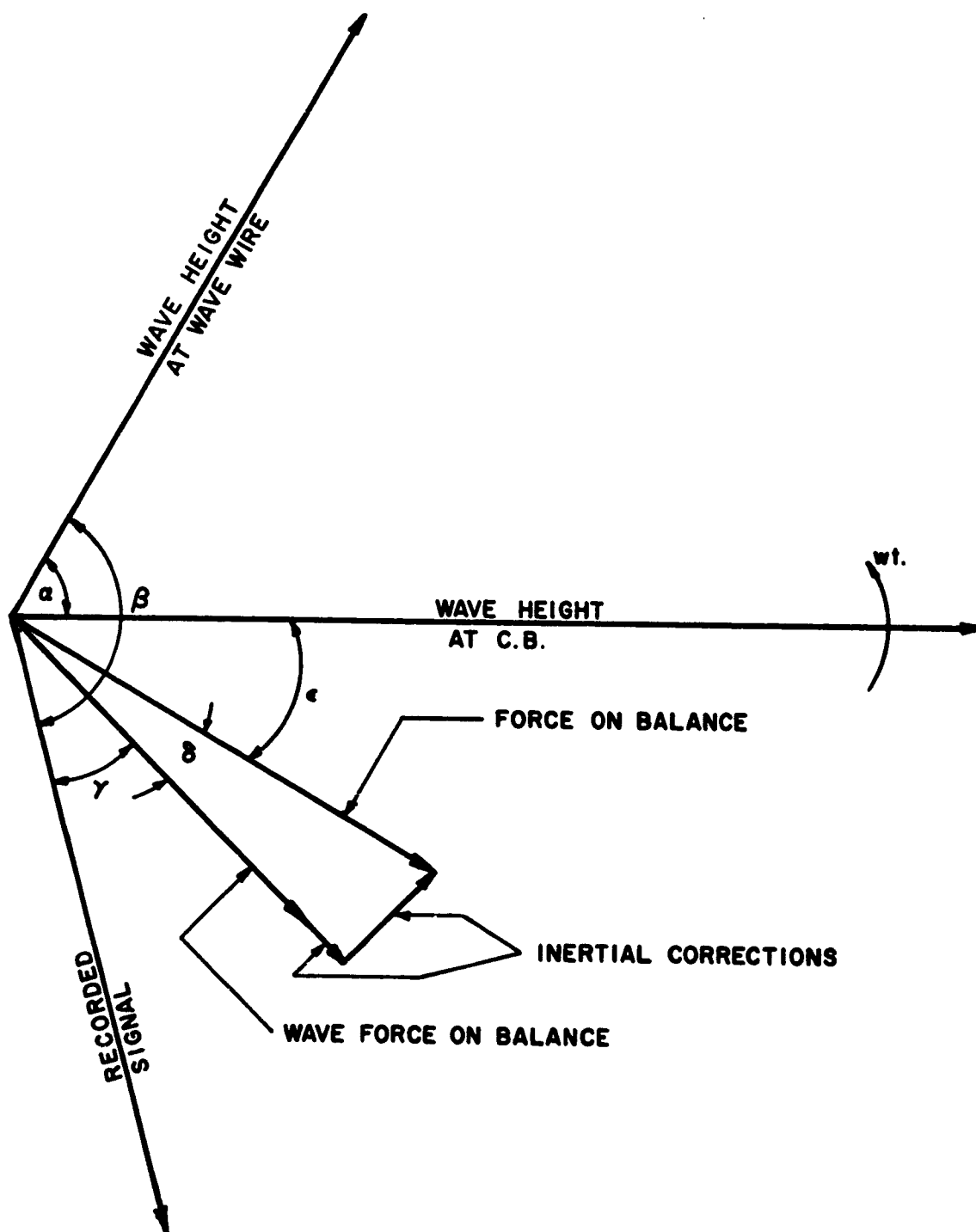


REPRODUCED FROM  
 10 X 10 TO THE INCH  
 10 X 10 TO THE INCH

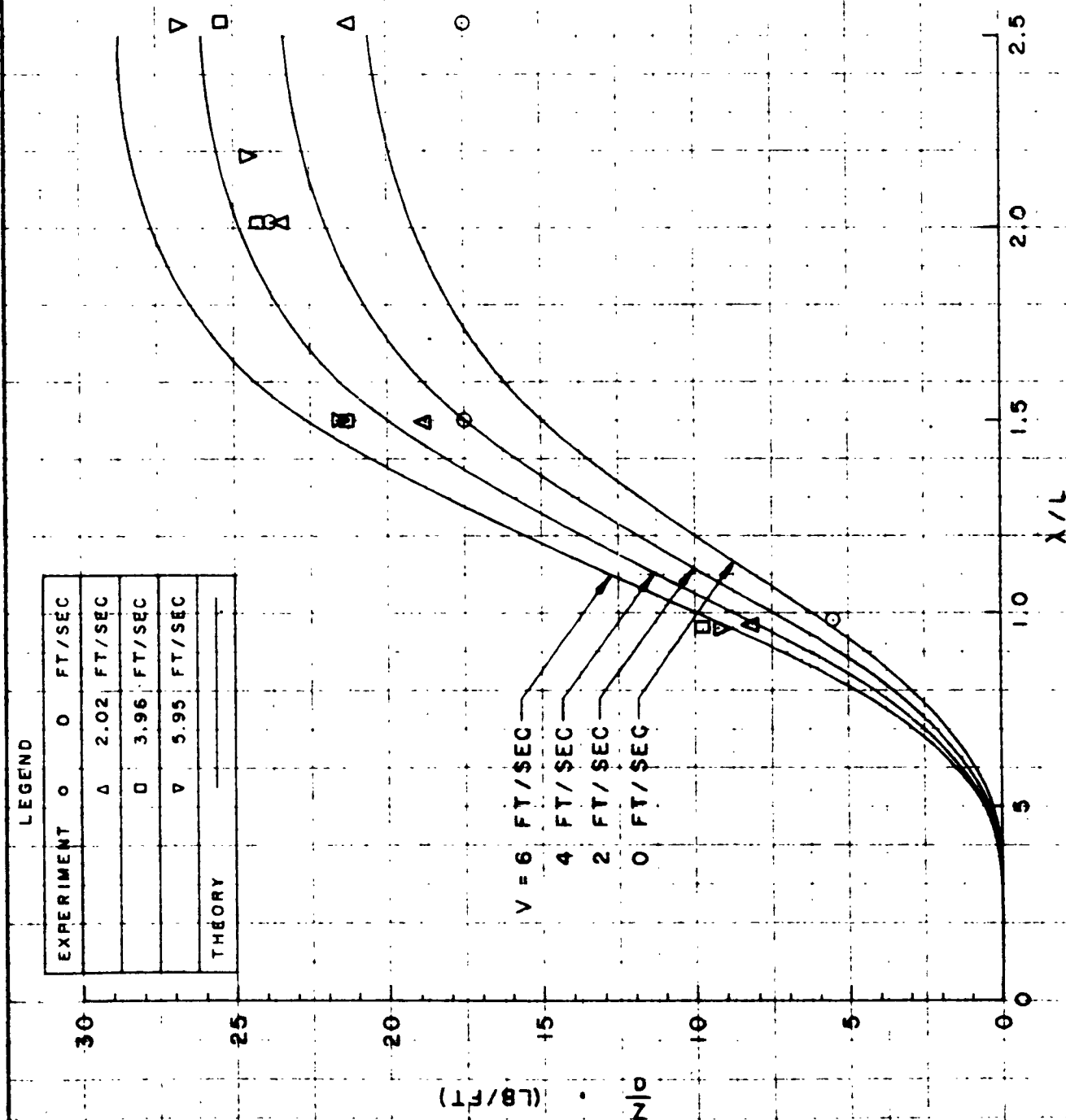
## OSCILLATING BEAM



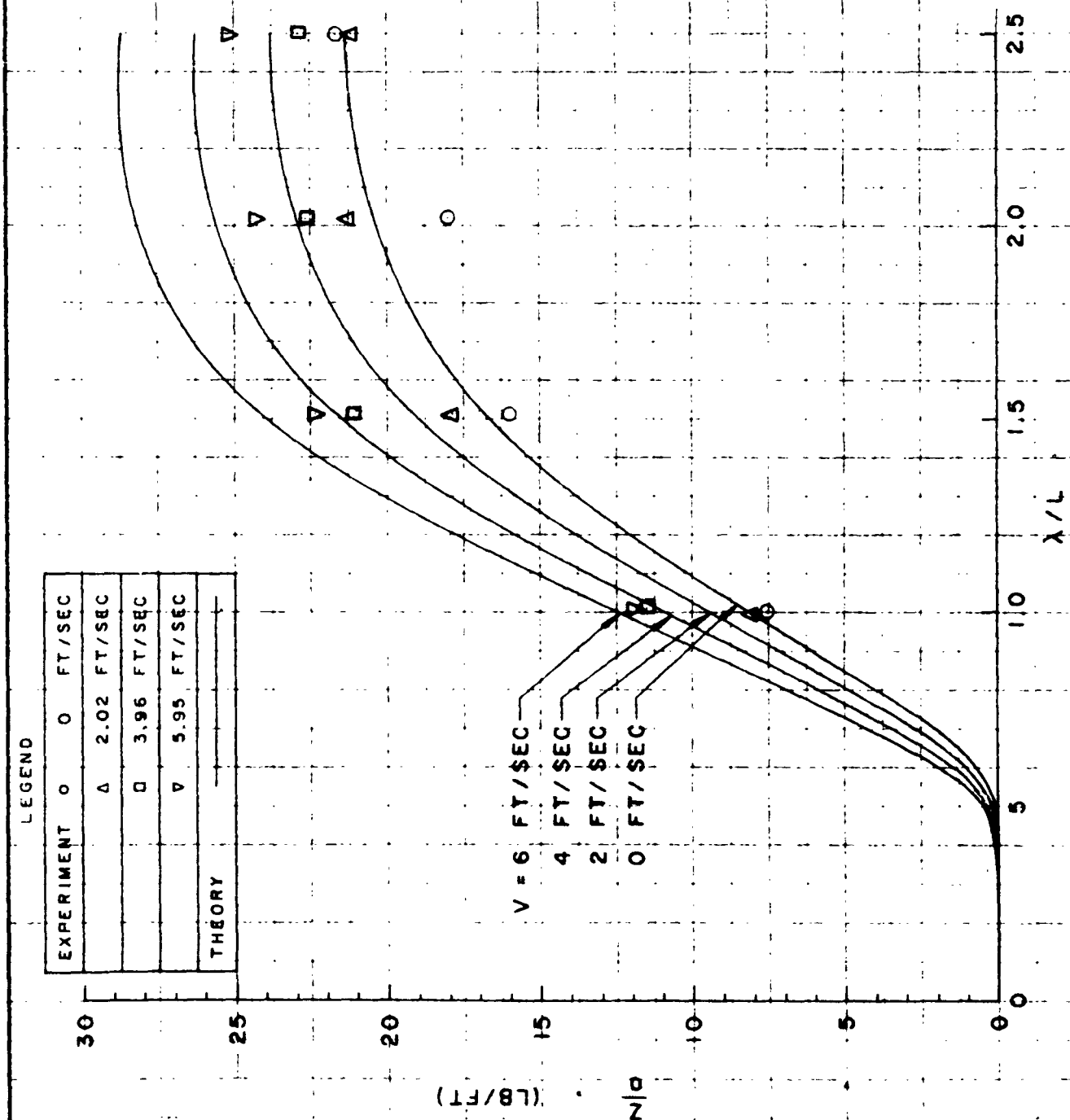
## PHASE DIAGRAM



# HEAVE FORCE PER UNIT WAVE AMPLITUDE vs WAVE LENGTH / BODY LENGTH AT 0° HEADING ANGLE

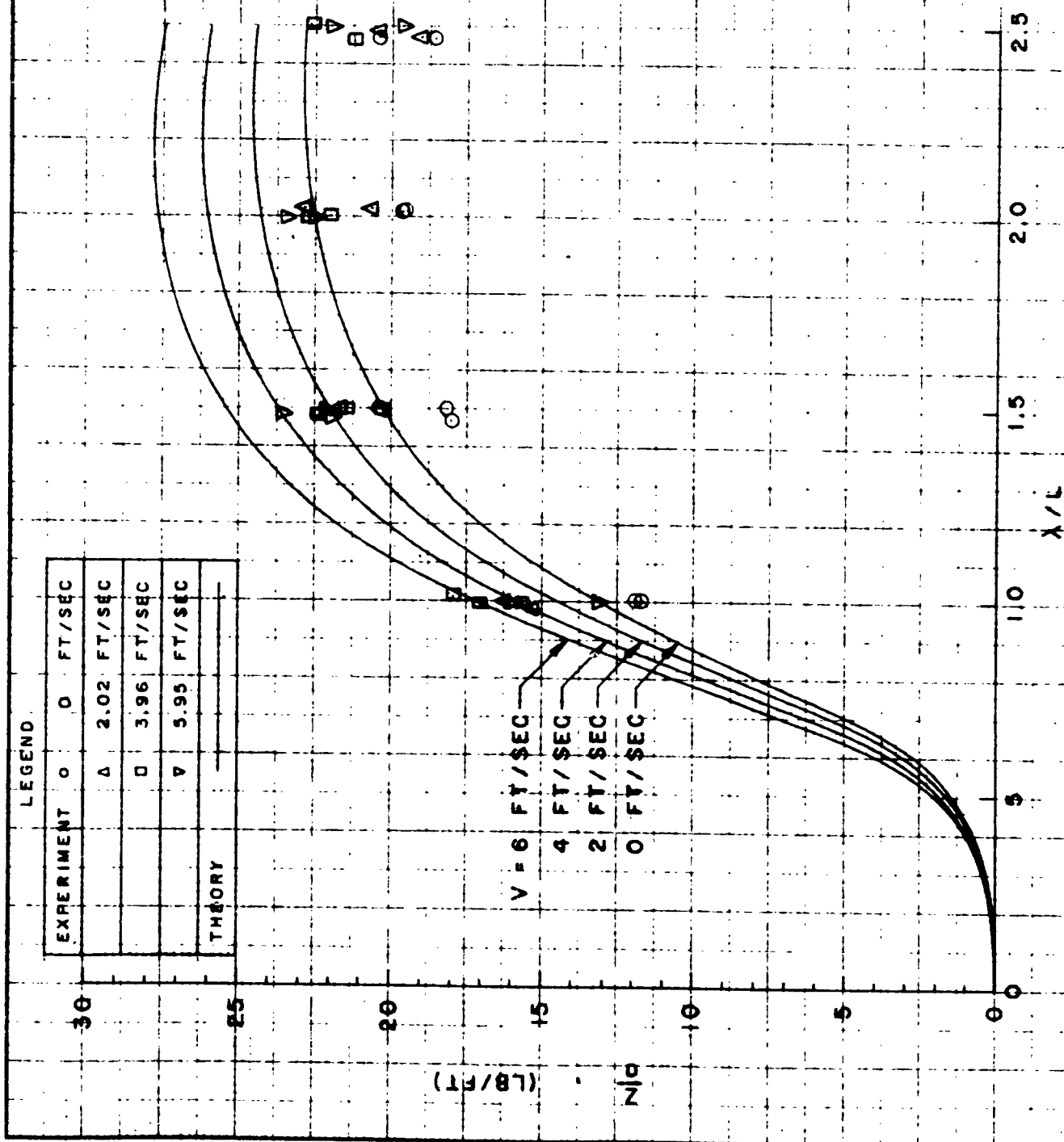


HEAVE FORCE PER UNIT WAVE AMPLITUDE  
VS  
WAVE LENGTH / BODY LENGTH  
AT 30° HEADING ANGLE

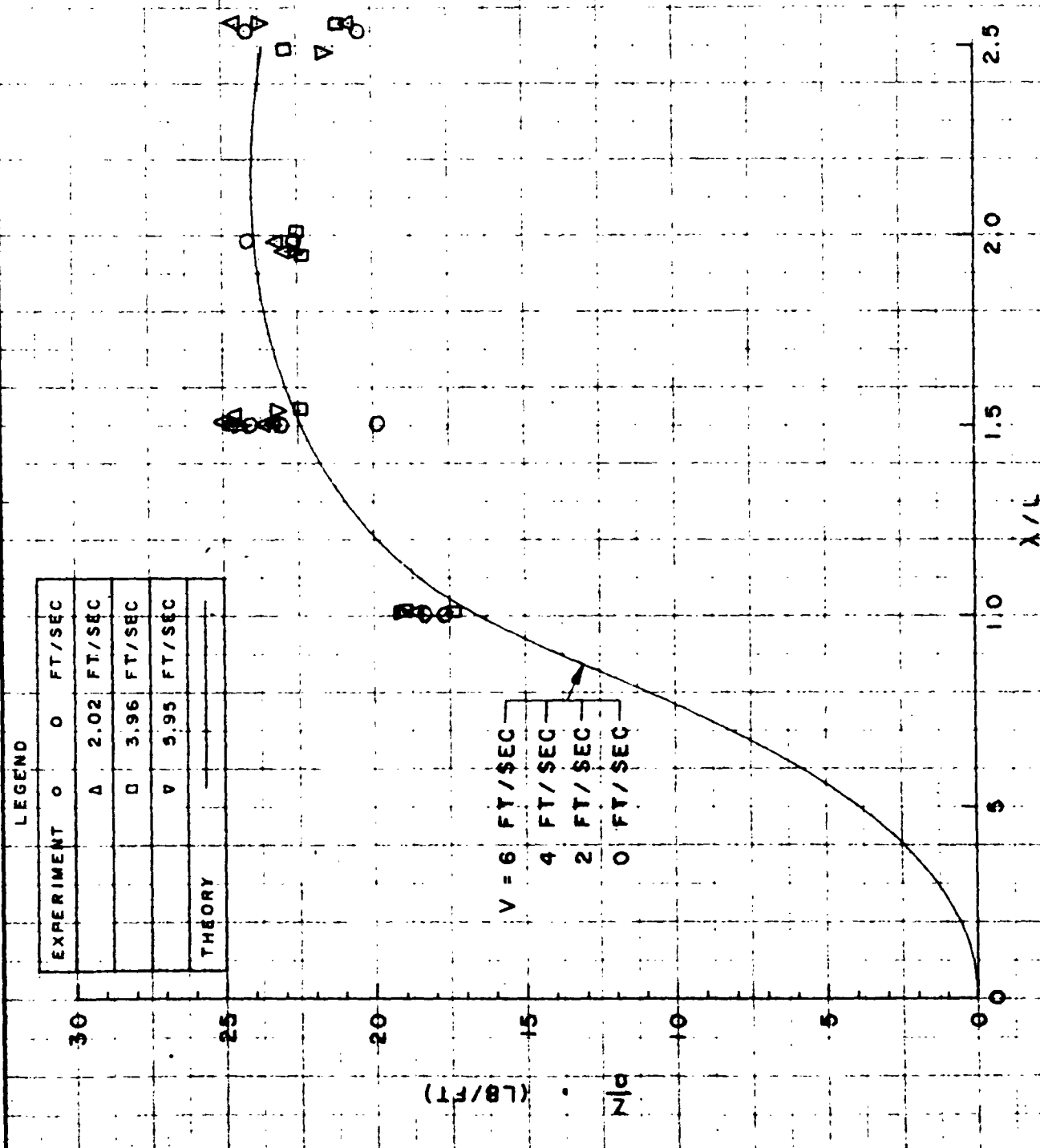




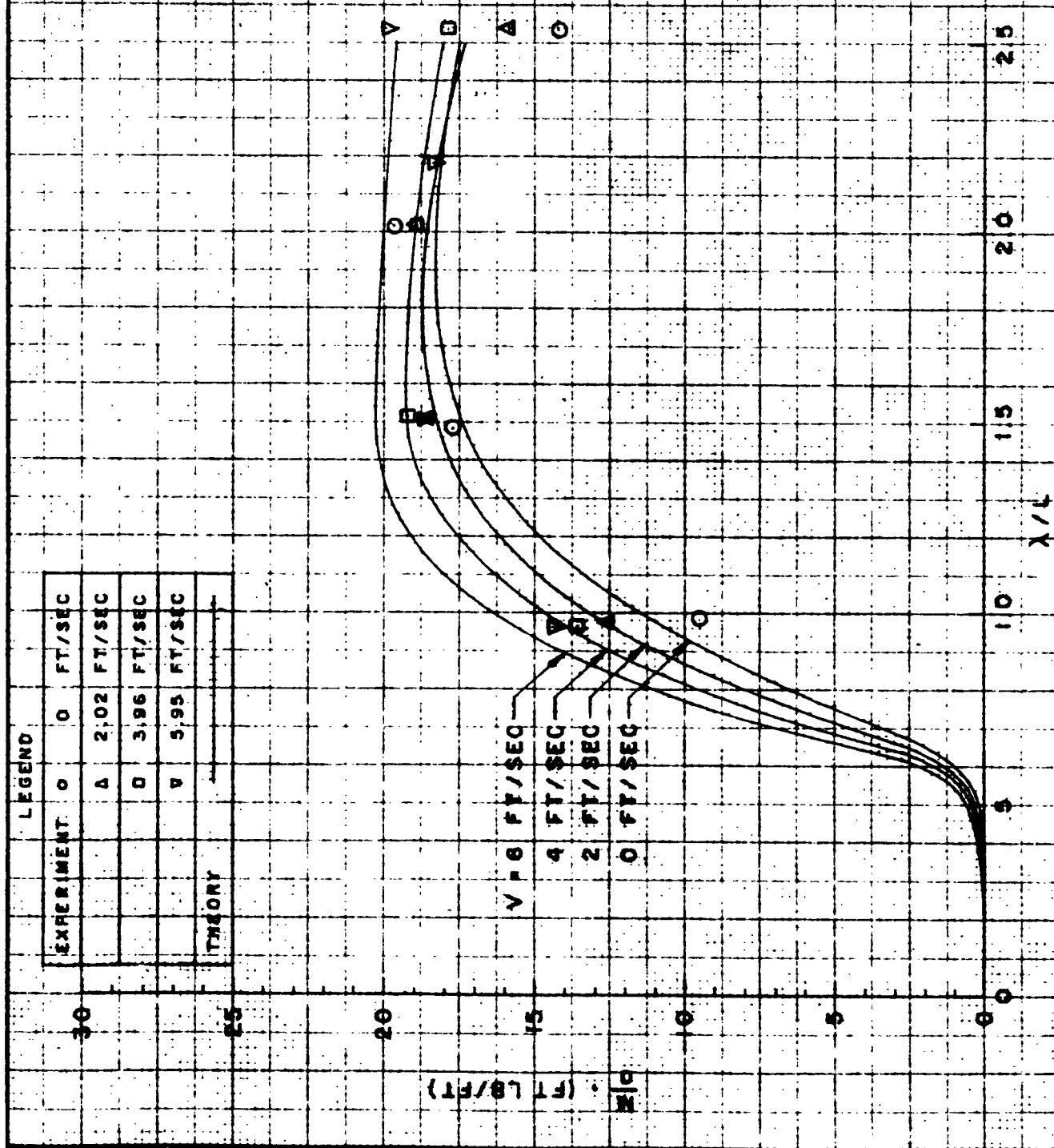
HEAVE FORCE PER UNIT WAVE AMPLITUDE  
 VS  
 WAVE LENGTH / BODY LENGTH  
 AT 60° HEADING ANGLE



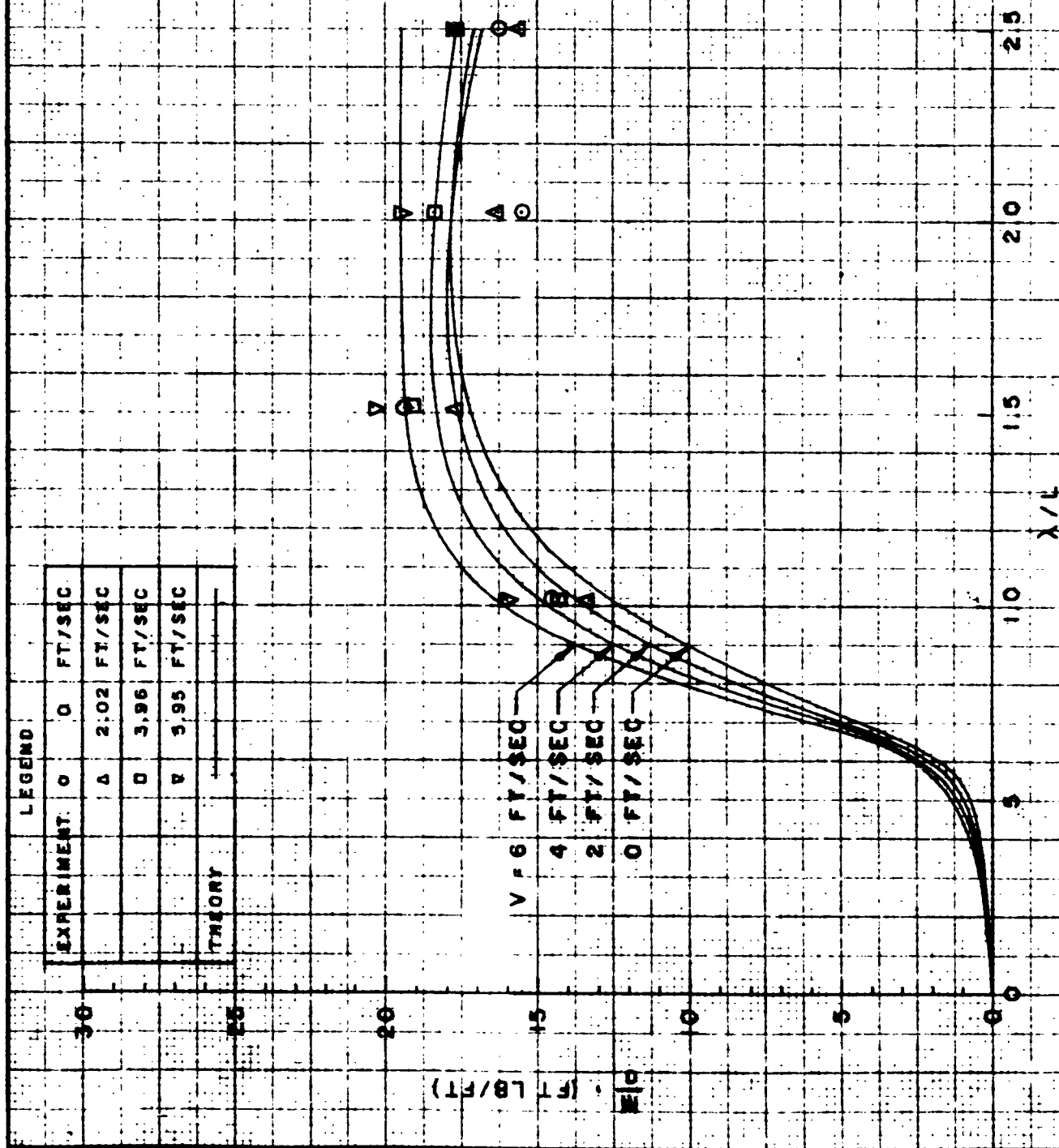
HEAVE FORCE PER UNIT WAVE AMPLITUDE  
 VS  
 WAVE LENGTH / BODY LENGTH  
 AT 90° HEADING ANGLE



PITCHING MOMENT PER UNIT WAVE AMPLITUDE  
VS  
WAVE LENGTH / BODY LENGTH  
AT 0° HEADING ANGLE

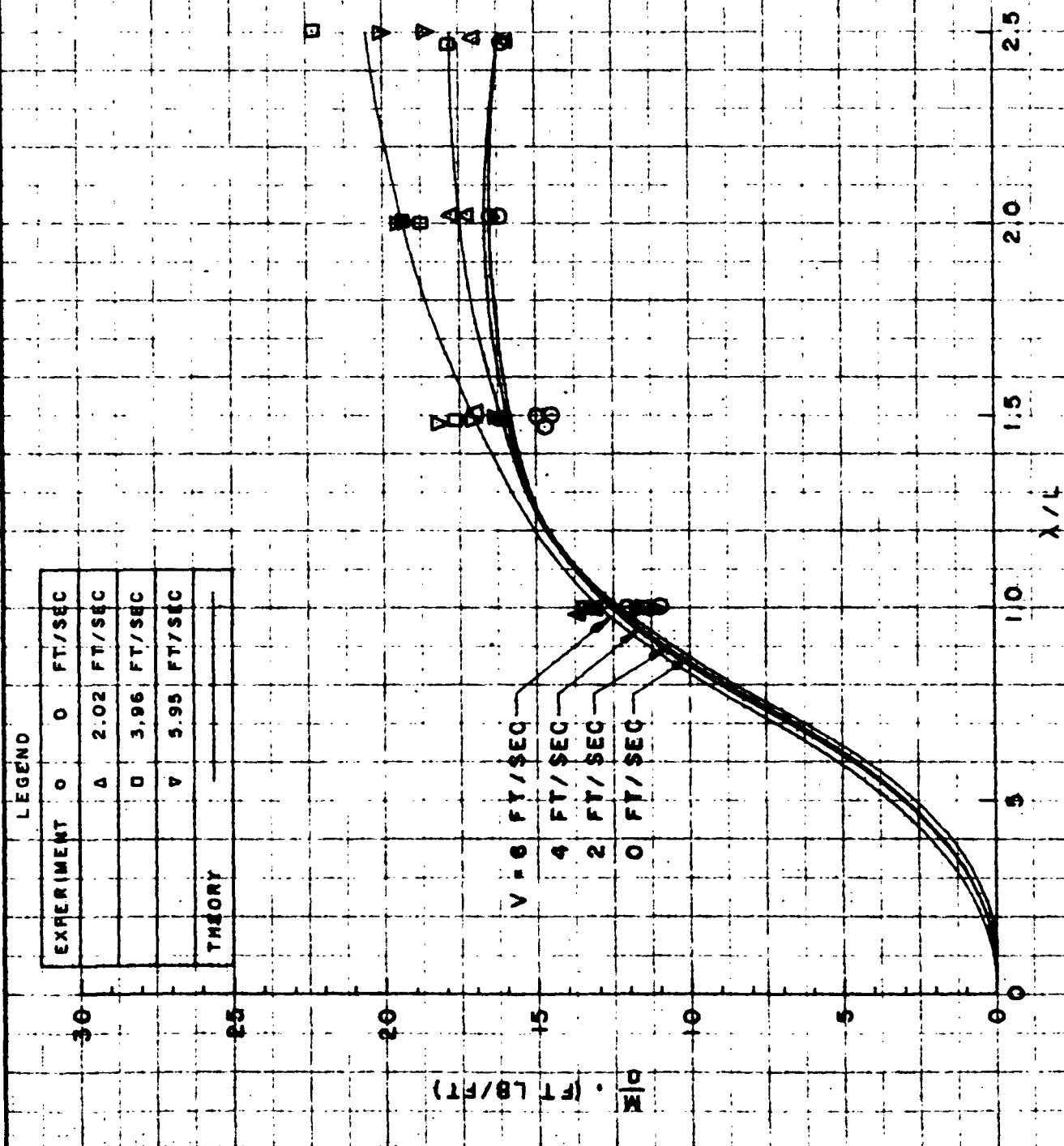


ALBANY, N. Y.  
MAY 11, 1901.  
TO THE  
NICHOLSON  
KENT & EASTON CO.  
—



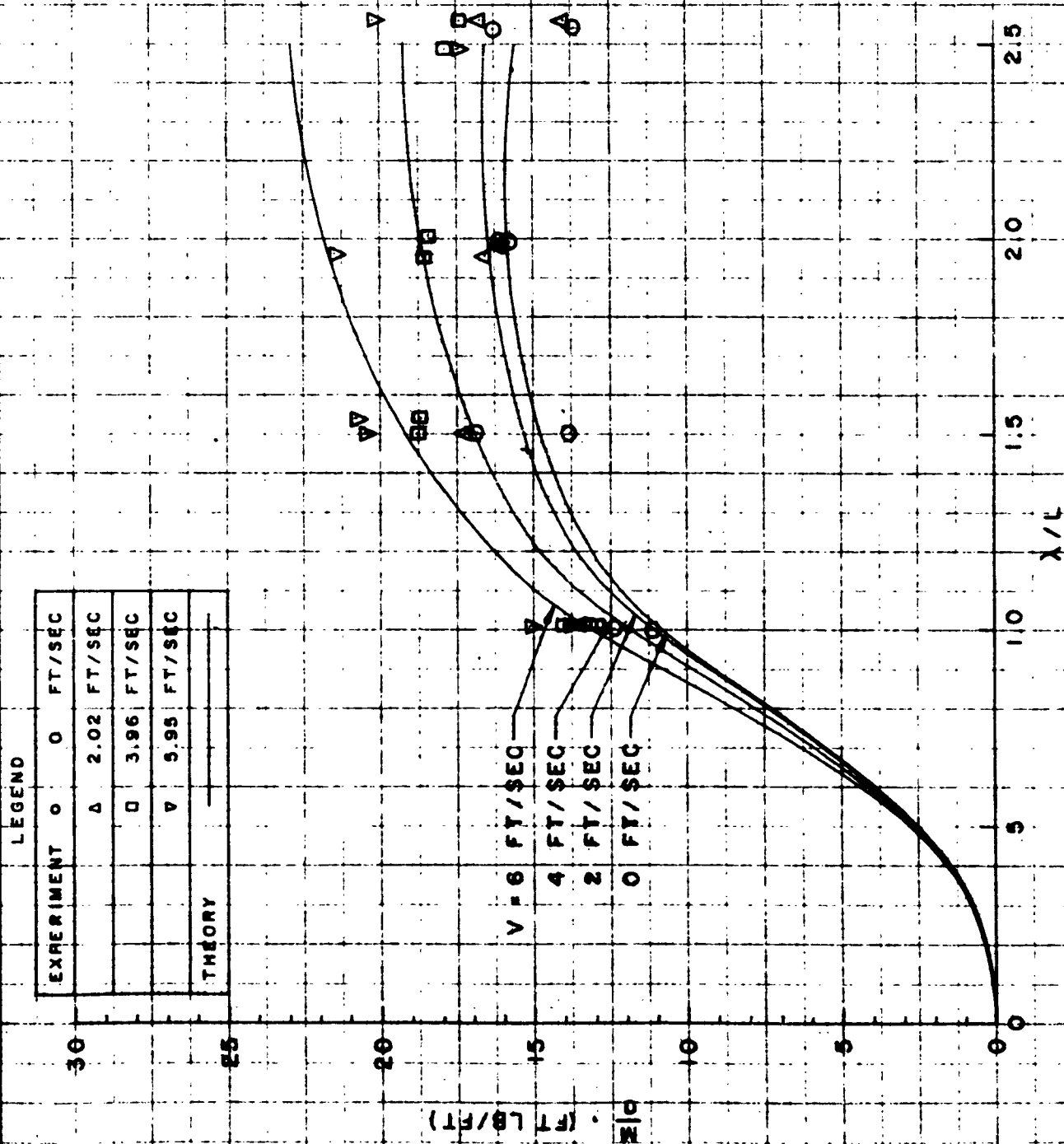
## PITCHING MOMENT PER UNIT WAVE AMPLITUDE

vs  
WAVE LENGTH / BODY LENGTH  
AT 60° HEADING ANGLE



## PITCHING MOMENT PER UNIT WAVE AMPLITUDE

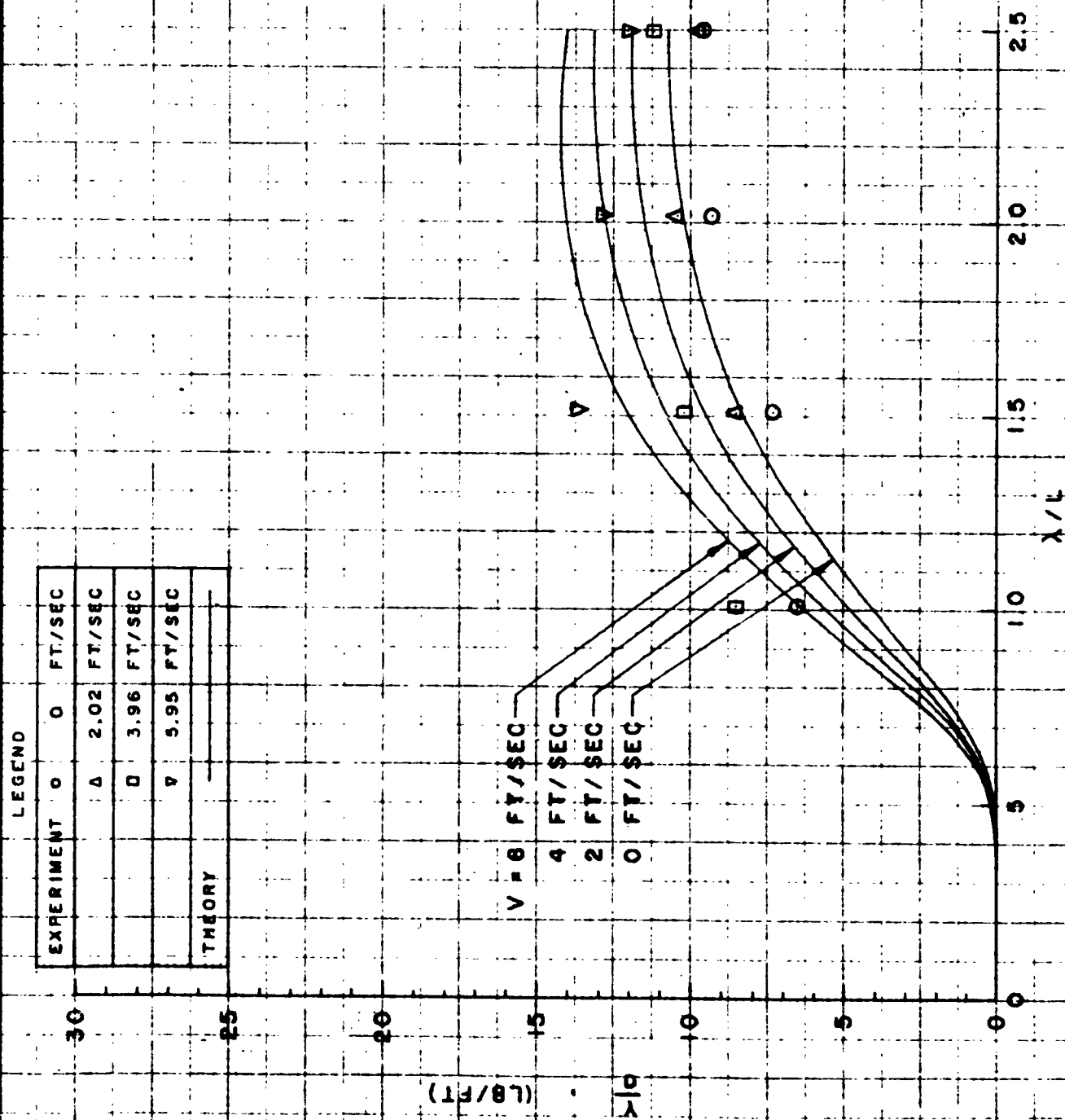
vs  
WAVE LENGTH / BODY LENGTH  
AT 90° HEADING ANGLE



## SIDE FORCE PER UNIT WAVE AMPLITUDE

vs

WAVE LENGTH / BODY LENGTH

AT 30° HEADING ANGLE  
(WITHOUT CONNING TOWER)

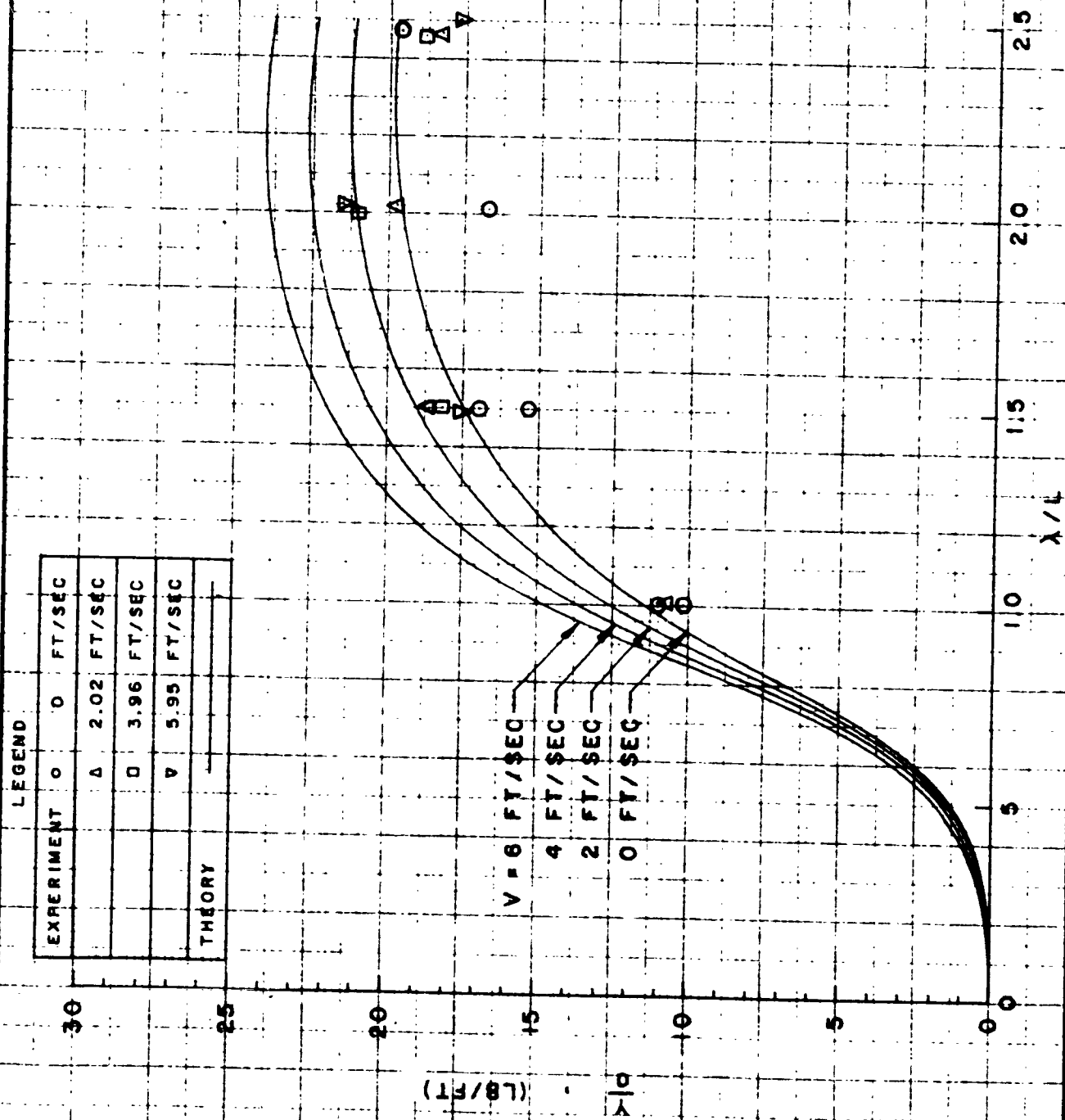
Tech- HONOLULU, HAWAII  
 2 JAN 1964

R-809

FIG. 15

# SIDE FORCE PER UNIT WAVE AMPLITUDE

vs  
 WAVE LENGTH / BODY LENGTH  
 AT 60° HEADING ANGLE  
 (WITHOUT CONNING TOWER)





SIDE FORCE PER UNIT WAVE AMPLITUDE

VS

WAVE LENGTH / BODY LENGTH

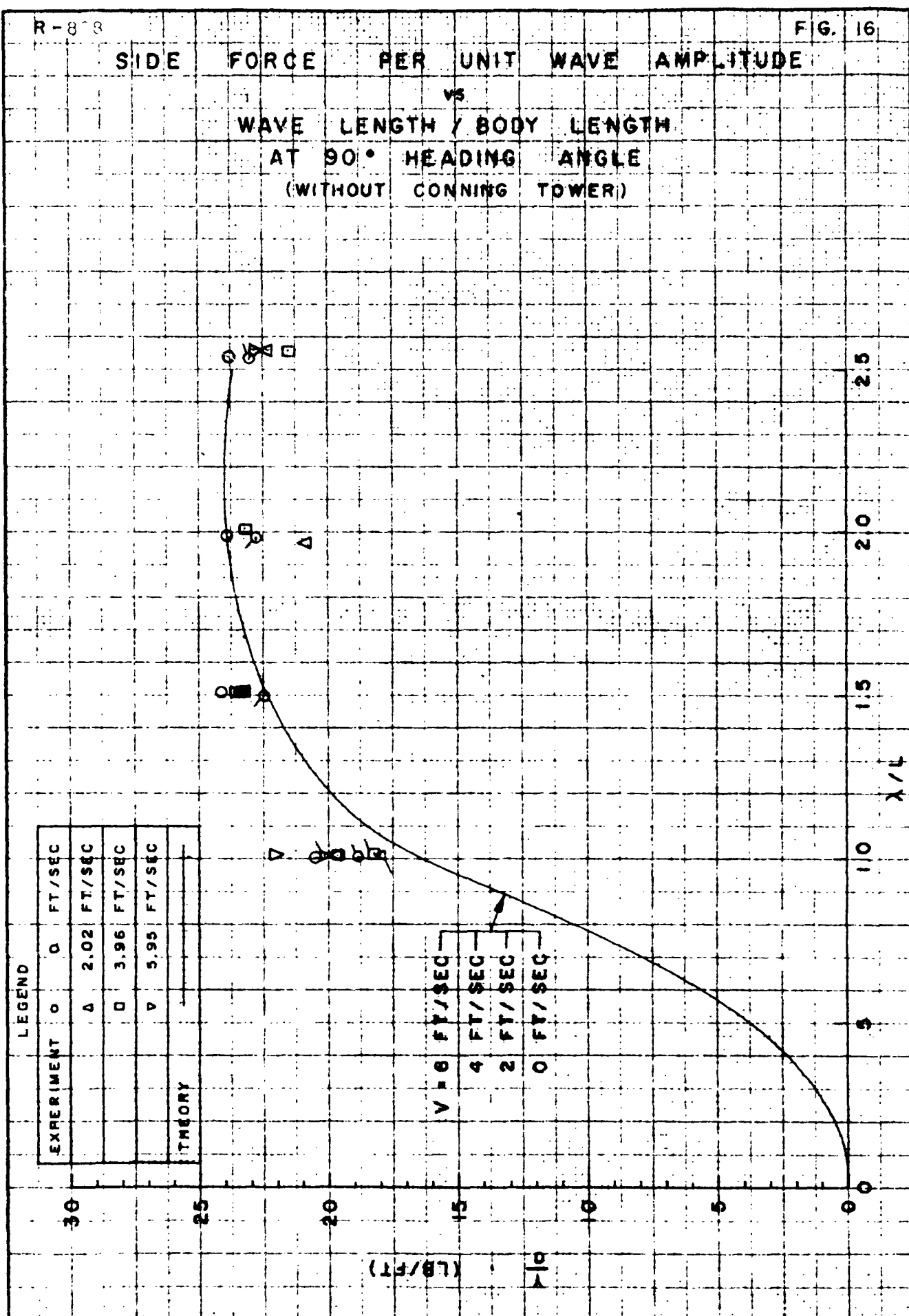
AT 90° HEADING ANGLE

(WITHOUT CONNING TOWER)

LEGEND

EXPERIMENT	0	0	FT/SEC
	Δ	2.02	FT/SEC
	□	3.96	FT/SEC
	▽	5.95	FT/SEC
THEORY			

V = 0 FT/SEC  
 4 FT/SEC  
 2 FT/SEC  
 0 FT/SEC



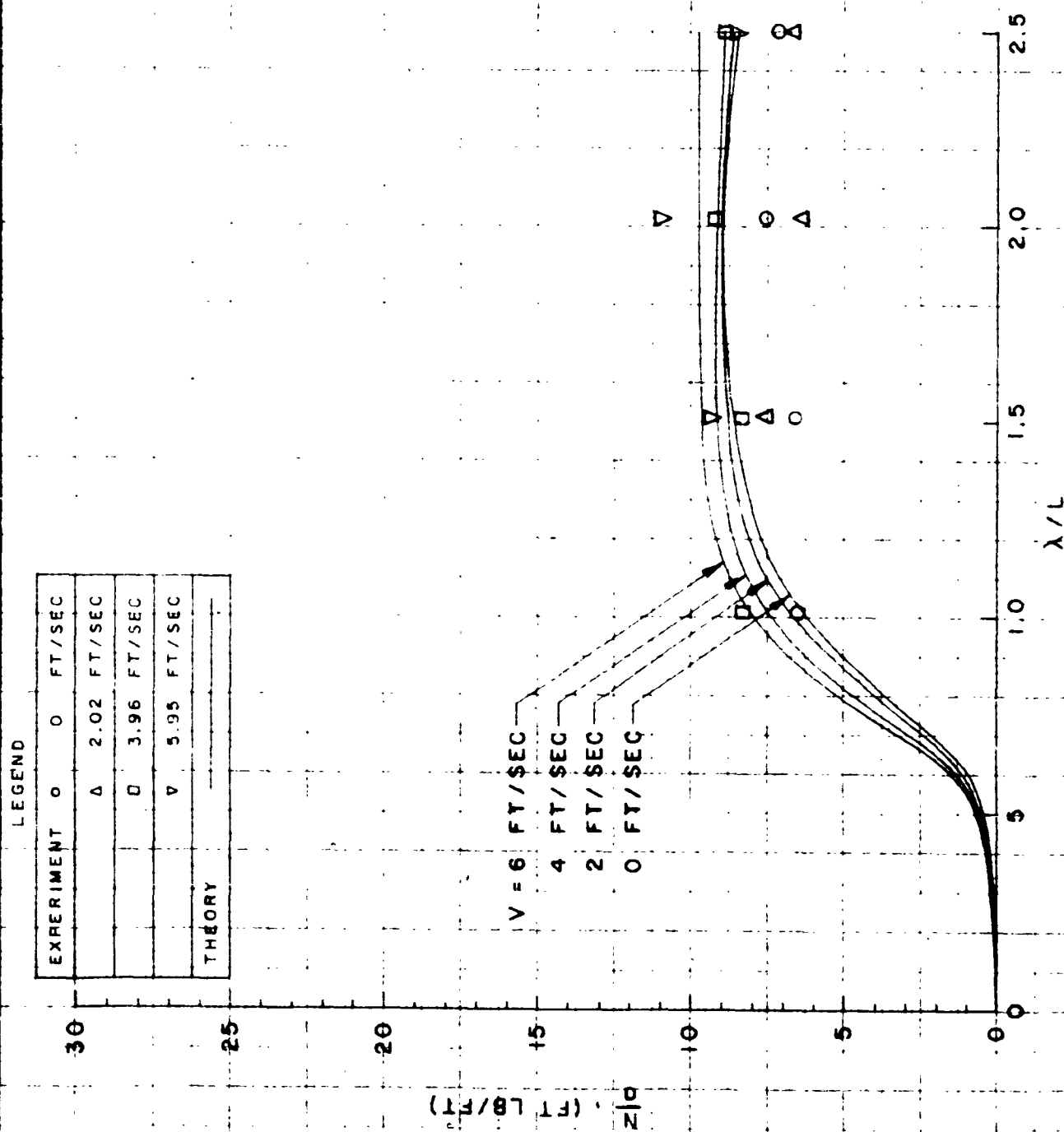
## YAWING MOMENT PER UNIT WAVE AMPLITUDE

vs

WAVE LENGTH / BODY LENGTH

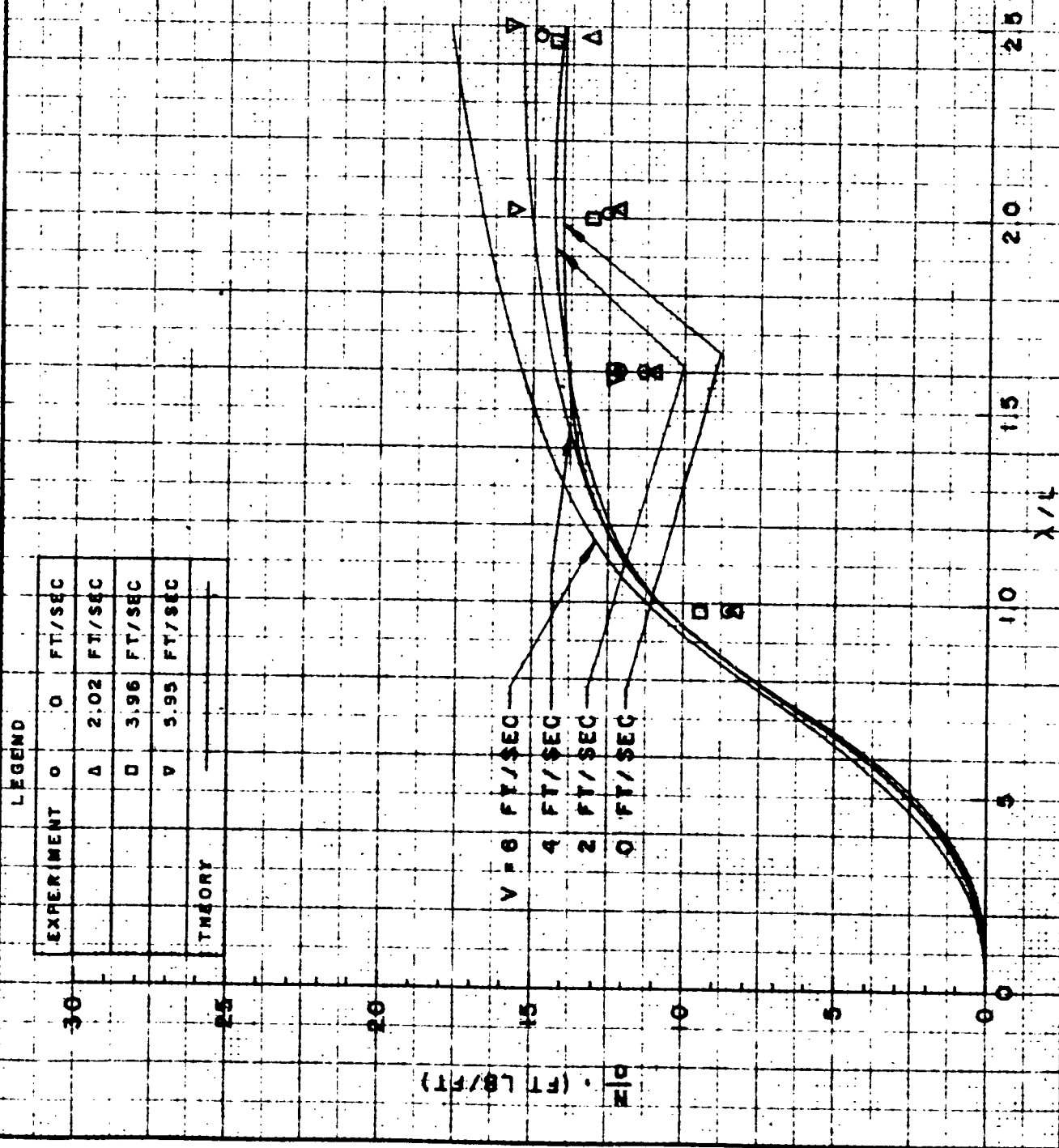
AT 30° HEADING ANGLE

(WITHOUT CONNING TOWER)



# YAWING MOMENT PER UNIT WAVE AMPLITUDE

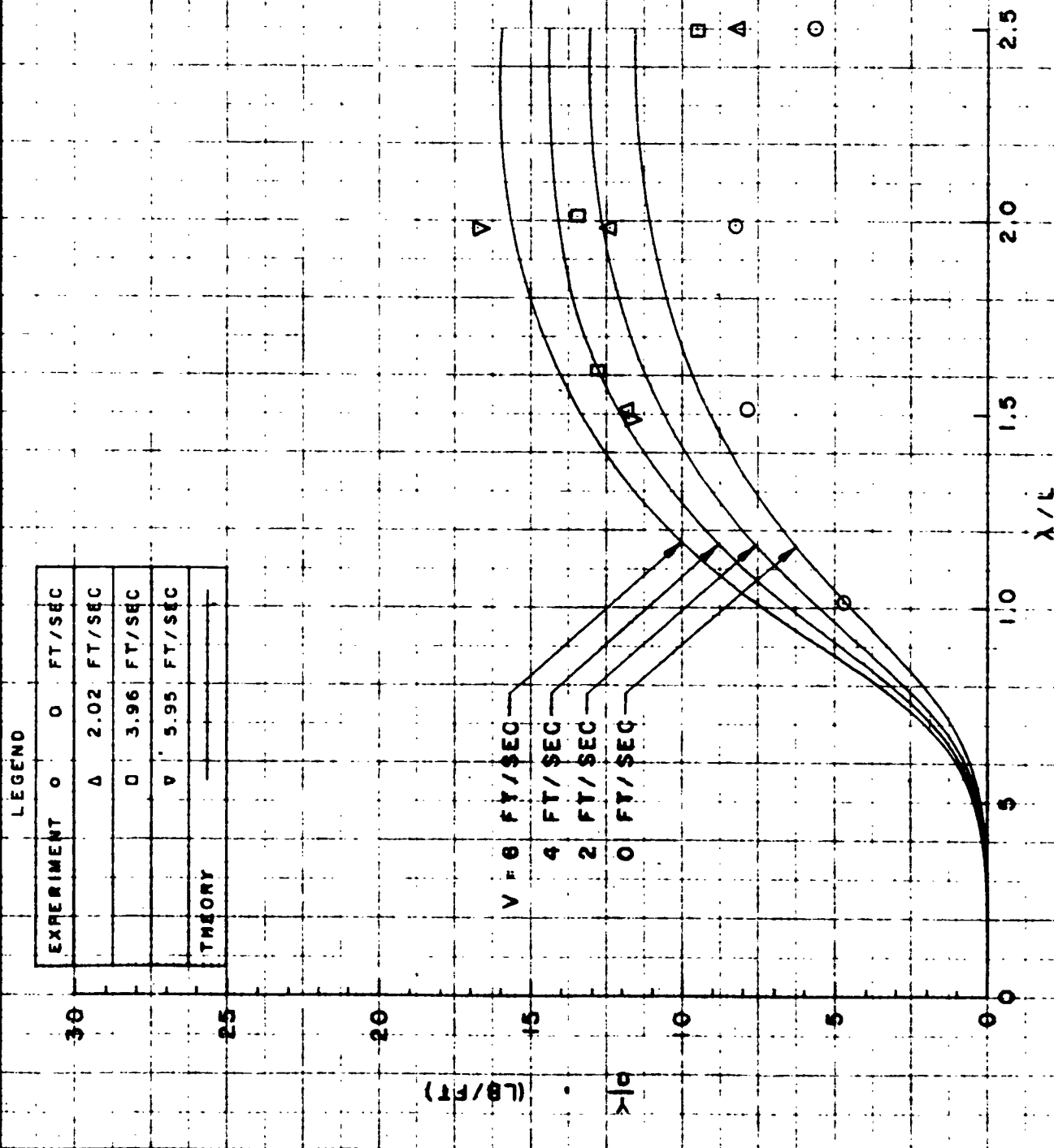
VS  
WAVE LENGTH / BODY LENGTH  
AT 60° HEADING ANGLE  
(WITHOUT CONNING TOWER)





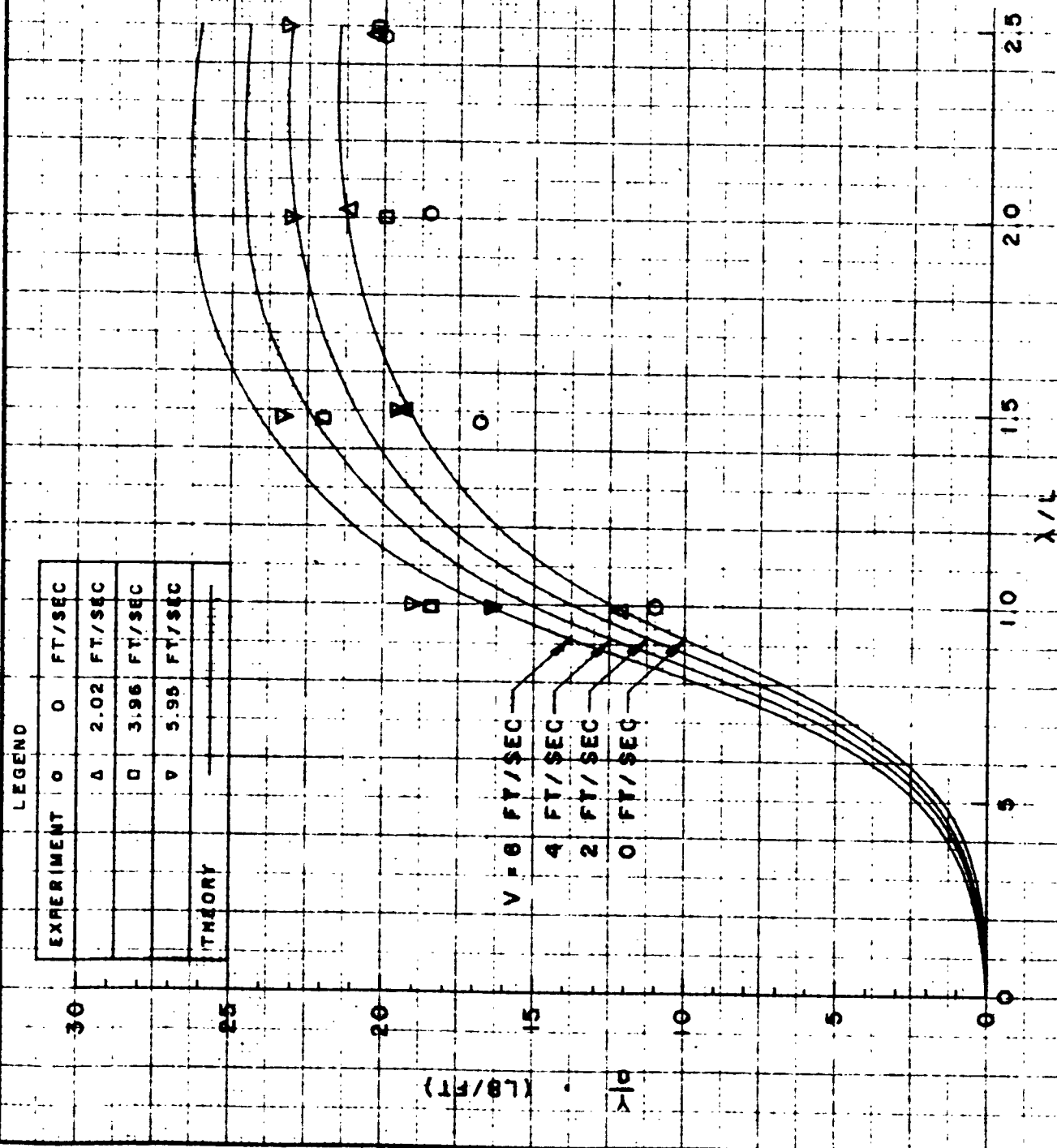
## SIDE FORCE PER UNIT WAVE AMPLITUDE

VS  
WAVE LENGTH / BODY LENGTH  
AT 30° HEADING ANGLE  
(WITH CONNING TOWER)



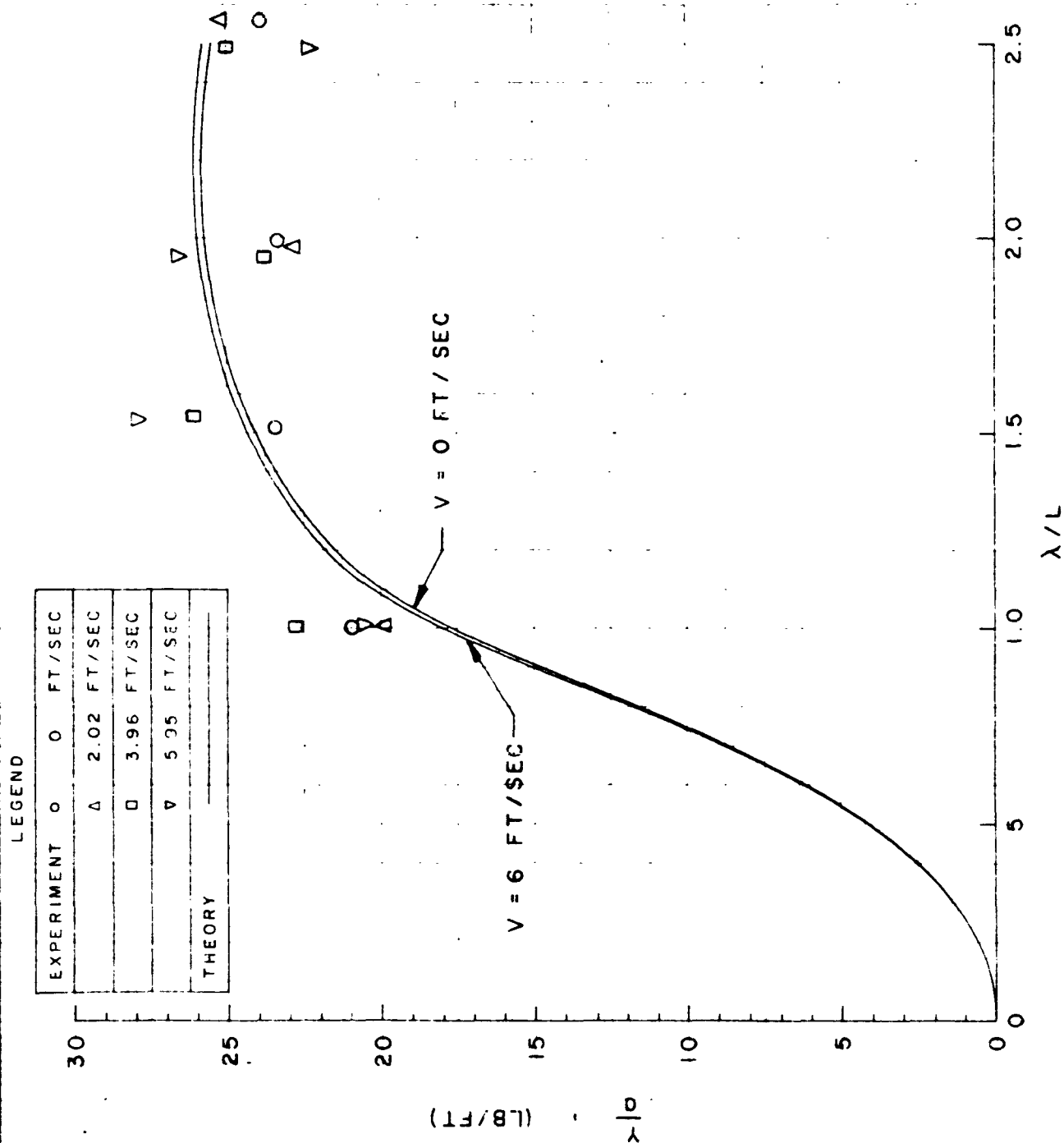
## SIDE FORCE PER UNIT WAVE AMPLITUDE

vs  
WAVE LENGTH / BODY LENGTH  
AT 60° HEADING ANGLE  
(WITH CONNING TOWER)



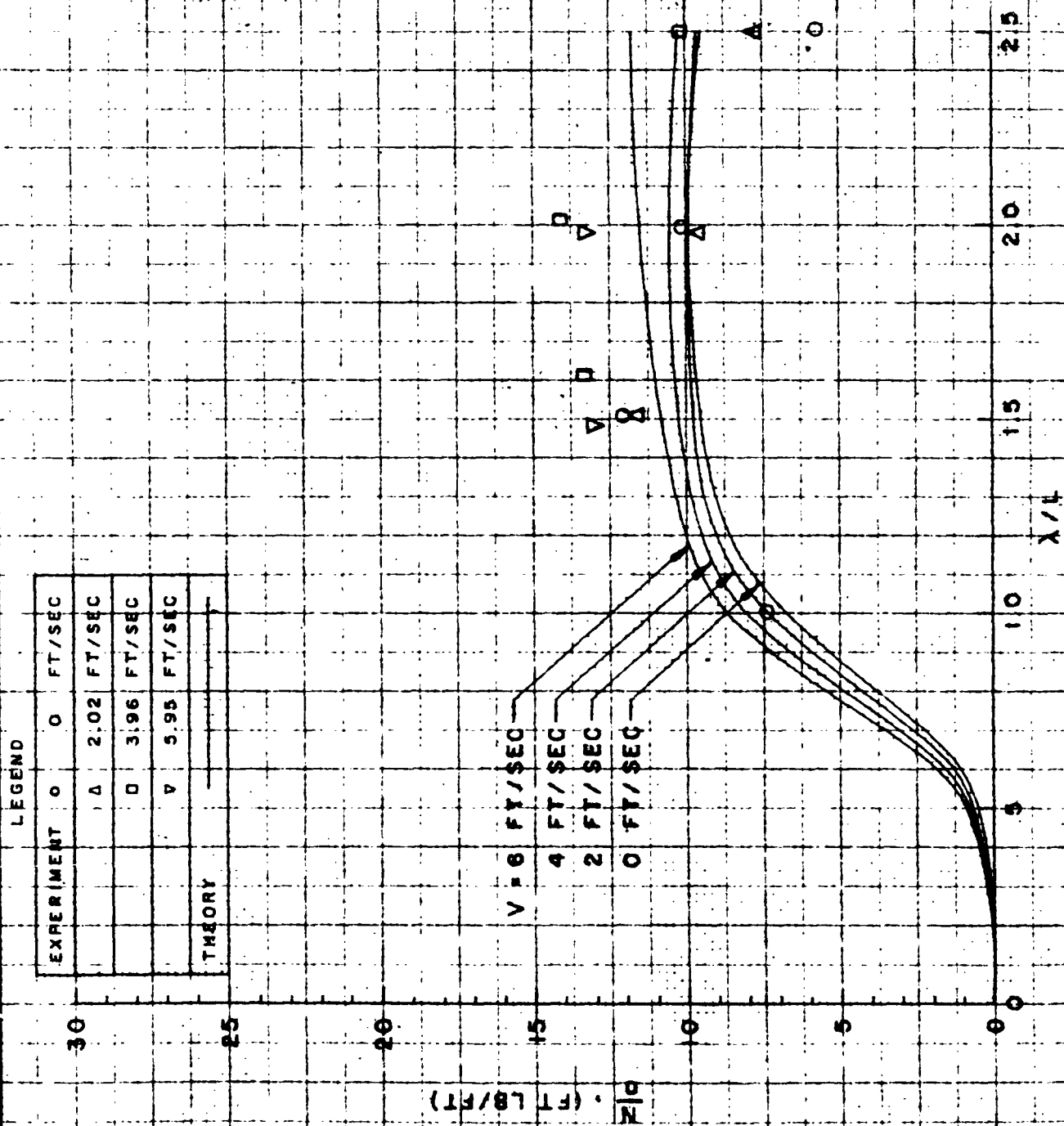
TEC  
HCO  
HTO  
10  
300  
REMARKS  
CONNING TOWER

SIDE FORCE PER UNIT WAVE AMPLITUDE  
 vs  
 WAVE LENGTH / BODY LENGTH  
 AT 90° HEADING ANGLE  
 (WITH CONNING TOWER)



[illegible]

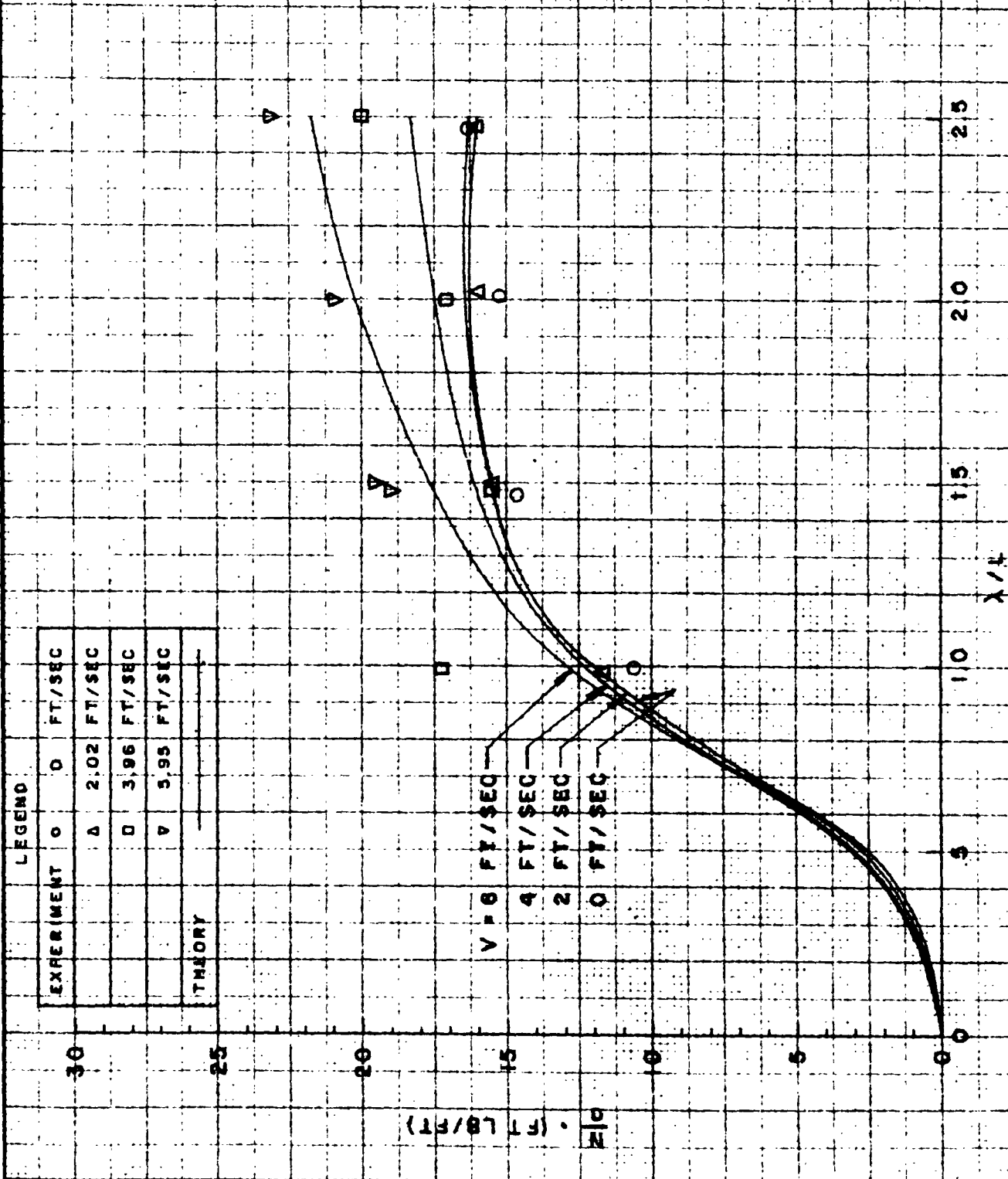
WAVE LENGTH / BODY LENGTH  
AT 30 ° HEADING ANGLE  
(WITH CONNING TOWER)





## YAWING MOMENT PER UNIT WAVE AMPLITUDE

VS  
WAVE LENGTH / BODY LENGTH  
AT 60° HEADING ANGLE  
(WITH CONNING TOWER)



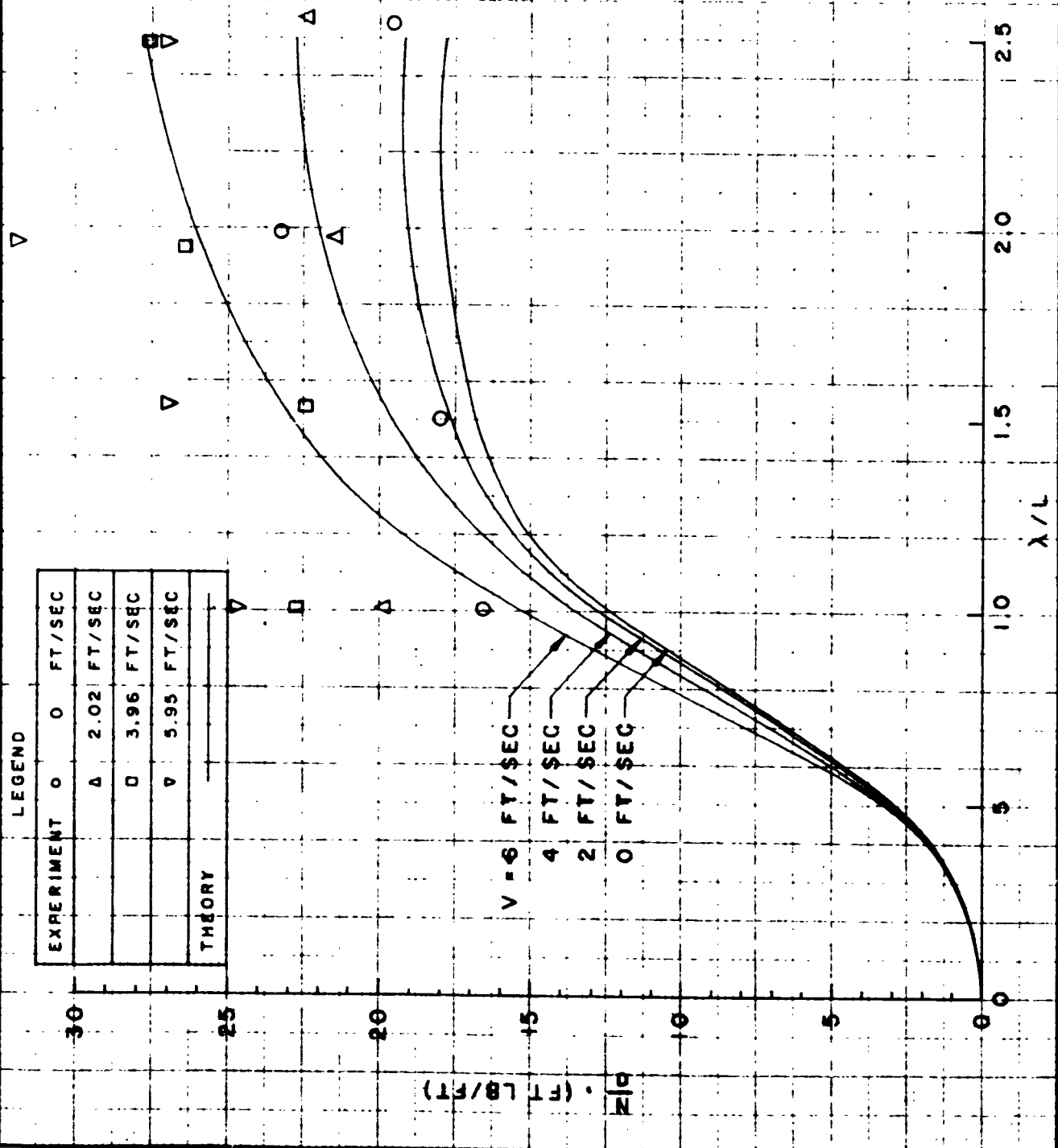
## YAWING MOMENT PER UNIT WAVE AMPLITUDE

VS

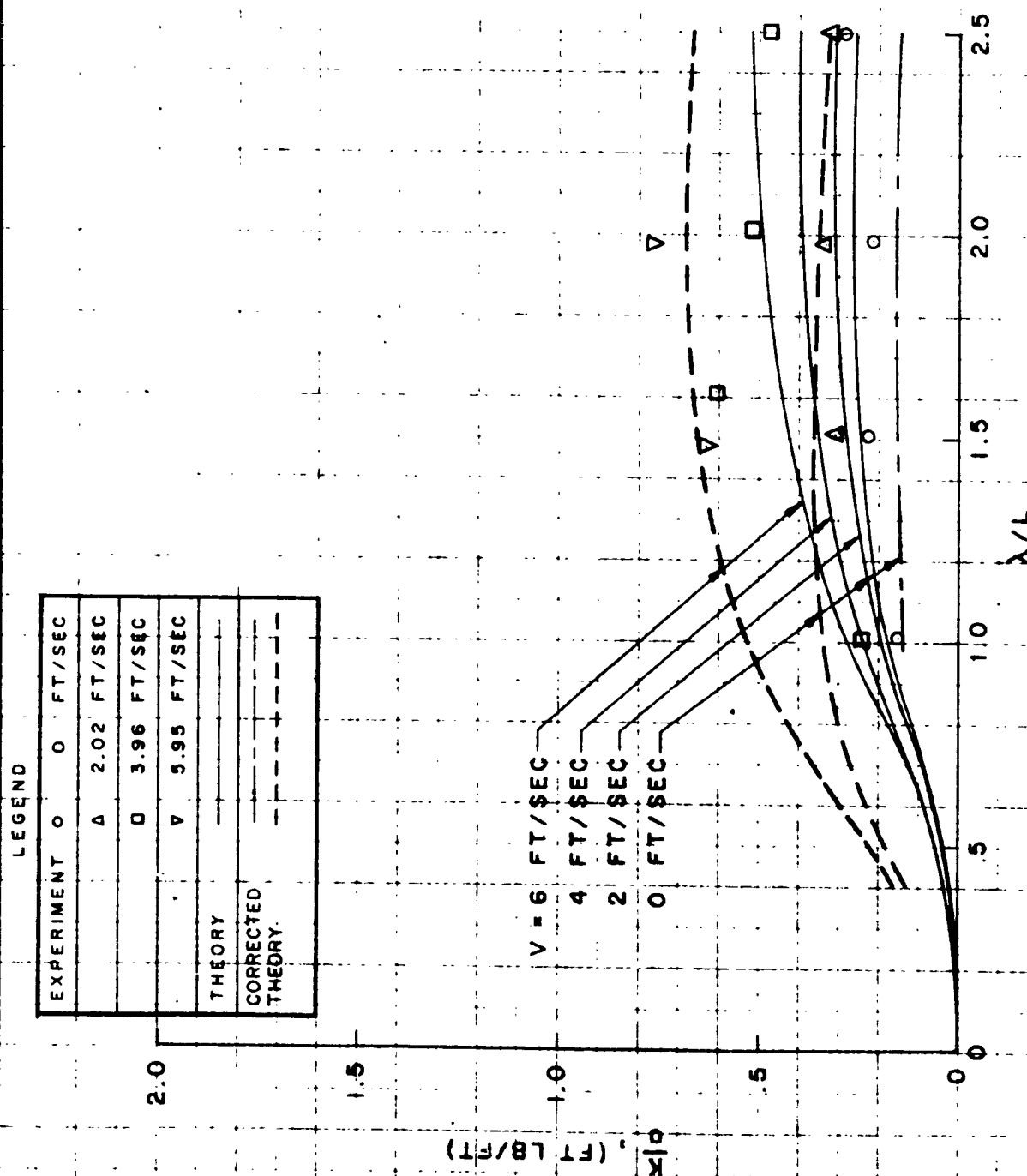
WAVE LENGTH / BODY LENGTH

AT 90° HEADING ANGLE

(WITH CONNING TOWER)



ROLL MOMENT PER UNIT WAVE AMPLITUDE  
vs  
WAVE LENGTH / BODY LENGTH  
AT 30° HEADING ANGLE  
(WITH CONNING TOWER)



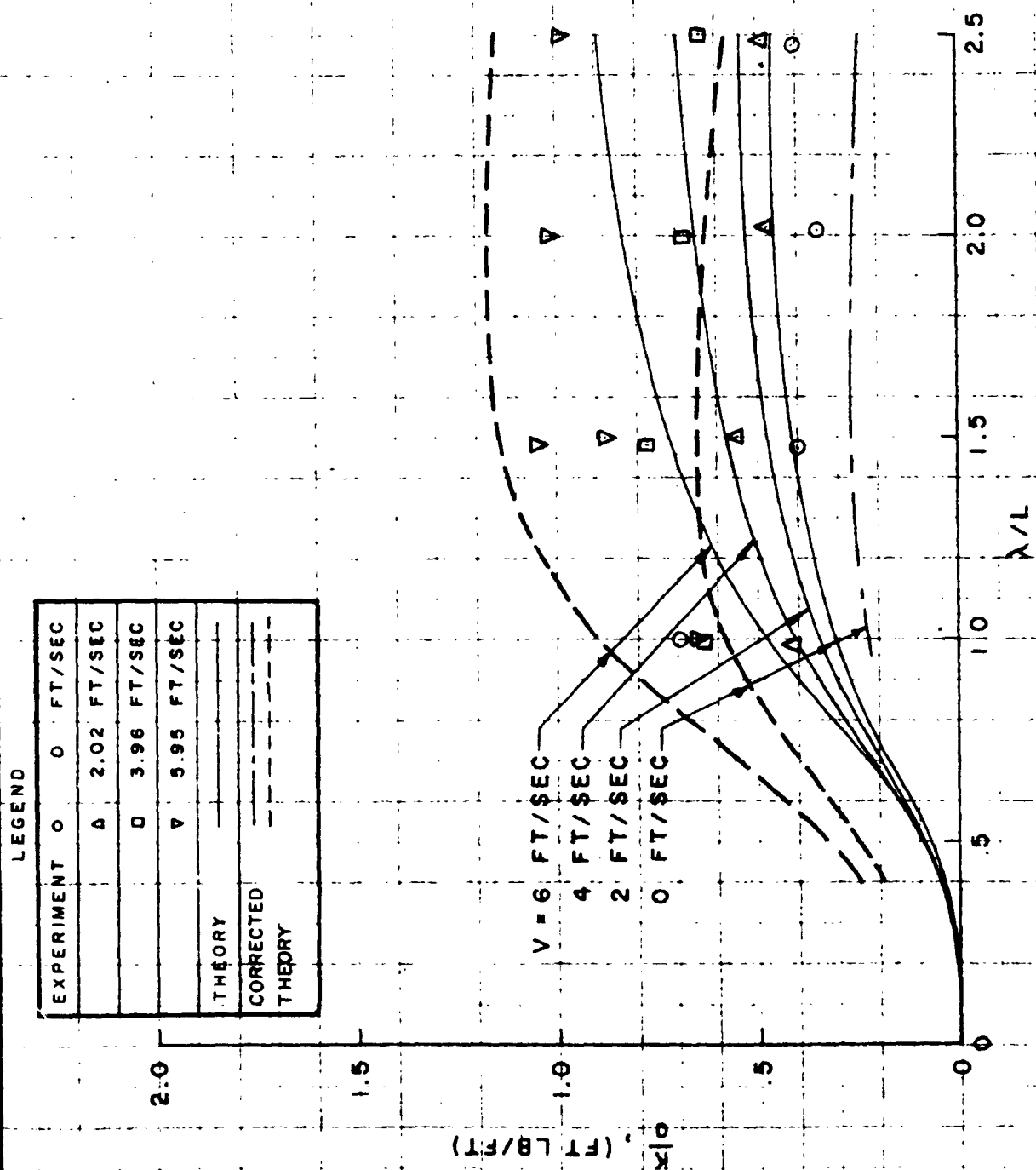
## ROLL MOMENT PER UNIT WAVE AMPLITUDE

VS

WAVE LENGTH / BODY LENGTH

AT 60° HEADING ANGLE

(WITH CONNING TOWER)



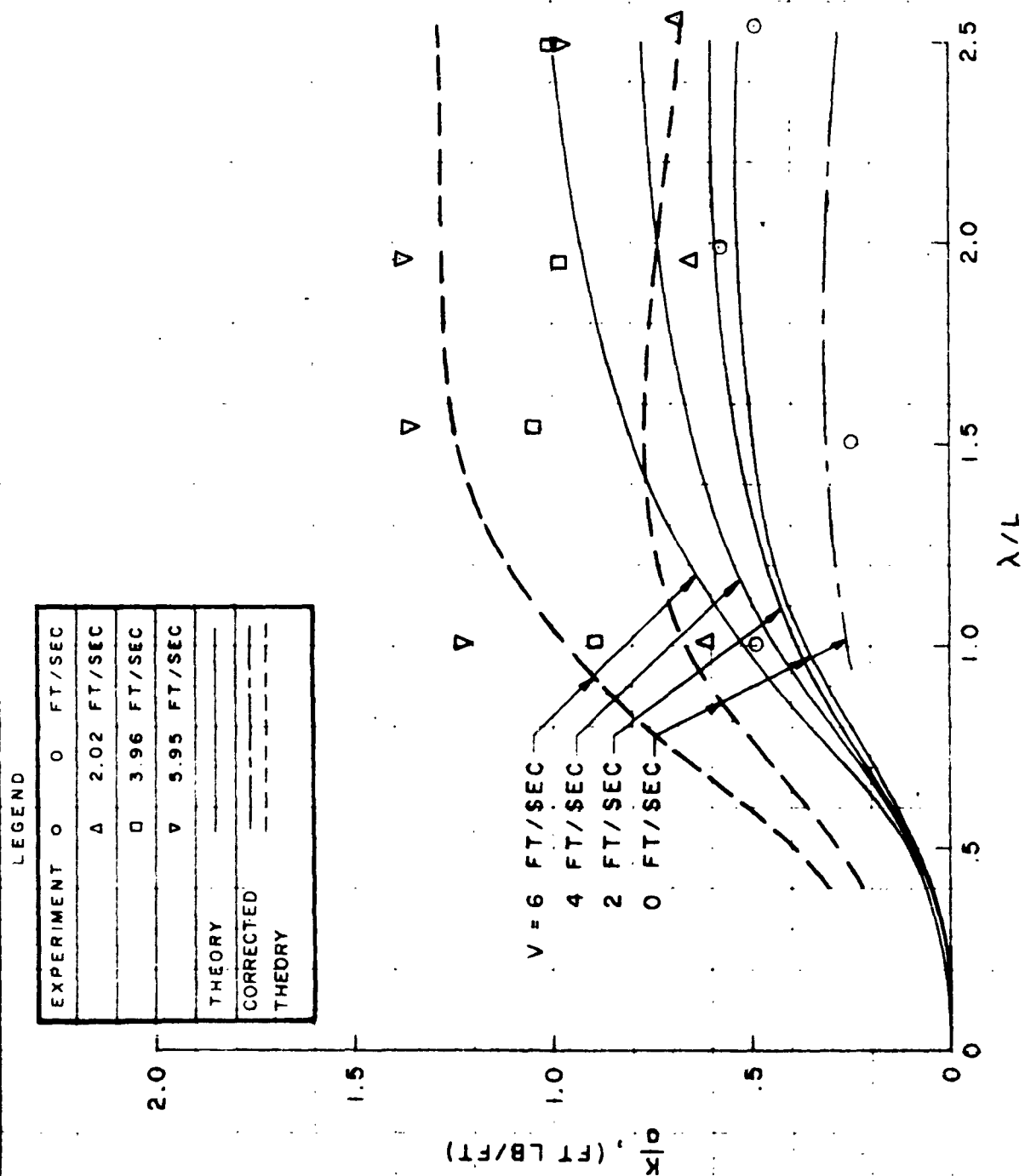
## ROLL MOMENT PER UNIT WAVE AMPLITUDE

vs

WAVE LENGTH / BODY LENGTH

AT 90° HEADING ANGLE

(WITH CONNING TOWER)



## PHASE LAG OF HEAVE FORCE

vs

FIG 29

WAVE LENGTH / BODY LENGTH

AT 0° HEADING ANGLE

LEGEND

EXPERIMENT	○	Q, FT/SEC
	△	2.02 FT/SEC
	□	3.96 FT/SEC
	▽	5.95 FT/SEC
THEORY	—	

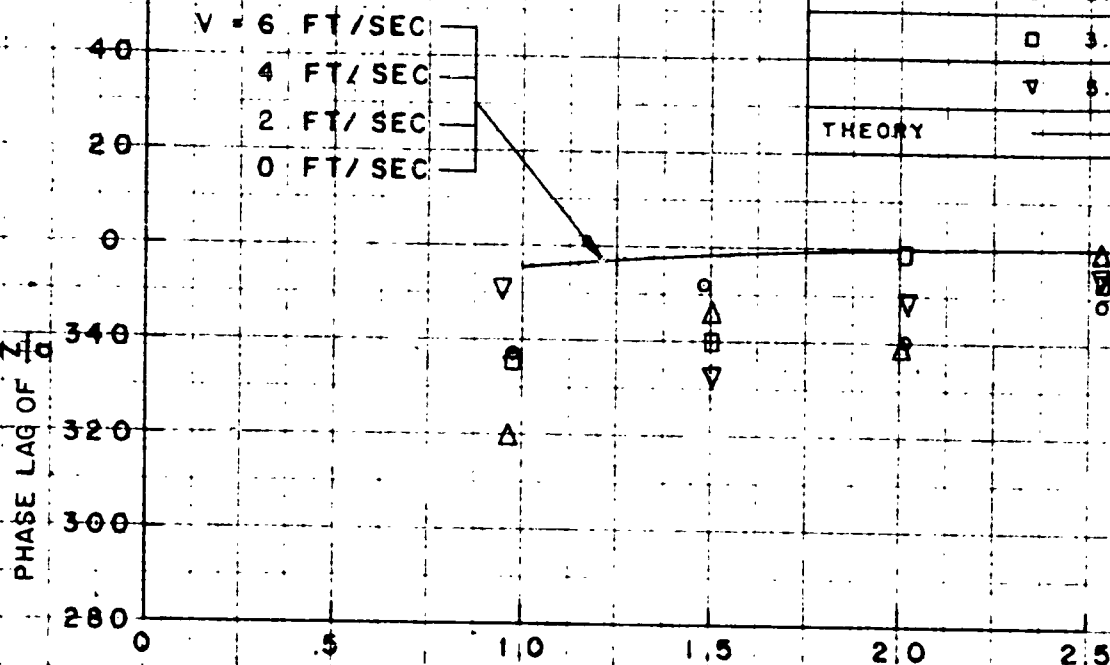


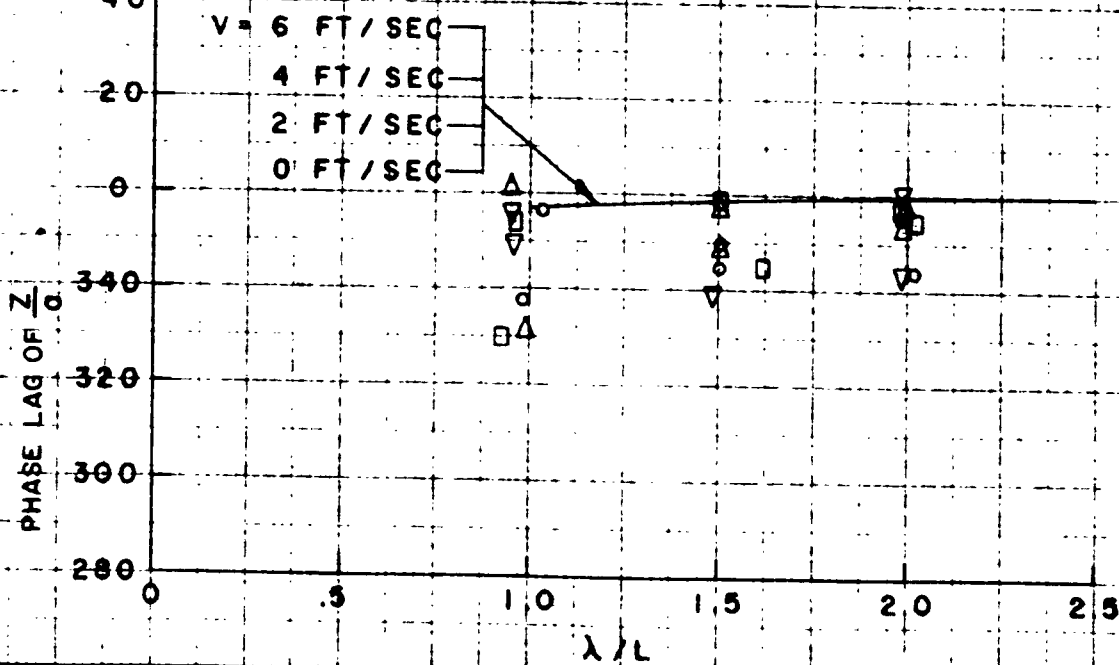
FIG. 30

## PHASE LAG OF HEAVE FORCE

vs

WAVE LENGTH / BODY LENGTH

AT 30° HEADING ANGLE



R-808

## PHASE LAG OF HEAVE FORCE

vs

WAVE LENGTH / BODY LENGTH

AT 60° HEADING ANGLE

LEGEND

EXPERIMENT	○	△	□	▽	FT/SEC
					2.02 FT/SEC
					3.96 FT/SEC
					5.95 FT/SEC

THEORY

FIG. 31

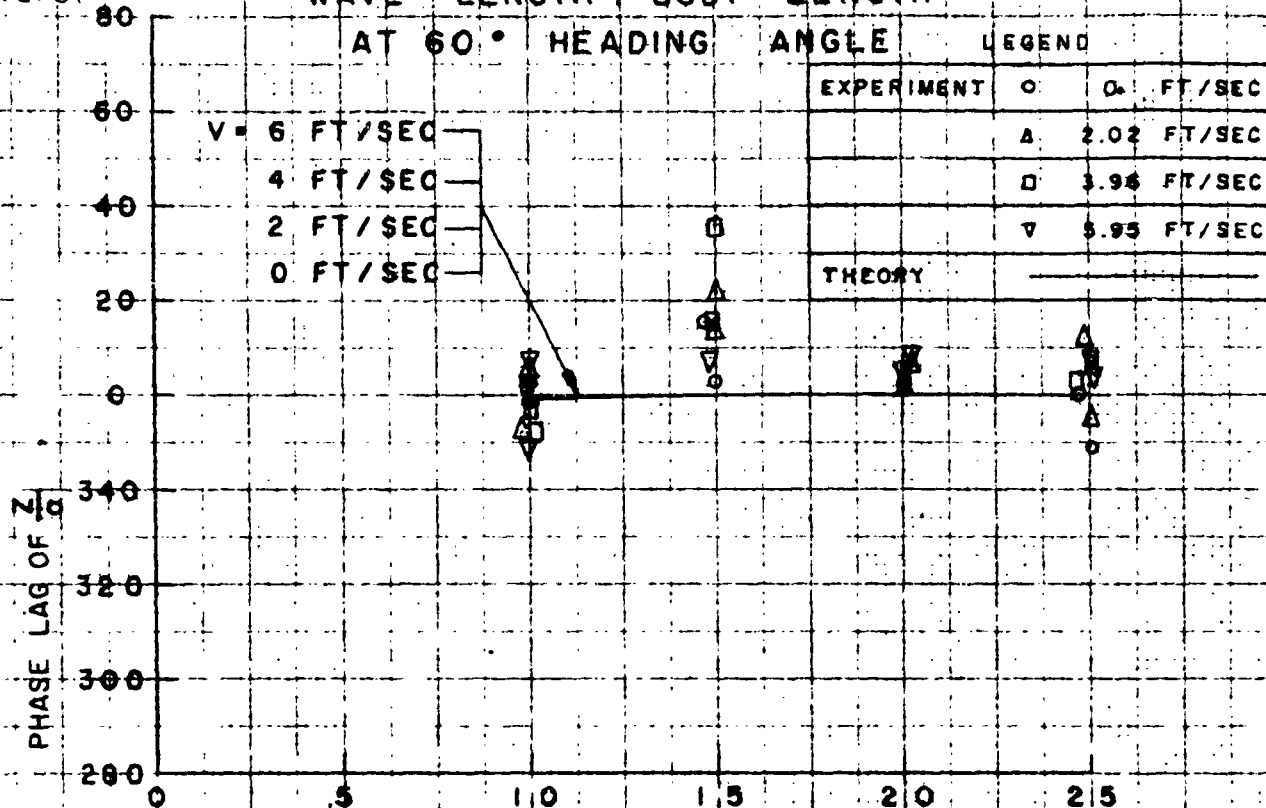


FIG. 32

## PHASE LAG OF HEAVE FORCE

vs

WAVE LENGTH / BODY LENGTH

AT 90° HEADING ANGLE

$V = 6 \text{ FT/SEC}$   
 $4 \text{ FT/SEC}$   
 $2 \text{ FT/SEC}$   
 $0 \text{ FT/SEC}$

PHASE LAG OF  $Z_a$ 

280

.5

1.0

1.5

2.0

2.5

 $\lambda/L$

R-60R

## PHASE LAG OF PITCHING MOMENT

vs

WAVE LENGTH / BODY LENGTH

AT 0° HEADING ANGLE

LEGEND

EXPERIMENT	O	FT/SEC
	Δ	2.02
	□	3.94
	▽	5.95

THEORY

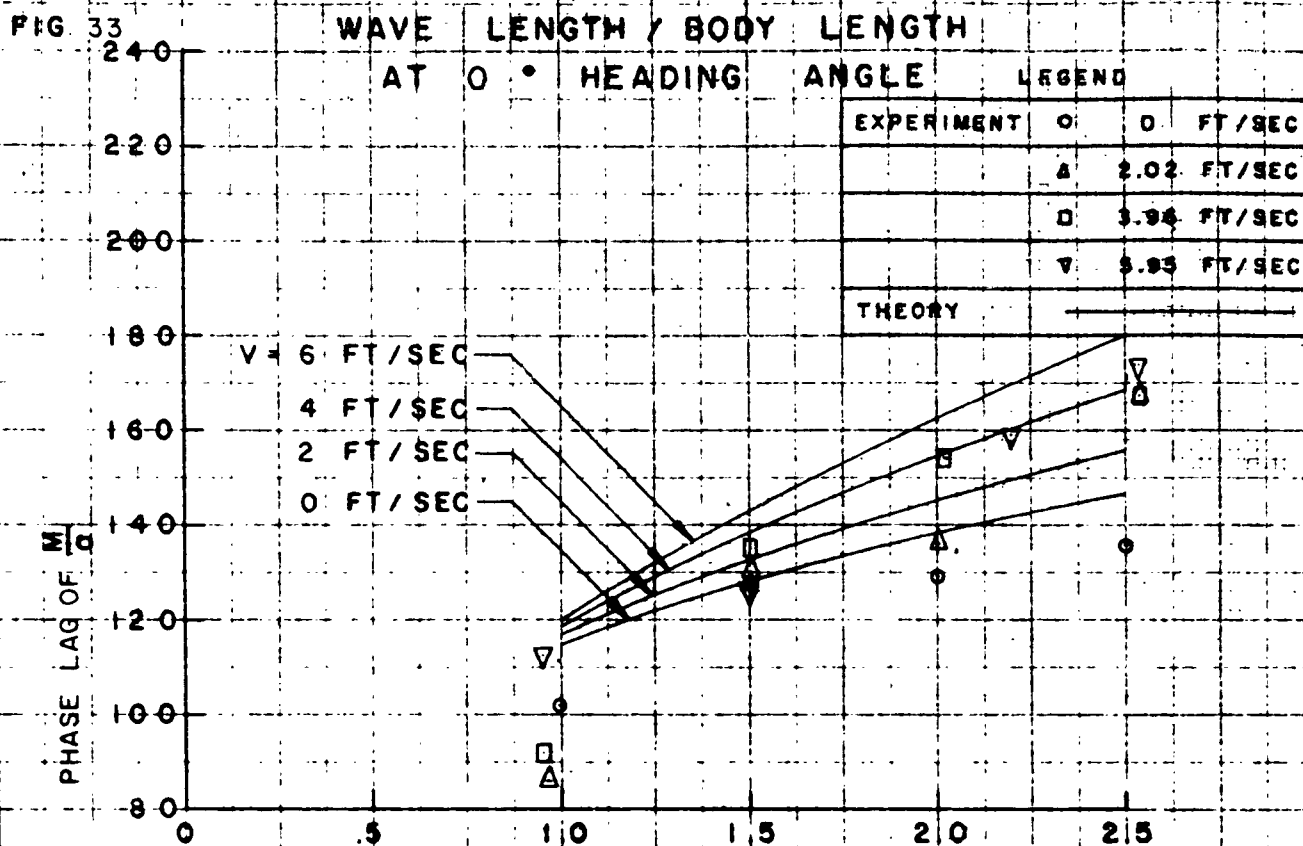


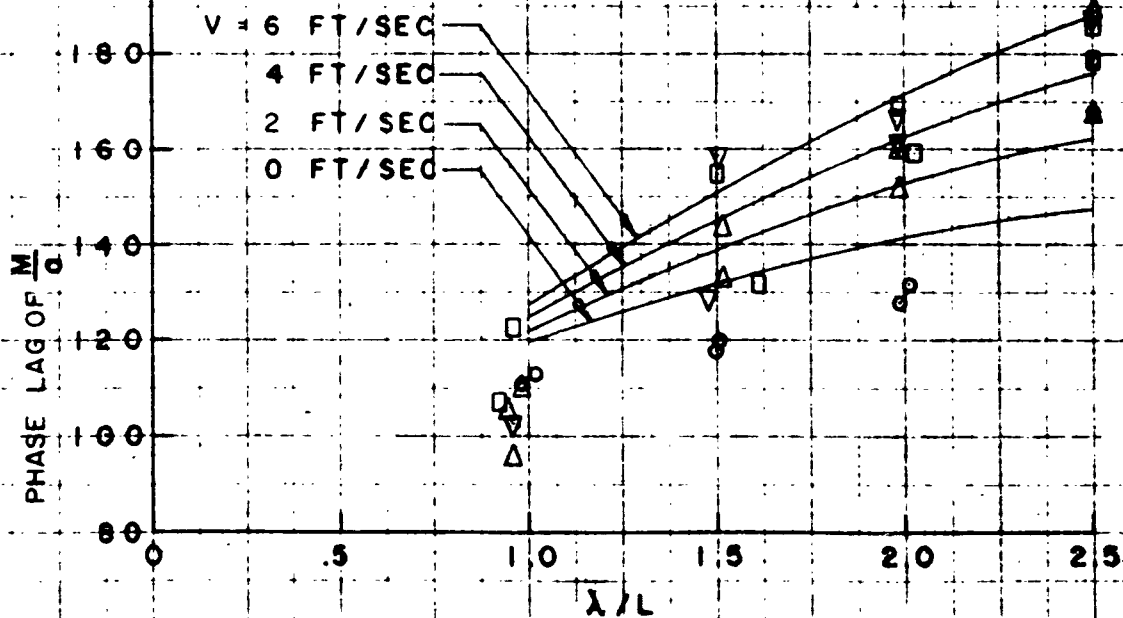
FIG. 34

## PHASE LAG OF PITCHING MOMENT

vs

WAVE LENGTH / BODY LENGTH

AT 30° HEADING ANGLE





## PHASE LAG OF PITCHING MOMENT

vs

WAVE LENGTH / BODY LENGTH

AT 60° HEADING ANGLE

LEGEND

EXPERIMENT	○	0 FT/SEC
	△	2.02 FT/SEC
	□	3.98 FT/SEC
	▽	5.95 FT/SEC
THEORY	—	

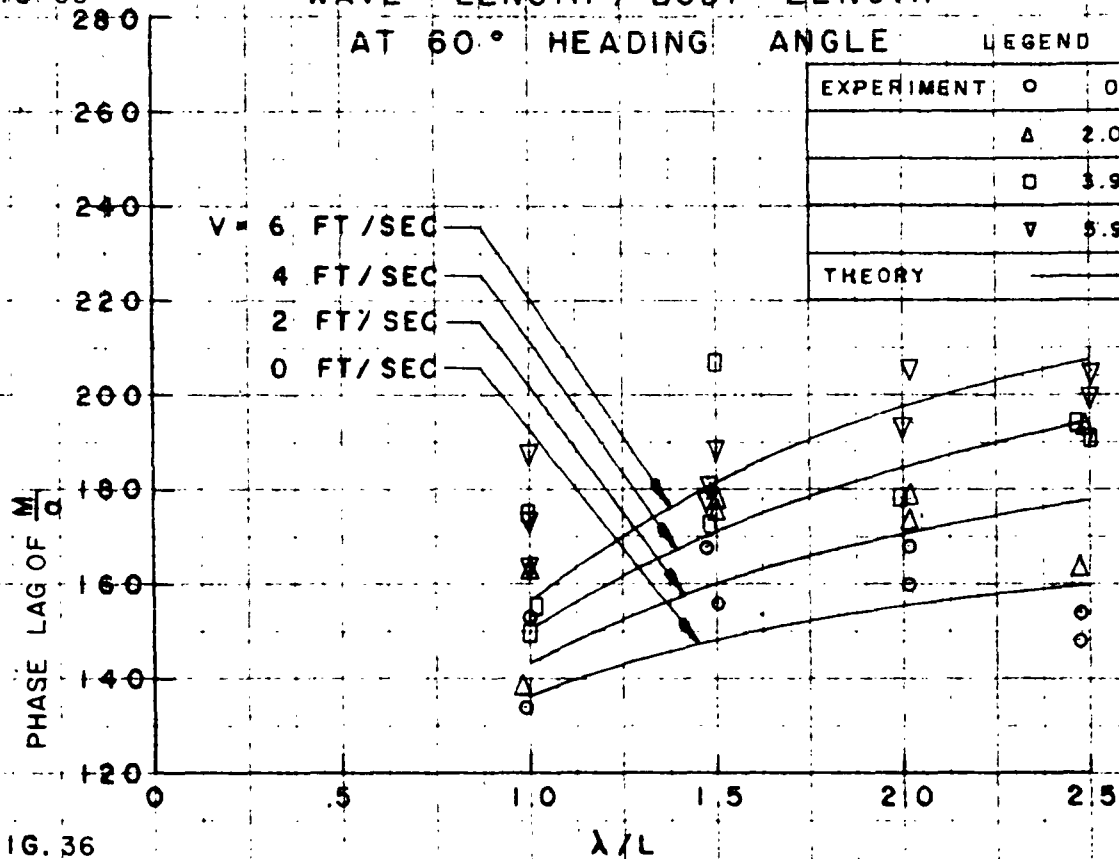


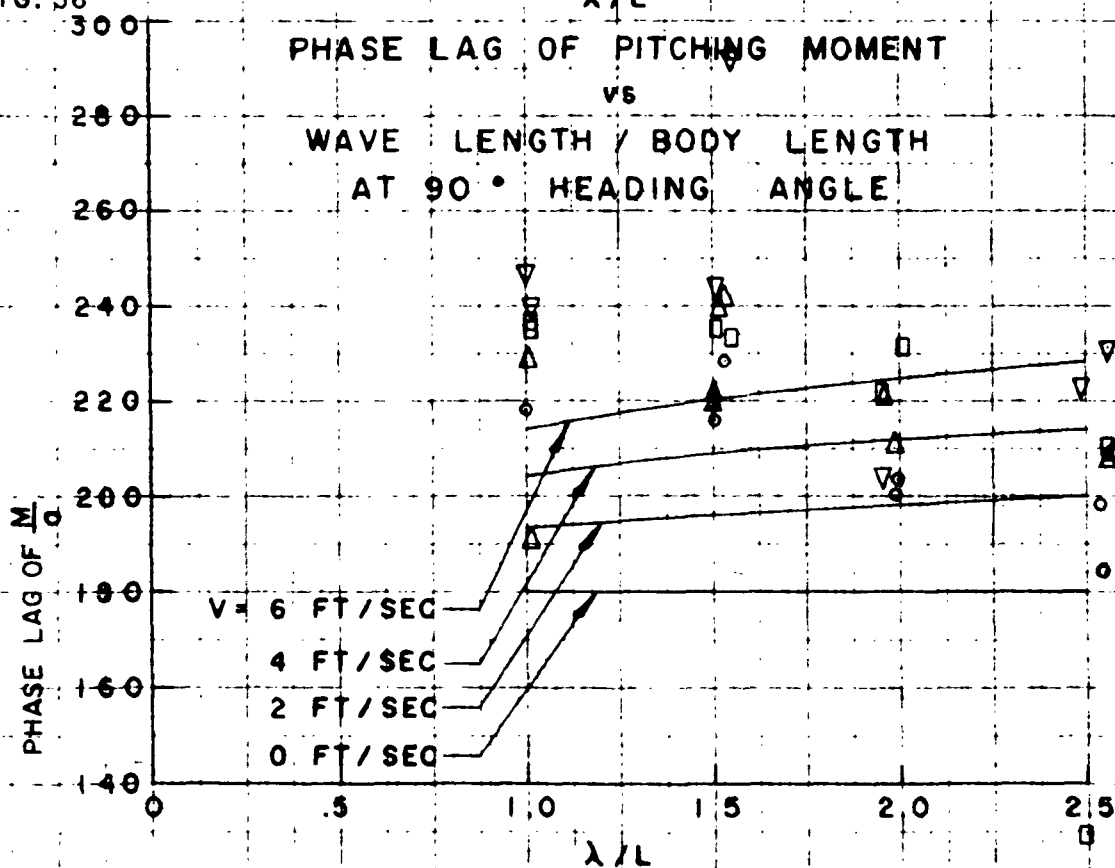
FIG. 36

## PHASE LAG OF PITCHING MOMENT

vs

WAVE LENGTH / BODY LENGTH

AT 90° HEADING ANGLE



# PHASE LAG OF SIDE FORCE

vs

FIG. 37

## WAVE LENGTH / BODY LENGTH

### AT 30° HEADING ANGLE

(WITHOUT CONNING TOWER)

LEGEND

EXPERIMENT	○	0 FT/SEC
	△	2.02 FT/SEC
	□	3.96 FT/SEC
	▽	5.95 FT/SEC
THEORY	—	

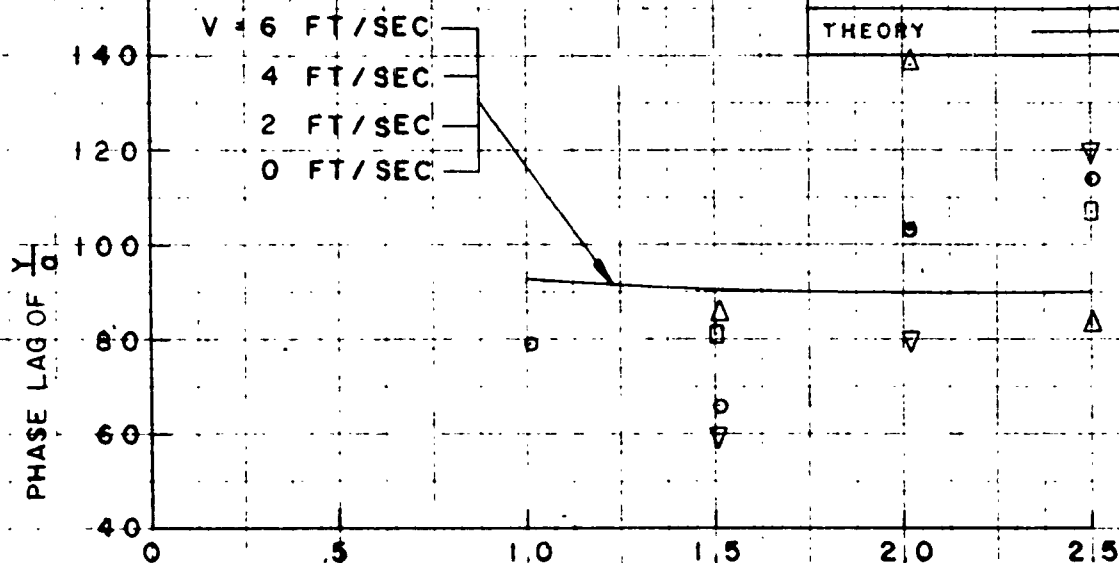


FIG. 38

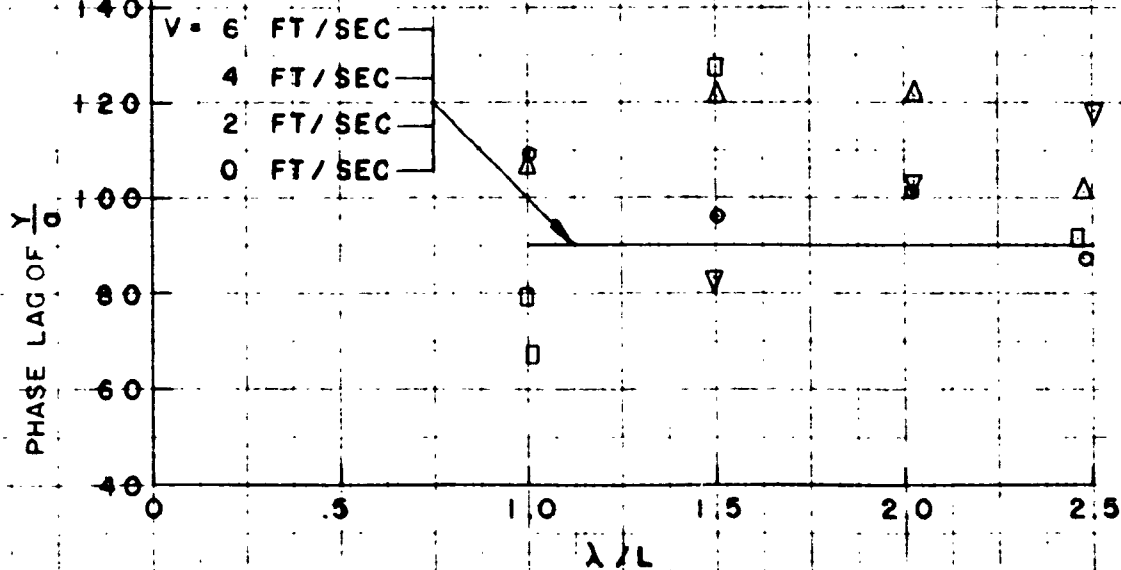
# PHASE LAG OF SIDE FORCE

vs

## WAVE LENGTH / BODY LENGTH

### AT 60° HEADING ANGLE

(WITHOUT CONNING TOWER)



# PHASE LAG OF SIDE FORCE

VS

## WAVE LENGTH / BODY LENGTH

### AT 90° HEADING ANGLE

LEGEND

(WITHOUT CONNING TOWER)

EXPERIMENT	O	0 FT/SEC
	Δ	2.02 FT/SEC
	□	3.96 FT/SEC
	▽	5.95 FT/SEC
THEORY	—	

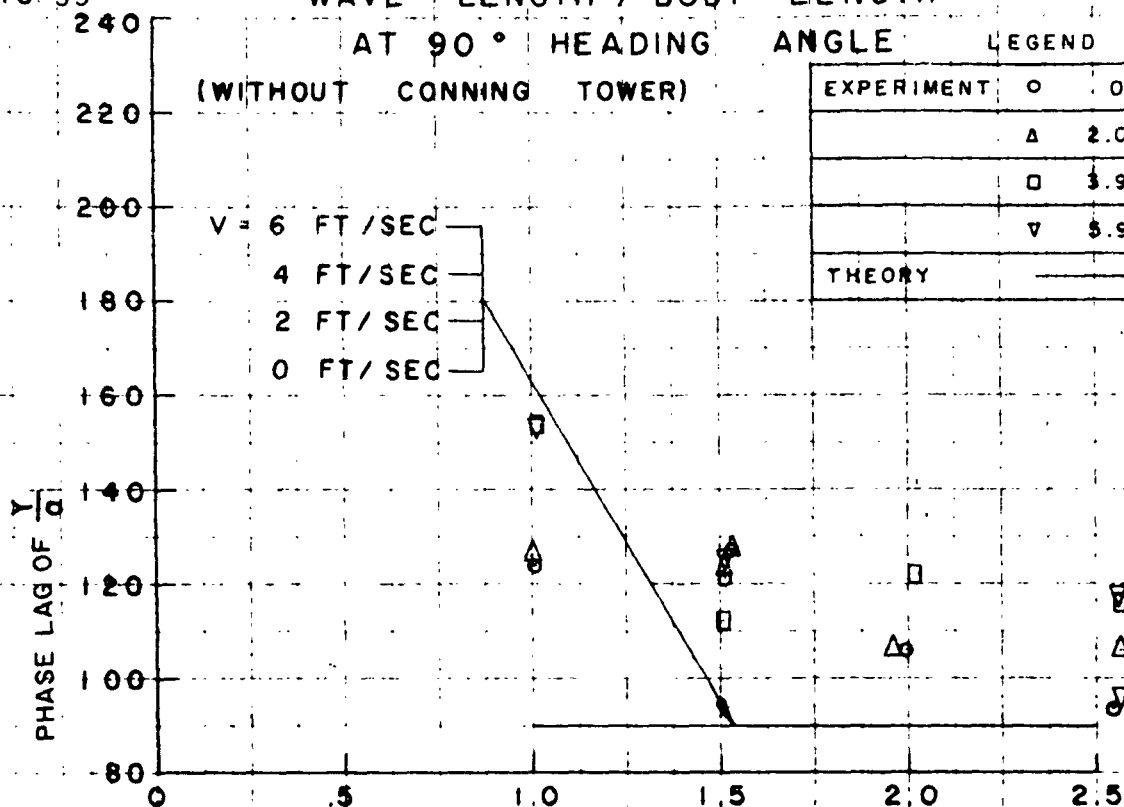


FIG. 40

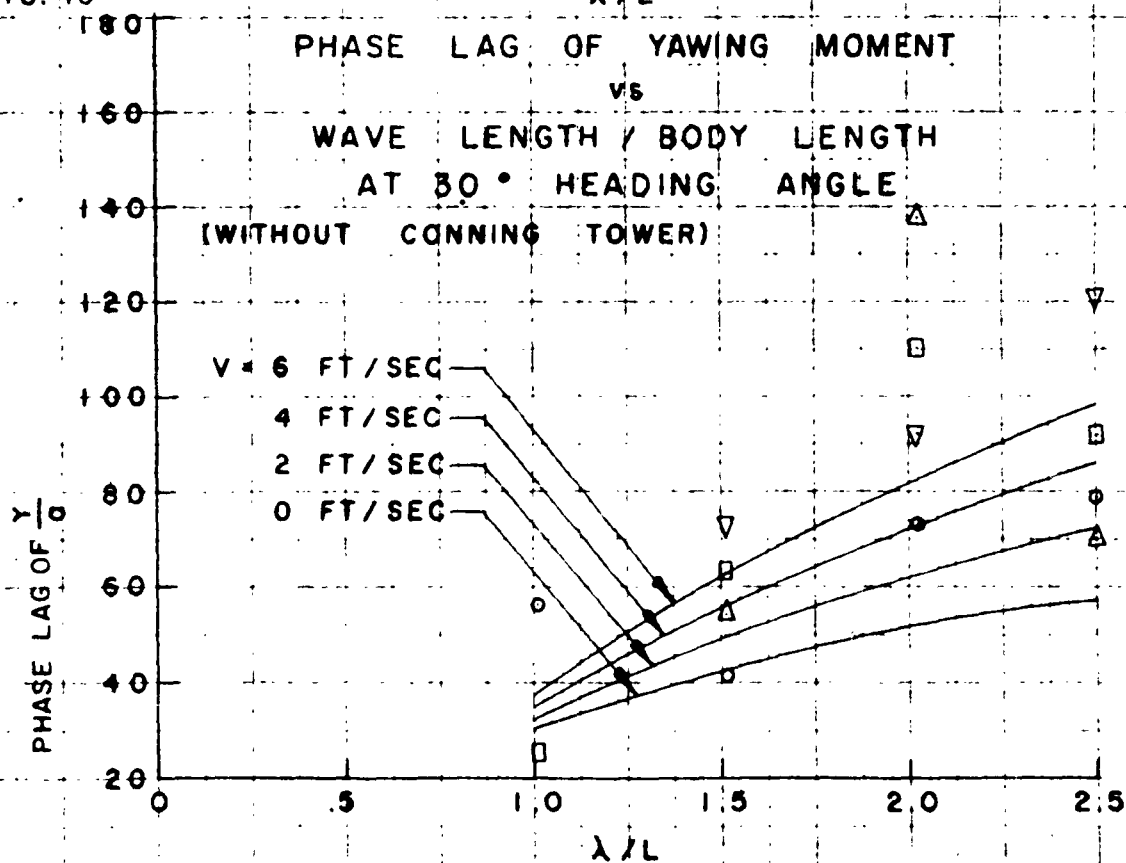
# PHASE LAG OF YAWING MOMENT

VS

## WAVE LENGTH / BODY LENGTH

### AT 30° HEADING ANGLE

(WITHOUT CONNING TOWER)



## PHASE LAG OF YAWING MOMENT

VS

FIG. 41

WAVE LENGTH / BODY LENGTH

AT 60° HEADING ANGLE

LEGEND

(WITHOUT CONNING TOWER)

EXPERIMENT	O	0 FT/SEC
	Δ	2.02 FT/SEC
	□	3.96 FT/SEC
	▽	5.95 FT/SEC
THEORY		

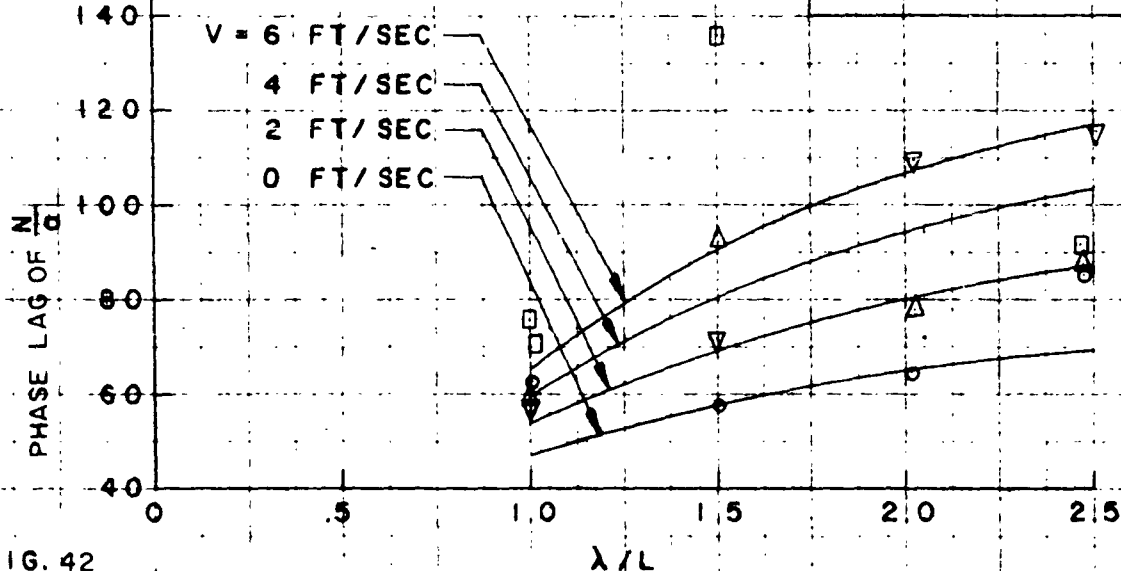


FIG. 42

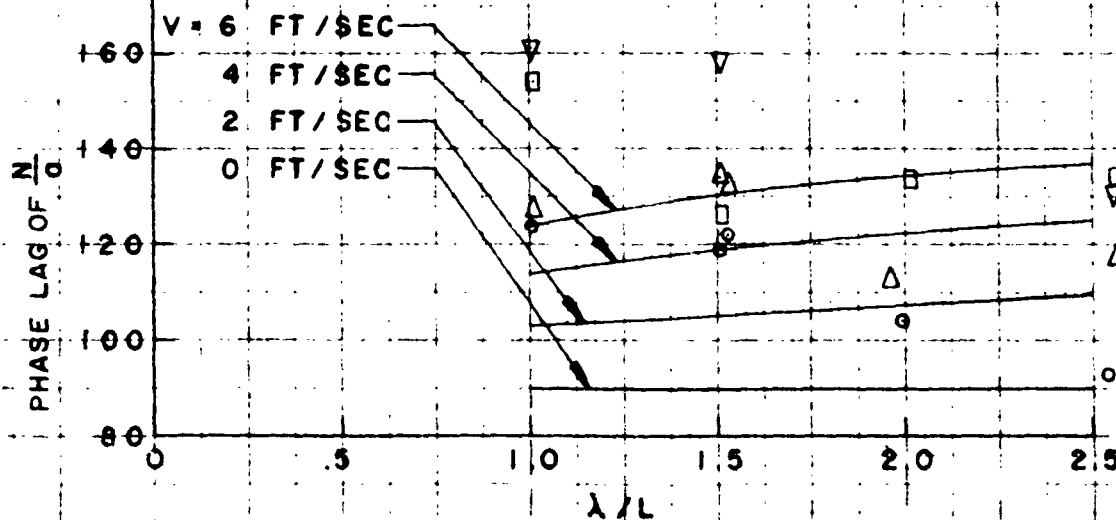
## PHASE LAG OF YAWING MOMENT

VS

WAVE LENGTH / BODY LENGTH

AT 90° HEADING ANGLE

(WITHOUT CONNING TOWER)



## PHASE LAG OF SIDE FORCE

vs

WAVE LENGTH / BODY LENGTH

AT 30° HEADING ANGLE

(WITH CONNING TOWER)

FIG. 43

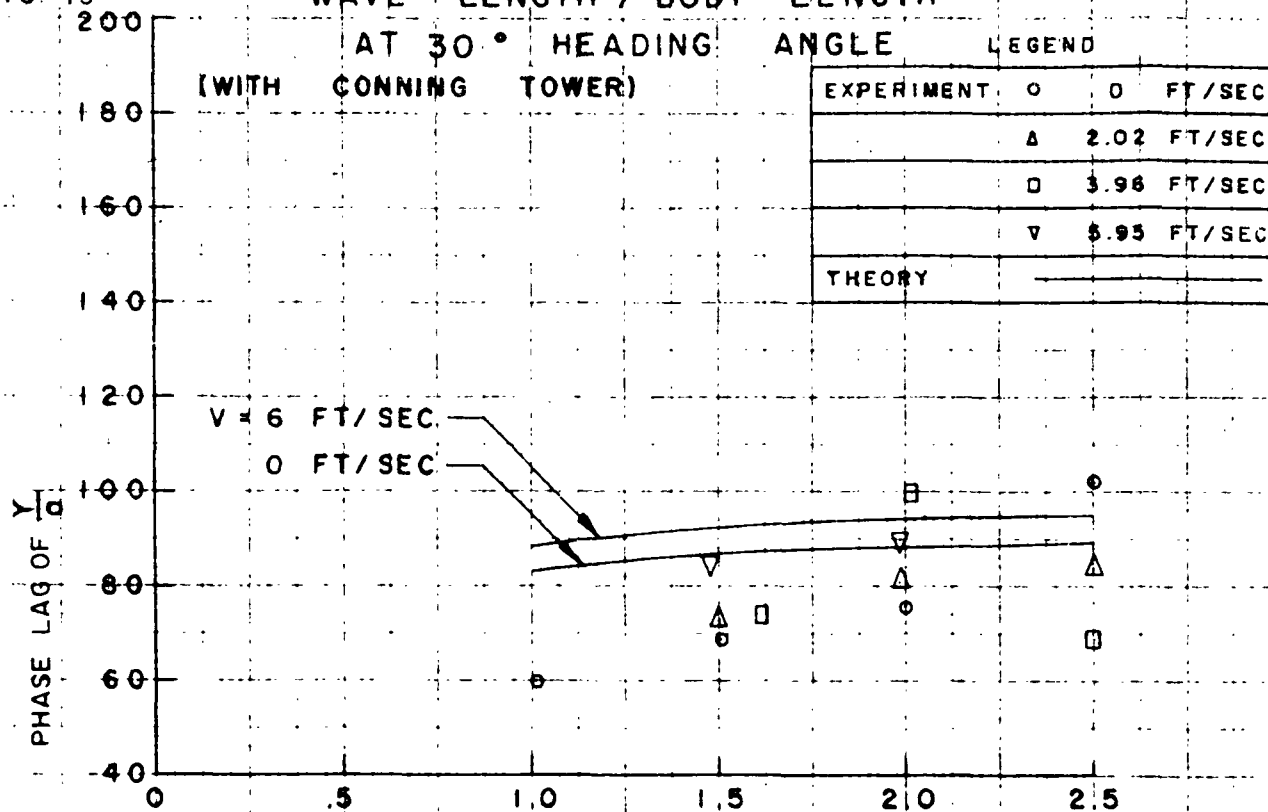


FIG. 44

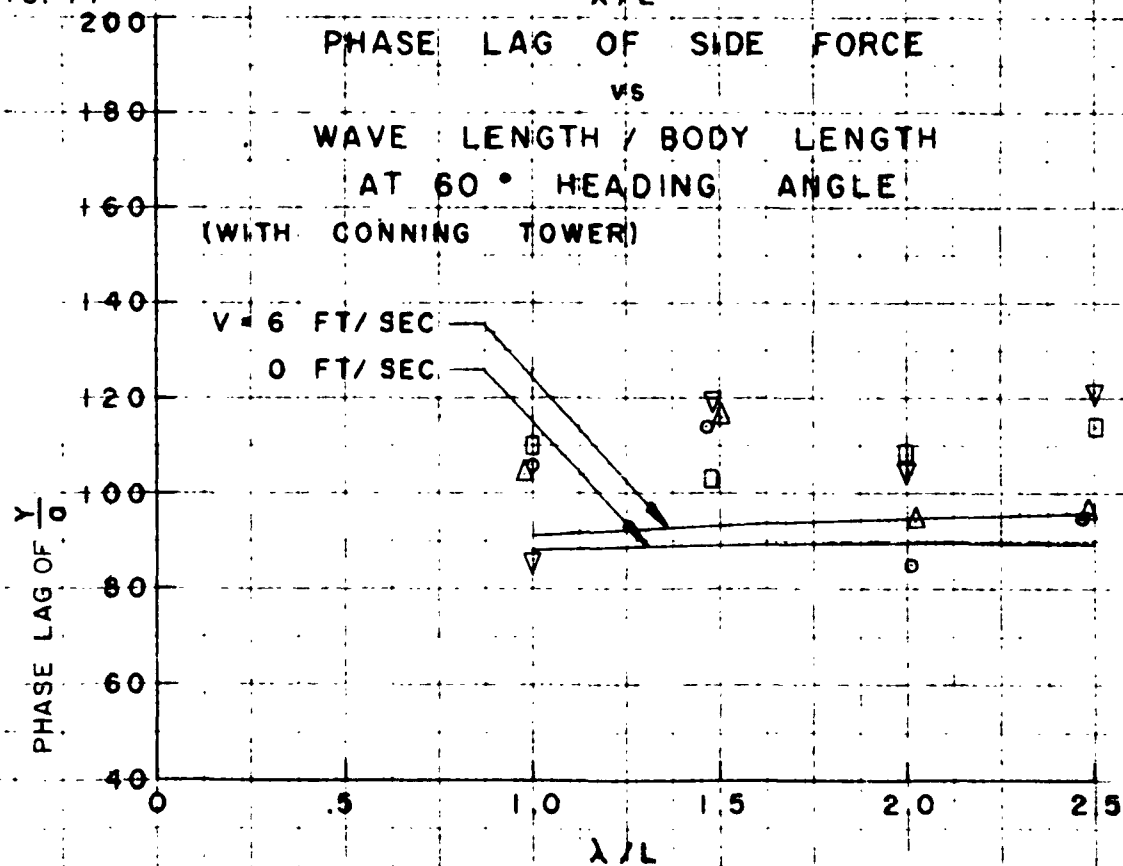
## PHASE LAG OF SIDE FORCE

vs

WAVE LENGTH / BODY LENGTH

AT 60° HEADING ANGLE

(WITH CONNING TOWER)



## PHASE LAG OF SIDE FORCE

vs

WAVE LENGTH / BODY LENGTH

AT 90° HEADING ANGLE

(WITH CONNING TOWER)

LEGEND

EXPERIMENT	○	0 FT/SEC
	△	2.02 FT/SEC
	□	3.96 FT/SEC
	▽	5.95 FT/SEC
THEORY		

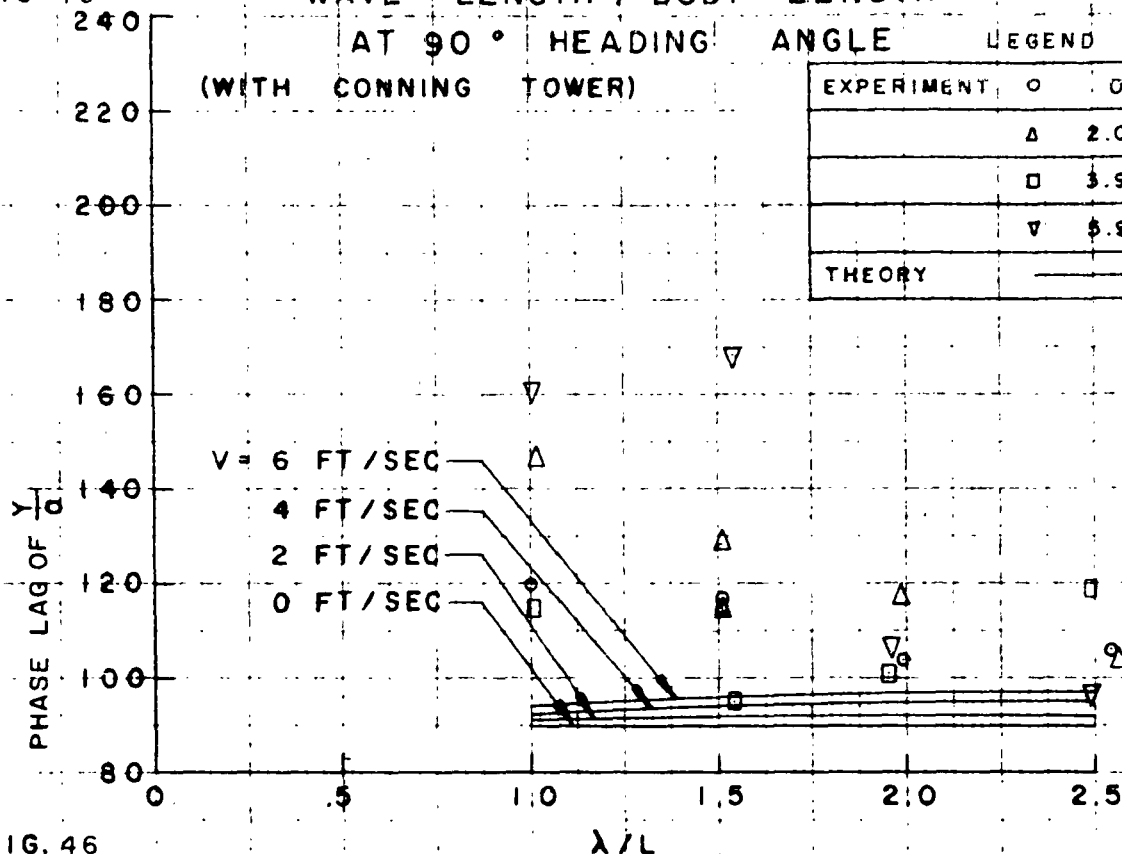


FIG. 46

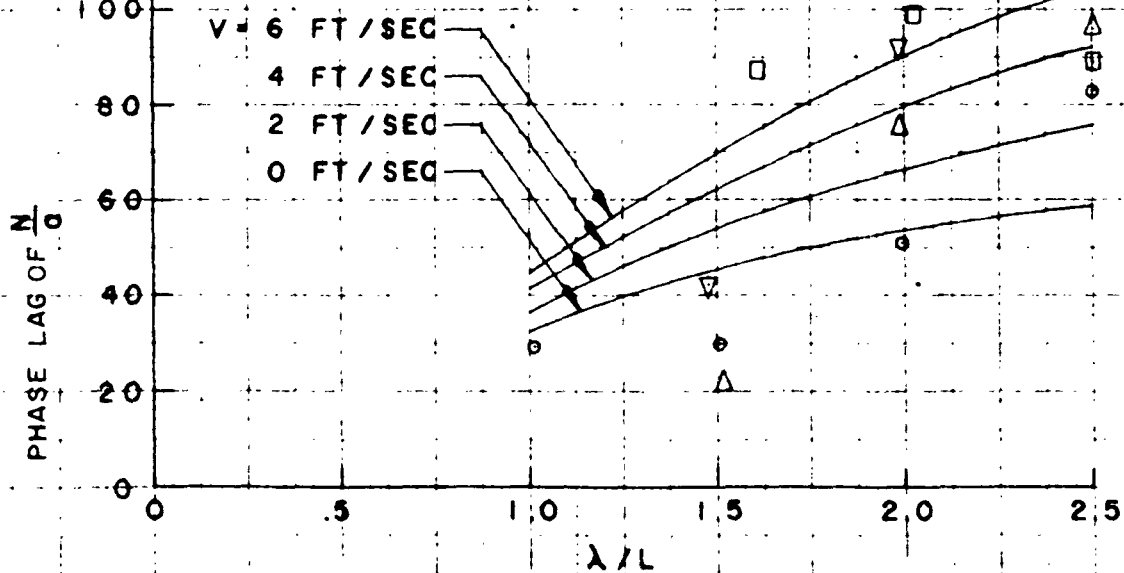
## PHASE LAG OF YAWING MOMENT

vs

WAVE LENGTH / BODY LENGTH

AT 30° HEADING ANGLE

(WITH CONNING TOWER)



# PHASE LAG OF YAWING MOMENT

vs

FIG 47

WAVE LENGTH / BODY LENGTH

AT 60° HEADING ANGLE

(WITH CONNING TOWER)

LEGEND

EXPERIMENT	○	0 FT/SEC
	△	2.02 FT/SEC
	□	3.96 FT/SEC
	▽	5.95 FT/SEC
THEORY	—	

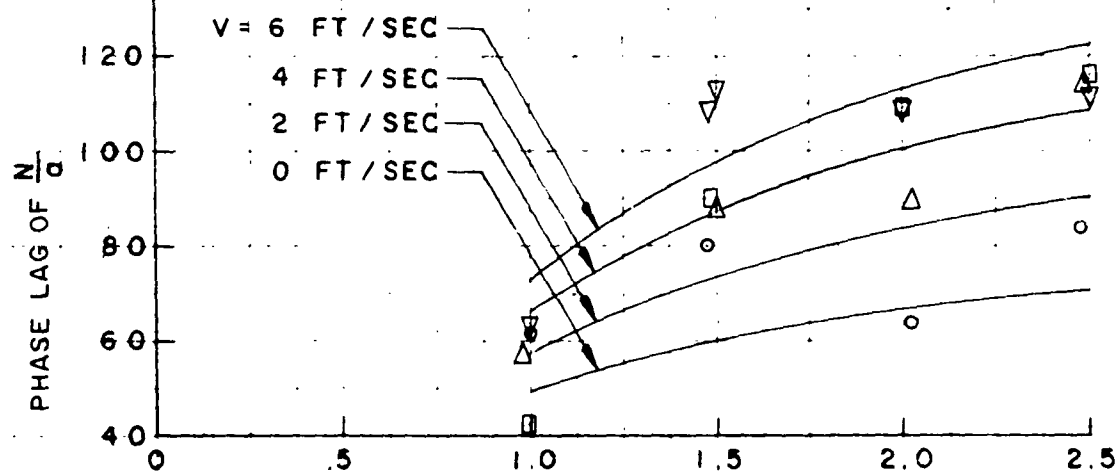


FIG. 48

λ/L

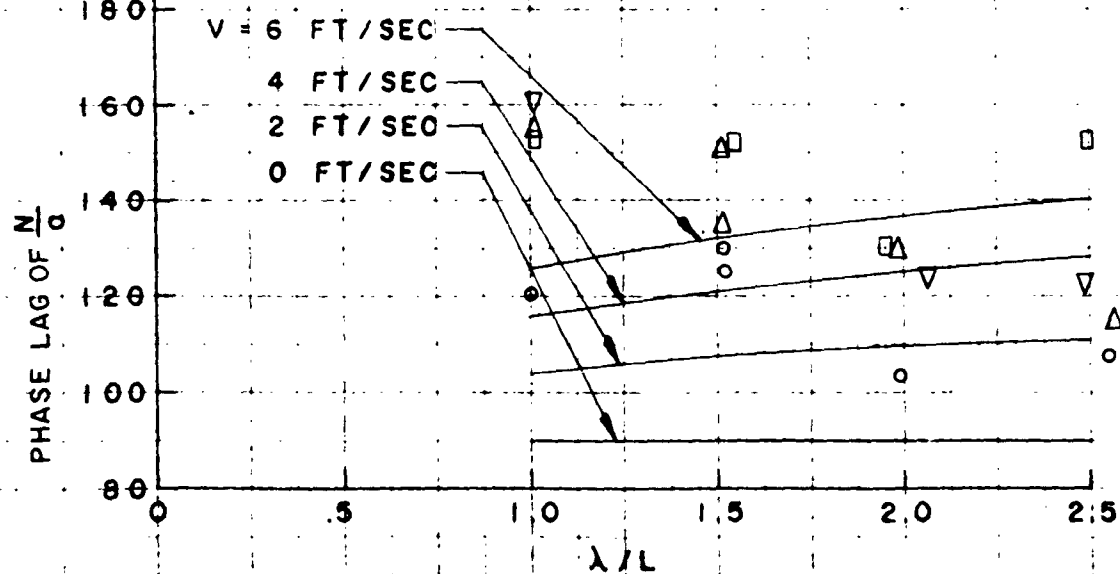
# PHASE LAG OF YAWING MOMENT

vs

WAVE LENGTH / BODY LENGTH

AT 90° HEADING ANGLE

(WITH CONNING TOWER)

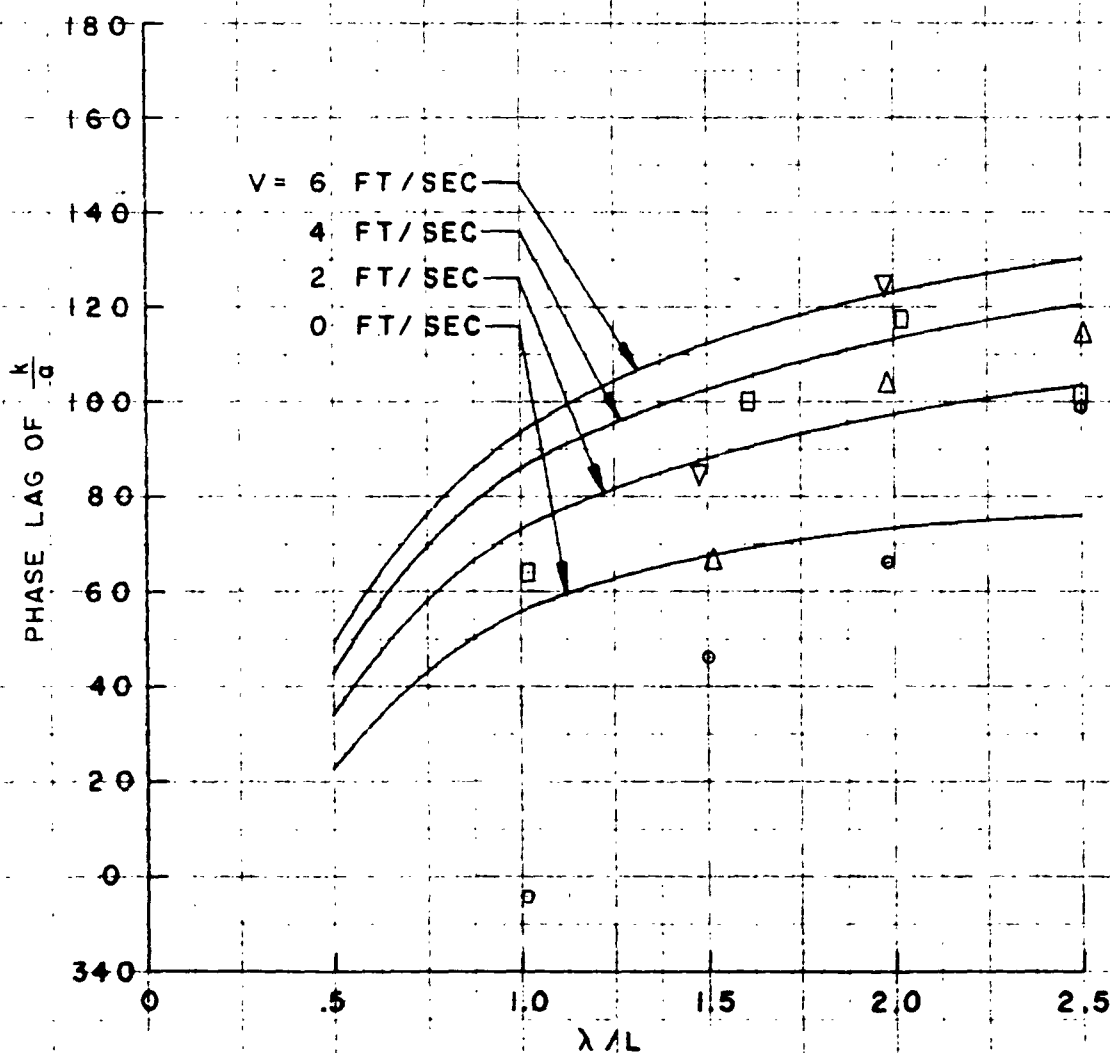


# PHASE LAG OF ROLL MOMENT vs

WAVE LENGTH / BODY LENGTH  
 AT 30° HEADING ANGLE  
 (WITH CONNING TOWER)

LEGEND

EXPERIMENT	○	0 FT/SEC
	Δ	2.02 FT/SEC
	□	3.96 FT/SEC
	▽	5.95 FT/SEC
THEORY	—	





R-808

## PHASE LAG OF ROLL MOMENT

vs

WAVE LENGTH / BODY LENGTH

AT 60° HEADING ANGLE

(WITH CONNING TOWER)

LEGEND

EXPERIMENT	O	0 FT/SEC
	Δ	2.02 FT/SEC
	□	3.96 FT/SEC
	▽	5.95 FT/SEC

THEORY

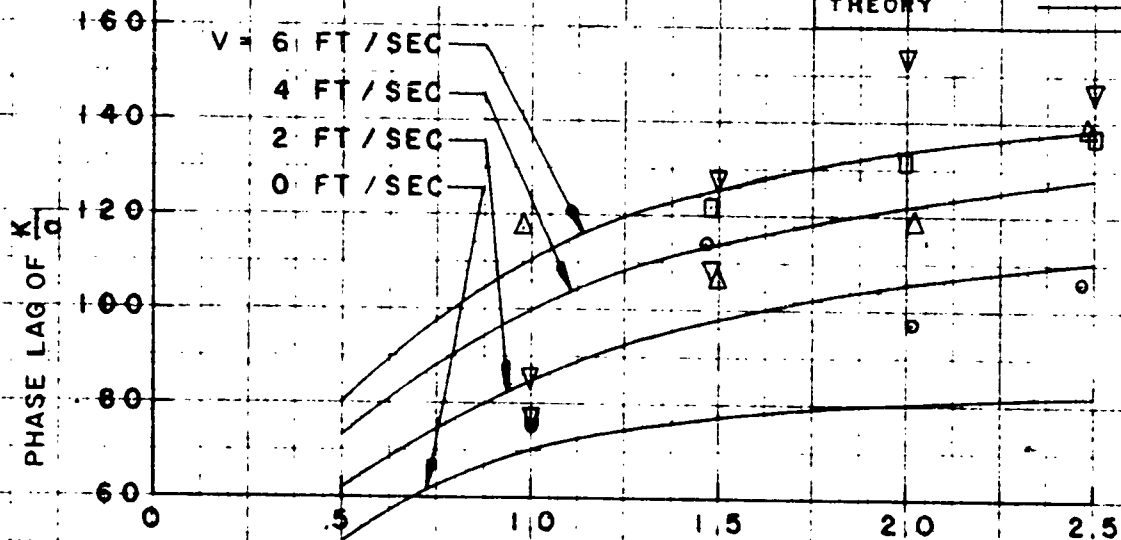


FIG. 51

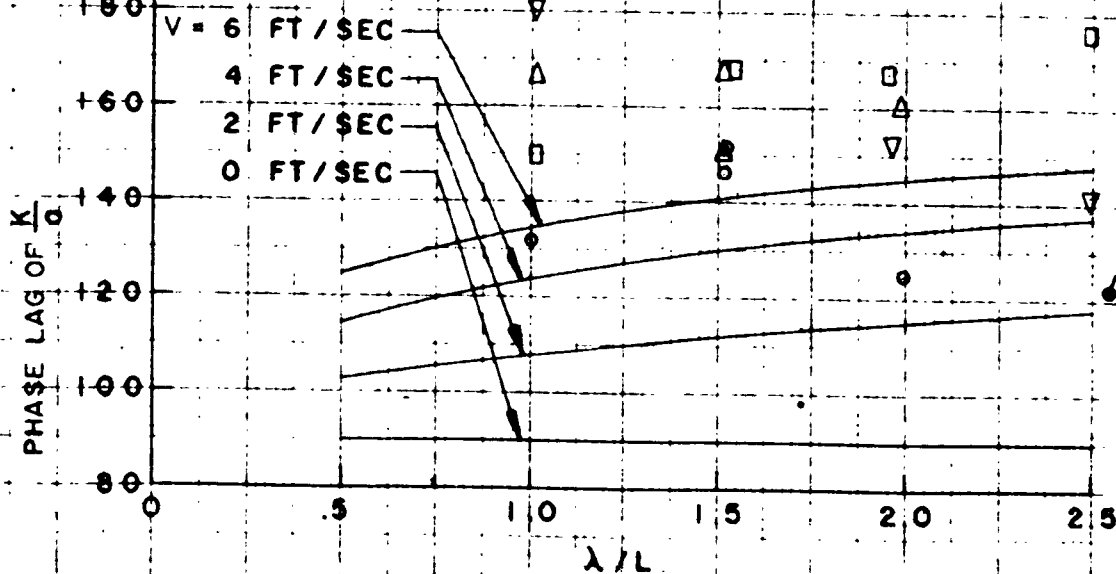
## PHASE LAG OF ROLL MOMENT

vs

WAVE LENGTH / BODY LENGTH

AT 90° HEADING ANGLE

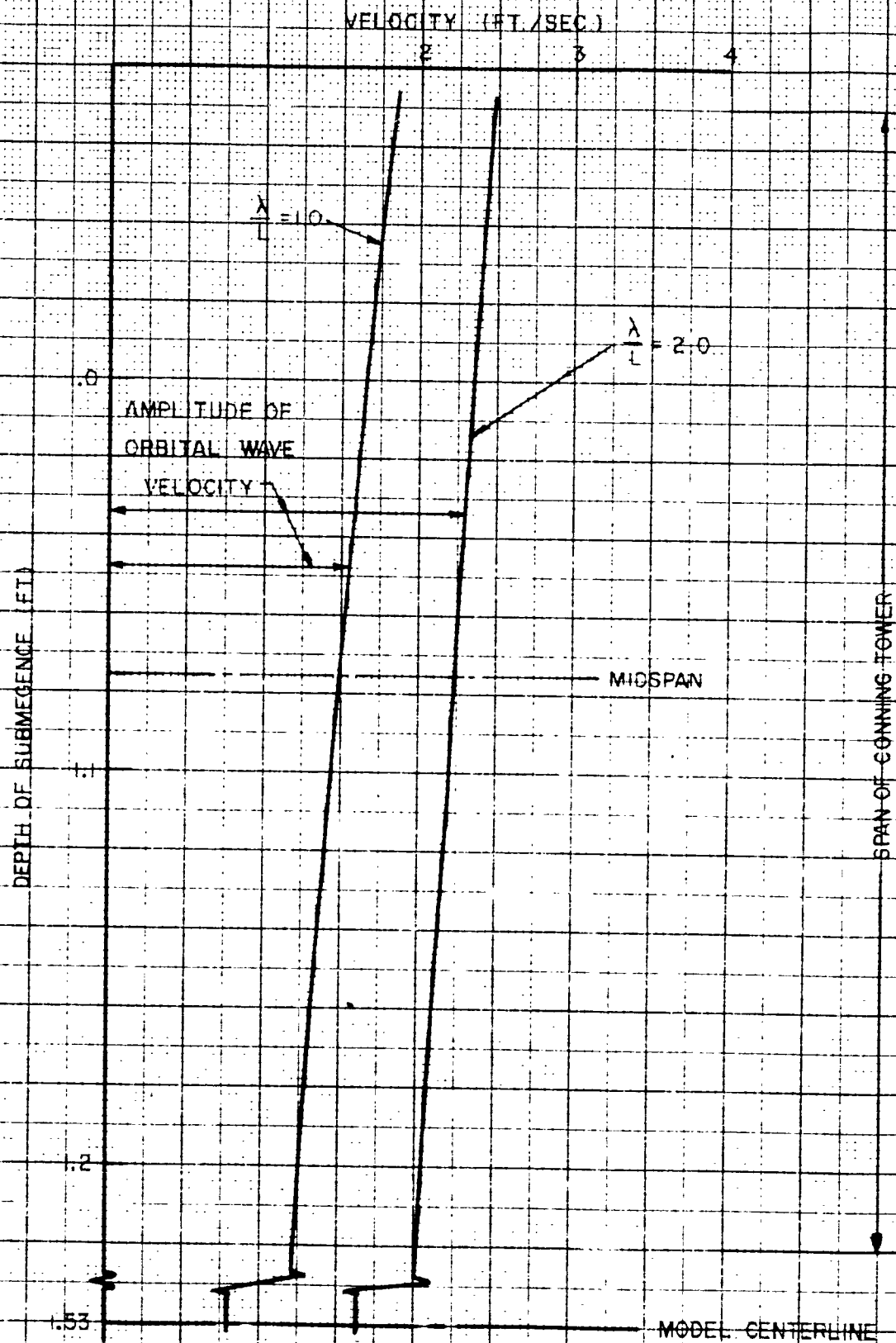
(WITH CONNING TOWER)



R-808

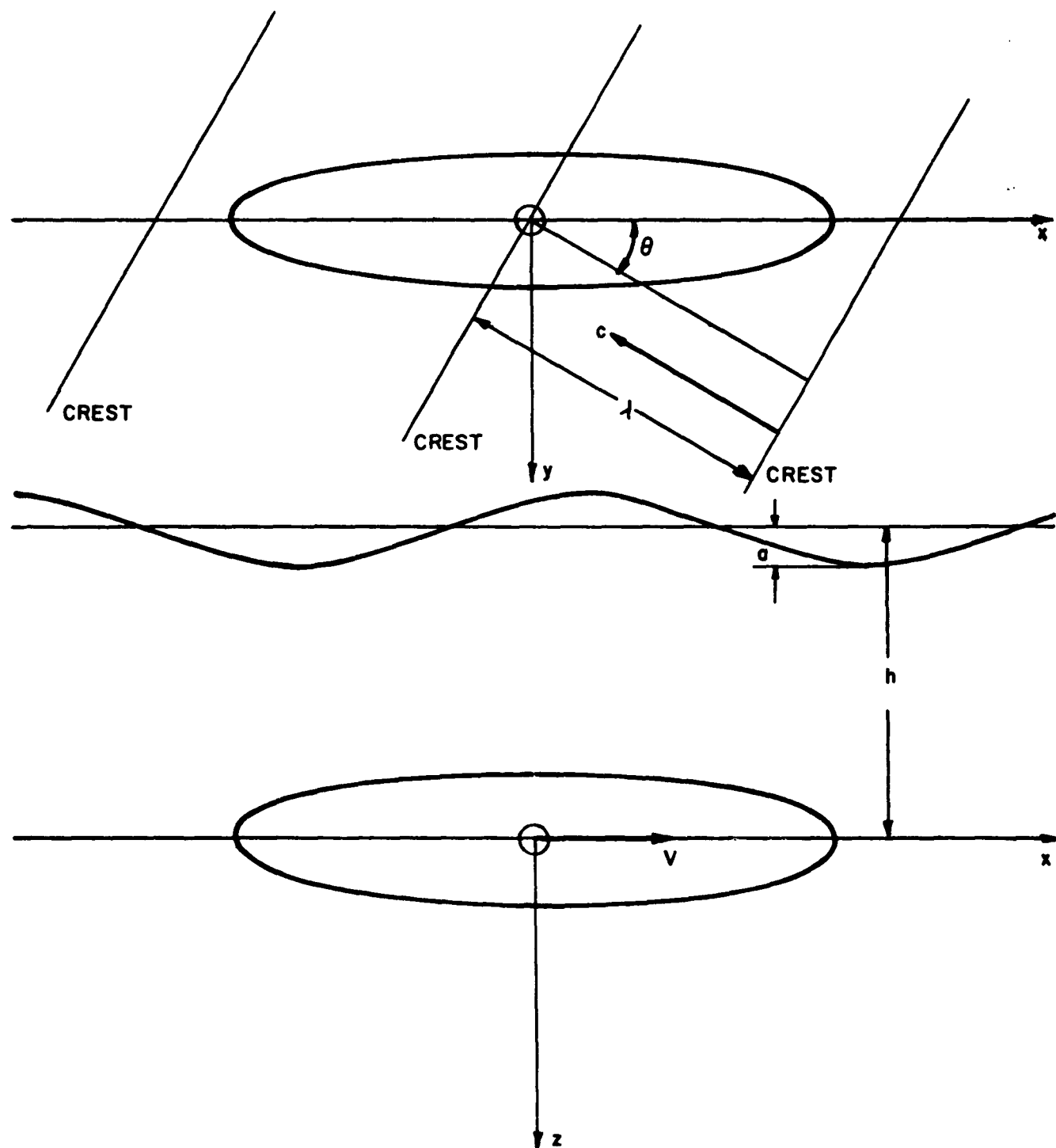
# VARIATION OF VELOCITY CORRECTIONS WITH DEPTH

FIG 52



10 X 10 TO THE 1/2 INCH  
 KENNEL & EGGEN CO.  
 2781-1112

## SYSTEM OF COORDINATES



# APPENDIX A: THEORETICAL ANALYSIS

The results presented here summarize the analysis originally reported in reference 3. The problem is the prediction of the forces and moments acting on a submerged slender body moving under a regular wave system. The coordinate system and other nomenclature are illustrated in Figure 53. The body is constrained to move in a straight line at constant depth and with no angle-of-attack relative to calm water. The wave system is at an arbitrary heading-angle to the course of the body. The effect of the presence of a free surface is neglected in determining the forces and moments.

With these assumptions, the expressions for the forces and moments acting on the body are derived. The side and heave force are

$$Y = \int_{x_s}^{x_b} \left[ \frac{D}{Dt} (A_{22} v_o) + m \frac{D v_o}{Dt} \right] dx \quad (A-1)$$

$$Z = \int_{x_s}^{x_b} \left[ \frac{D}{Dt} (A_{33} w_o) + m \frac{D w_o}{Dt} \right] dx \quad (A-2)$$

where  $D/Dt = \partial/\partial t - V \partial/\partial x$ ,  $w_o$  and  $v_o$  are the wave orbital velocities at the point  $(x, 0, 0)$  of the body, and  $A_{22}$  and  $A_{33}$  are the two-dimensional stripwise added masses in the Y and Z directions due to translational motion in the Y and Z direction respectively, given by:

$$A_{33} = \rho \pi R^2 \text{ (at all sections)}$$

$$A_{22} = \rho \pi R^2 \text{ (at sections where there is no conning tower)}$$

$$A_{22} = \frac{\pi \rho}{4 b^2} \left[ (b + R)^4 - 12 R^2 b^2 \right] \text{ (at fairwater sections)}$$

For the yaw and pitching moment the following equations were used:

$$N = \int_{x_s}^{x_b} x \frac{dY}{dx} dx \quad (A-3)$$

$$M = - \int_{x_s}^{x_b} x \frac{dZ}{dx} dx \quad (A-4)$$

For the roll moment

$$K = + \int_{x_s}^{x_b} \frac{D}{Dt} (A_{42} v_o) dx \quad (A-5)$$

where  $A_{42}$ , the stripwise added mass moment about the x axis due to flow in the y direction is given by:

$$A_{42} = \rho \left[ \frac{(b - R)^3}{4} \left( \frac{R}{b} \right)^{1/2} \left( \frac{14}{3} \frac{R}{b} + 1 + \frac{R^2}{b^2} \right) + \frac{(b - R)^2 (b + R)^4}{8 b^3} \left( \frac{\pi}{2} + \sin^{-1} \frac{b - R}{b + R} \right) \right] \quad (A-6)$$

The wave orbital velocities at  $(x, 0, 0)$  are given by the following equations:

$$v_o = -kac \sin \theta e^{-kh} e^{ik [x \cos \theta + (V \cos \theta - c)t]} \quad (A-7)$$

$$w_o = -ik ac e^{-kh} e^{ik [x \cos \theta + (V \cos \theta - c)t]} \quad (A-8)$$

These results were applied to a series-58 hull with dimensions given in Table I of this report. The forces and

moments were evaluated for a submergence of 2.5 model diameters. The origin of the coordinate system was taken at the center-of-buoyancy and consequently the moments were calculated relative to the CB. These results were transferred vectorially to give the magnitude of the forces and moments acting at the center of the balance. The computed phase lags are relative to the wave height ( $\eta$ ) at the CB given by

$$\eta = a \cos \omega t. \quad (A-9)$$

## APPENDIX B: INERTIAL CORRECTIONS

The flexibility of the structure, used to support the strut, caused the records of the force and moment output to include inertial forces which were due to the motion of the model in response to the wave forces. The corrections, made necessary by these inertial forces, are discussed in this appendix.

The linear and angular displacement ( $\delta$  and  $\beta$ ) of the model in the x,y plane relative to the strut were measured and recorded. These displacements were proportional to the force and moment ( $-k_\delta \delta$  and  $-k_\beta \beta$ ) that were applied to the model by the balance, where  $k_\delta$  and  $k_\beta$  were the calibrated spring constants of the balance. The wave force and moment relative to the center-of-buoyancy (Y and N) are the quantities which must be found. Using the usual nomenclature for the linearized hydrodynamic forces acting on a submerged body, the equations of motion of the model relative to the center-of-buoyancy are:

$$Y + Y_{\ddot{y}}\ddot{y} + Y_{\dot{y}}\dot{y} + Y_{\ddot{\beta}}\ddot{\beta} + Y_{\dot{\beta}}\dot{\beta} + Y_{\beta}\beta - k_\delta \delta = m\ddot{y} - m\xi\ddot{\beta} \quad (B-1)$$

and

$$N + N_{\ddot{y}}\ddot{y} + N_{\dot{y}}\dot{y} + N_{\ddot{\beta}}\ddot{\beta} + N_{\dot{\beta}}\dot{\beta} + N_{\beta}\beta - k_\beta \beta + \ell k_\delta \delta = I_{zz}\ddot{\beta} - m\xi\ddot{y} \quad (B-2)$$

where  $\ell$  is the distance from the center of the balance to the center-of-buoyancy and  $\xi$  is the distance from the center-of-gravity to the center-of-buoyancy which are both positive when the center-of-buoyancy is forward. The hydrodynamic derivatives and the moment of inertia ( $I_{zz}$ ) are all relative to the center-of-buoyancy. The total linear translation of the

model along the y-axis was found to be large in comparison with the total angular displacement. Therefore, the angular displacement  $\beta$  is assumed to be entirely due to the distortion of the balance, while the total linear translation is denoted as  $y$ , and the linear distortion of the balance in the y-direction is  $\delta$  ( $< y$ ). The hydrodynamic inertia coupling terms  $Y_{\dot{\beta}}$  and  $N_{\dot{y}}$  are taken to be zero in this analysis. Solving these equations for the force and moment due to the wave forces and transferring the moment axis to the center of the balance results in the following expressions:

$$Y = (m - Y_{\ddot{y}}) \ddot{y} - Y_{\dot{y}} \dot{y} - m \xi \ddot{\beta} - Y_{\ddot{\beta}} \ddot{\beta} - Y_{\dot{\beta}} \dot{\beta} + k_{\delta} \delta \quad (B-3)$$

and

$$\begin{aligned} N + lY = & [(m - Y_{\ddot{y}})l - m\xi] \ddot{y} - [lY_{\dot{y}} + N_{\dot{y}}] \dot{y} + \\ & \alpha [(I_{zz} - N_{\ddot{\beta}}) - m\xi l] \ddot{\beta} - [N_{\dot{\beta}} + Y_{\dot{\beta}}l] \dot{\beta} - \\ & [N_{\beta} + Y_{\beta}l] \beta + k_{\beta} \beta \end{aligned} \quad (B-4)$$

Assuming simple harmonic motion with frequency ( $\omega$ ) equal to the frequency of wave encounter for the displacements of  $y$ ,  $\delta$ , and  $\beta$  and assuming that all of these motions are in phase with each other, equations B-3 and B-4 become:

$$Y_0 = -\omega^2 y_0 (m - Y_{\ddot{y}}) - i\omega y_0 Y_{\dot{y}} + \omega^2 \beta_0 m l - i\omega \beta_0 Y_{\dot{\beta}} - Y_{\beta} \beta_0 + k_{\delta} \delta_0 \quad (B-5)$$

and

$$\begin{aligned} N_0 + lY_0 = & -\omega^2 y_0 [(m - Y_{\ddot{y}})l - m\xi] - i\omega y_0 [lY_{\dot{y}} + N_{\dot{y}}] - \\ & \omega^2 \beta_0 [I_{zz} - N_{\ddot{\beta}} - m\xi l] - i\omega \beta_0 [N_{\dot{\beta}} + Y_{\dot{\beta}}l] - \\ & [N_{\beta} + Y_{\beta}l] \beta_0 + k_{\beta} \beta_0 \end{aligned} \quad (B-6)$$

where an  $e^{i\omega t}$  has been cancelled from each term;  $y_0$ ,  $\beta_0$ , and  $\delta_0$  denote the real amplitudes of the respective motions and  $N_0$  and  $Y_0$  are the complex amplitudes of the wave force and



moment. In these equations, the hydrodynamic terms involving  $\beta_o$  were small in comparison with  $y_o$  and the terms  $i\omega y_o lY_{\dot{y}}$ ,  $\omega^2 y_o m \dot{y}$  and  $i\omega y_o lY_{\dot{y}}$  were small in comparison with the remaining terms. Neglecting these terms, equations B-5 and B-6 reduce to:

$$Y_o = -\omega^2 y_o (m - Y_{\dot{y}}) + k_{\delta} \delta_o \quad (B-7)$$

and

$$N_o + lY_o = -\omega^2 y_o (m - Y_{\dot{y}}) l - i\omega y_o N_{\dot{y}} + k_{\beta} \beta_o \quad (B-8)$$

In equations B-7 and B-8, the terms  $k_{\delta} \delta_o$  and  $k_{\beta} \beta_o$  represent the recorded balance forces; the left-hand sides ( $Y_o$  and  $N_o + lY_o$ ), represent the complex amplitudes of the force and moment applied to the model by the wave forces relative to the center of the balance, and the remaining terms are corrections to the forces measured by the balance, which are necessary because of the model motion of amplitude  $y_o$  and frequency  $\omega$  in response to the wave force excitation. From these equations, the phase and magnitude corrections to the measured force and moment may be found.

The corrections indicated by equations B-7 and B-8 were evaluated for several tests. The acceleration ( $\omega^2 y_o$ ) and frequency ( $\omega$ ) were measured from the records and the velocity ( $\omega y_o$ ) was calculated. However, the recorded accelerations at frequency  $\omega$  were indiscernable because of the hash in the accelerometer records so that an estimate of the worst possible value for the magnitude of the acceleration was the best information that could be obtained. Using this value, it was found that the phase correction was always less than 5-degrees and that the magnitude correction was less than 10 percent for 90 percent of the runs. As a result, including these corrections in the calculation of the experimental forces and moments was considered to be not worth the time involved. For those cases investigated, the inclusion of

these corrections did not lessen the scatter in the results for either the magnitude or phase of the measured forces and moments. In all cases, when the magnitude corrections are included, the magnitude is reduced. The side force data corrected on the basis of the previous analysis are shown as the flagged points in Figure 16 and in Figure 19 for the yaw moment.

# DISTRIBUTION LIST

Copies		Copies	
50	Commanding Officer and Director David Taylor Model Basin Washington 7, D. C. Attn: Code 513	9	Chief, Bureau of Ships Department of the Navy Washington 25, D. C. Attn: Code 320 (Lab N.G.T.) (1)
10	Commander Armed Services Technical Information Agency Arlington Hall Station Arlington 12, Virginia Attn: TIPDR		335 (Technical Information Branch) (3)
			345 (Ship Silencing Branch) (1)
			420 (Preliminary Design Branch) (1)
			421 (Preliminary Design Branch) (1)
1	Commander Boston Naval Shipyard Boston, Massachusetts		440 (Hull Design Branch) (1)
			442 (Scientific and Research) (1)
1	California Institute of Technology Pasadena 4, California Attn: Dr. T. Y. Wu	1	Chief, Bureau of Yards and Docks Department of the Navy Washington 25, D. C. Attn: Code D-400 (Research Div.)
1	Commander Charleston Naval Shipyard Charleston, South Carolina	2	Iowa Institute of Hydraulic Research State University of Iowa Iowa City, Iowa Attn: Dr. H. Rouse, Director Dr. L. Landweber
1	Colorado State University Department of Civil Engineering Fort Collins, Colorado Attn: Mr. A. R. Chamberlain, Chief Engineering, Mathematics and Physics Research	2	Institute of Mathematical Sciences New York University 25 Waverly Place New York 3, New York Attn: Prof. J. Stoker (1) Prof. A. Peters (1)
1	University of Notre Dame Notre Dame Indiana Attn: Dr. A. G. Strandhagen Dept. of Engineering Science	1	Commander Long Beach Naval Shipyard Long Beach, California
1	Chief of Naval Research (Code 438) Department of the Navy Washington 25, D. C.	1	Commander Mare Island Naval Shipyard Vallejo, California
2	Chief, Bureau of Naval Weapons (R) Department of the Navy Washington 25, D. C.	1	Administrator U. S. Maritime Administration Department of Commerce Washington 25, D. C. Attn: Mr. Vito L. Russo, Deputy Chief, Office of Ship Construction
1	Special Projects Office Department of the Navy Washington 25, D. C. Attn: Chief Scientist		

## Copies

- 1 Maritime College  
State University of New York  
Fort Schulyer  
New York 65, New York  
Attn: Prof. J. J. Foody, Head  
Engineering Department
- 1 Massachusetts Institute of  
Technology  
Cambridge 39, Massachusetts  
Attn: Department of Naval  
Architecture and  
Marine Engineering
- 1 Commander  
Military Sea Transportation Service  
Department of the Navy  
3800 Newark Street, N. W.  
Washington 25, D. C.
- 1 Director  
National Aeronautics and Space  
Administration  
1512 H Street, N. W.  
Washington 25, D. C.
- 1 Director  
National Bureau of Standards  
Washington 25, D. C.  
Attn: Dr. G. B. Schubauer  
(Fluid Mechanics)
- 1 Mr. A. M. O. Smith  
Douglas Aircraft Company, Inc.  
El Segundo Division  
El Segundo,  
California
- 1 Oceanics, Inc.  
114 East 40th Street  
New York 16,  
New York
- 1 Director  
National Science Foundation  
1951 Constitution Avenue, N. W.  
Washington, D. C.
- 6 Director  
U. S. Naval Research Laboratory  
Code 2020  
Washington 25, D. C.

## Copies

- 1 Commander  
New York Naval Shipyard  
Brooklyn, New York
- 1 New York University  
University Heights  
New York 53, New York  
Attn: Dr. W. J. Pierson, Jr.
- 1 Commander  
Norfolk Naval Shipyard  
Portsmouth, Virginia
- 25 Commanding Officer  
Office of Naval Research  
Navy 100, Fleet Post Office  
New York, New York
- 1 Commanding Officer  
Office of Naval Research Branch Office  
1000 Geary Street  
San Francisco 9, California
- 1 Commanding Officer  
Office of Naval Research Branch Office  
1030 East Green Street  
Pasadena 1, California
- 1 Commanding Officer  
Office of Naval Research Branch Office  
346 Broadway  
New York 13, New York
- 1 Commanding Officer  
Office of Naval Research Branch Office  
The John Crerar Library Building  
85 East Randolph Street  
Chicago 1, Illinois
- 1 Commander  
Pearl Harbor Naval Shipyard  
Navy 120, Fleet Post Office  
San Francisco, California
- 1 Pennsylvania State University  
University Park, Pennsylvania  
Attn: Director  
Ordnance Research Laboratory
- 1 Commander  
Philadelphia Naval Shipyard  
Philadelphia, Pennsylvania

## Copies

1 Commander  
Portsmouth Naval Shipyard  
Portsmouth, New Hampshire

1 Commander  
Puget Sound Naval Shipyard  
Bremerton, Washington

1 Commander  
San Francisco Naval Shipyard  
San Francisco, California

1 Society of Naval Architects and  
Marine Engineers  
74 Trinity Place  
New York 6, New York

1 Dr. L. C. Straub, Director  
St. Anthony Falls Hydraulic  
Laboratory  
University of Minnesota  
Minneapolis 14, Minnesota

3 University of California  
Berkeley 5, California  
Attn: Department of Engineering  
Prof. H. A. Schade, Head  
Dept. of Naval Architecture (1)  
Prof. J. Johnson (1)  
Prof. J. V. Wehausen,  
Institute of Engineering  
Research (1)

1 University of Maryland  
College Park, Maryland  
Attn: Institute for Fluid Dynamics  
and Applied Mathematics

1 University of Michigan  
Ann Arbor, Michigan  
Attn: Prof. R. B. Couch, Chairman  
Department of Naval  
Architecture and Marine  
Engineering

1 Commanding Officer  
Headquarters  
U. S. Army Transportation Command  
Fort Eustis, Virginia  
Attn: Research Reference Center

## Copies

2 U. S. Coast Guard  
1300 E Street, N. W.  
Washington 25, D. C.  
Attn: Secretary, Ship Structure  
Committee (1)  
Commandant (1)

1 Chief, Applied Naval Architecture  
Department of Nautical Science  
U. S. Merchant Marine Academy  
Kings Point, Long Island, New York

1 Superintendent  
U. S. Naval Academy  
Annapolis, Maryland  
Attn: Library

1 Superintendent  
U. S. Naval Postgraduate School  
Monterey, California

1 Commander  
U. S. Naval Proving Ground  
Dahlgren, Virginia

1 Commanding Officer  
U. S. Naval Repair Facility  
U. S. Naval Station  
San Diego, California

1 Administrator  
Webb Institute of Naval Architecture  
Crescent Beach Road  
Glen Cove, Long Island, New York  
Attn: Technical Library

1 Director  
Woods Hole Oceanographic Institute  
Woods Hole, Massachusetts  
Attn: Dr. C. Iselin, Senior Oceanographer

1 Editor  
Engineering Index, Inc.  
29 West 39th Street  
New York, New York

1 Librarian  
Society of Naval Architects and  
Marine Engineers  
74 Trinity Place  
New York 6, New York

<p>Davidson Laboratory Report No. 808 WAVE FORCES ON SUBMERGED BODIES by Charles J. Henry, Milton Martin, and Paul Kaplan, June 1961</p> <p>A series of experiments, in which the forces and moments acting on a slender, submerged body-of-revolution moving under regular waves were measured, provided data to verify theoretical predictions of these forces and moments. The measured and predicted results over a range of speeds, heading angles, and wave lengths agreed. The measured and predicted roll moments, acting on the same model but with a conning tower, did not agree; however, the measured and predicted heave and side forces and the pitch and yaw moments did agree.</p>	<p>UNCLASSIFIED</p>	<p>Davidson Laboratory Report No. 808 WAVE FORCES ON SUBMERGED BODIES by Charles J. Henry, Milton Martin, and Paul Kaplan, June 1961</p> <p>A series of experiments, in which the forces and moments acting on a slender, submerged body-of-revolution moving under regular waves were measured, provided data to verify theoretical predictions of these forces and moments. The measured and predicted results over a range of speeds, heading angles, and wave lengths agreed. The measured and predicted roll moments, acting on the same model but with a conning tower, did not agree; however, the measured and predicted heave and side forces and the pitch and yaw moments did agree.</p>	<p>UNCLASSIFIED</p>
<p>Davidson Laboratory Report No. 808 WAVE FORCES ON SUBMERGED BODIES by Charles J. Henry, Milton Martin, and Paul Kaplan, June 1961</p> <p>A series of experiments, in which the forces and moments acting on a slender, submerged body-of-revolution moving under regular waves were measured, provided data to verify theoretical predictions of these forces and moments. The measured and predicted results over a range of speeds, heading angles, and wave lengths agreed. The measured and predicted roll moments, acting on the same model but with a conning tower, did not agree; however, the measured and predicted heave and side forces and the pitch and yaw moments did agree.</p>	<p>UNCLASSIFIED</p>	<p>Davidson Laboratory Report No. 808 WAVE FORCES ON SUBMERGED BODIES by Charles J. Henry, Milton Martin, and Paul Kaplan, June 1961</p> <p>A series of experiments, in which the forces and moments acting on a slender, submerged body-of-revolution moving under regular waves were measured, provided data to verify theoretical predictions of these forces and moments. The measured and predicted results over a range of speeds, heading angles, and wave lengths agreed. The measured and predicted roll moments, acting on the same model but with a conning tower, did not agree; however, the measured and predicted heave and side forces and the pitch and yaw moments did agree.</p>	<p>UNCLASSIFIED</p>